



National Library  
of Canada

Bibliothèque nationale  
du Canada

Canadian Theses Service

Services des thèses canadiennes

Ottawa, Canada  
K1A 0N4

## CANADIAN THESES

### NOTICE

The quality of this microfiche is heavily dependent upon the quality of the original thesis submitted for microfilming. Every effort has been made to ensure the highest quality of reproduction possible.

If pages are missing, contact the university which granted the degree.

Some pages may have indistinct print especially if the original pages were typed with a poor typewriter ribbon or if the university sent us an inferior photocopy.

Previously copyrighted materials (journal articles, published tests, etc.) are not filmed.

Reproduction in full or in part of this film is governed by the Canadian Copyright Act, R.S.C. 1970, c. C-30. Please read the authorization forms which accompany this thesis.

**THIS DISSERTATION  
HAS BEEN MICROFILMED  
EXACTLY AS RECEIVED**

## THÈSES CANADIENNES

### AVIS

La qualité de cette microfiche dépend grandement de la qualité de la thèse soumise au microfilmage. Nous avons tout fait pour assurer une qualité supérieure de reproduction.

S'il manque des pages, veuillez communiquer avec l'université qui a conféré le grade.

La qualité d'impression de certaines pages peut laisser à désirer, surtout si les pages originales ont été dactylographiées à l'aide d'un ruban usé ou si l'université nous a fait parvenir une photocopie de qualité inférieure.

Les documents qui font déjà l'objet d'un droit d'auteur (articles de revue, examens publiés, etc.) ne sont pas microfilmés.

La reproduction, même partielle, de ce microfilm est soumise à la Loi canadienne sur le droit d'auteur, SRC 1970, c. C-30. Veuillez prendre connaissance des formules d'autorisation qui accompagnent cette thèse.

**LA THÈSE A ÉTÉ  
MICROFILMÉE TELLE QUE  
NOUS L'AVONS REÇUE**

**Canada**



National Library  
of Canada

Bibliothèque nationale  
du Canada

TC -

Ottawa, Canada  
K1A 0N4

0-315-22910-1

CANADIAN THESES ON MICROFICHE SERVICE - SERVICE DES THÈSES CANADIENNES SUR MICROFICHE

**PERMISSION TO MICROFILM - AUTORISATION DE MICROFILMER**

• Please print or type - Écrire en lettres moulées ou dactylographier

**AUTHOR - AUTEUR**

Full Name of Author - Nom complet de l'auteur

GEORGE ROBERT GILLSON

Date of Birth - Date de naissance

30/6/1958

Canadian Citizen - Citoyen canadien

☒ Yes Oui

☐ No Non

Country of Birth - Lieu de naissance

CANADA

Permanent Address - Residence fixe

#5-100 HENDERSON AVE  
THORNHILL, ONT L3T 2K8

**THESIS - THÈSE**

Title of Thesis - Titre de la thèse

A Study of Analyte Species in the ICP by  
Atomic Fluorescence / Atomic Absorption Spectroscopy

Degree for which thesis was presented  
Grade pour lequel cette thèse fut présentée

Ph.D

Year this degree conferred  
Année d'obtention de ce grade

1985

University - Université

Alberta

Name of Supervisor - Nom du directeur de thèse

Gary Horlick

**AUTHORIZATION - AUTORISATION**

Permission is hereby granted to the NATIONAL LIBRARY OF CANADA to  
microfilm this thesis and to lend or sell copies of the film.

The author reserves other publication rights, and neither the thesis nor extensive  
extracts from it may be printed or otherwise reproduced without the  
author's written permission.

L'autorisation est, par la présente, accordée à la BIBLIOTHÈQUE NATIONALE  
DU CANADA de microfilmer cette thèse et de prêter ou de vendre des ex-  
emplaires du film.

L'auteur se réserve les autres droits de publication; ni la thèse ni de longs ex-  
traits de celle-ci ne doivent être imprimés ou autrement reproduits sans  
l'autorisation écrite de l'auteur.

ATTACH FORM TO THESIS - VEUILLEZ JOINDRE CE FORMULAIRE À LA THÈSE

Signature

Date

George Gillson

17/6/1985

THE UNIVERSITY OF ALBERTA

A STUDY OF ANALYTE SPECIES IN THE ICP BY  
ATOMIC FLUORESCENCE/ATOMIC ABSORPTION SPECTROSCOPY

by

GEORGE ROBERT GILLSON

A THESIS

SUBMITTED TO THE FACULTY OF GRADUATE STUDIES AND RESEARCH  
IN PARTIAL FULFILMENT OF THE REQUIREMENTS FOR THE DEGREE  
OF DOCTOR OF PHILOSOPHY

DEPARTMENT OF CHEMISTRY

EDMONTON, ALBERTA

FALL 1985

THE UNIVERSITY OF ALBERTA

RELEASE FORM

NAME OF AUTHOR: GEORGE ROBERT GILLSON

TITLE OF THESIS: A STUDY OF ANALYTE SPECIES IN THE ICP BY  
ATOMIC FLUORESCENCE/ATOMIC ABSORPTION  
SPECTROSCOPY

DEGREE FOR WHICH THESIS WAS PRESENTED: Ph.D.

YEAR THIS DEGREE GRANTED: 1985

Permission is hereby granted to THE UNIVERSITY OF ALBERTA LIBRARY to reproduce single copies of this thesis and to lend or sell such copies for private, scholarly or scientific research purposes only.

The author reserves other publication rights, and neither the thesis nor extensive extracts from it may be printed or otherwise reproduced without the author's written permission.

(Signed) *George Gillson*  
PERMANENT ADDRESS:

#5-100 Henderson Ave.

Thornhill, Ont.

DATED 14/6/85



THE UNIVERSITY OF ALBERTA  
FACULTY OF GRADUATE STUDIES AND RESEARCH

The undersigned certify that they have read, and recommend to the Faculty of Graduate Studies and Research, for acceptance, a thesis entitled A STUDY OF ANALYTE SPECIES IN THE ICP BY ATOMIC FLUORESCENCE/ATOMIC ABSORPTION SPECTROSCOPY submitted by GEORGE ROBERT GILLSON in partial fulfilment of the requirements for the degree of DOCTOR OF PHILOSOPHY

Barry Horlick  
Supervisor

B. Katschul

Robert Tidorev

June W. Sims

Dallas Habens

MRB  
External Examiner

DATE 14/6/85

## ABSTRACT

The inductively coupled plasma (ICP) has gained widespread acceptance as a source for analytical atomic emission spectroscopy and recently, it was introduced as an ion source for analytical mass spectrometry (ICP-MS). Via numerous studies of the spatial analyte emission patterns of the discharge, knowledge of the excited analyte ions and atoms contained therein has been acquired. Analogous studies of ground state analyte populations, of particular relevance for ICP-MS, have not been as extensive.

In this thesis work, the response of ground state analyte ion and atom population distributions to changes in plasma operating parameters (power, aerosol carrier flowrate) was thoroughly investigated. Initial studies centered around atomic absorption measurements. Later, using the technique of laser-induced atomic fluorescence, radial profiles of relative ground state analyte ion and atom densities were acquired for a variety of observation heights and operating conditions. Attention was focussed on Ca although Sr and Mo were also studied. Equipment constructed for the investigations includes a pulsed hollow cathode lamp control unit, photodiode array spectrometer and computer controlled torch positioning system.

In general, for a fixed aerosol carrier flowrate, large ground state ion fluorescence signals can be obtained over a wide range of powers and observation heights. These signals were, however, seen to be critically dependent on aerosol carrier flowrate. Spatially averaged atomic absorption measurements provide independent confirmation of the fluorescence results. Good agreement was also seen when ion fluorescence measurements were compared to corresponding ion count rates from ICP-MS.

With a few simple modifications, the experimental system could be set up to measure lateral emission intensity. For comparison to fluorescence results, sets of lateral emission profiles were acquired. These differed markedly from the fluorescence profiles in their response to changes in the operating conditions and/or observation zone. The trends seen in emission were also compared to trends seen in excited state fluorescence. This latter study has important ramifications for future fluorescence studies which might be undertaken.

Although useful in their own right, relative density measurements are not appropriate for in-depth characterization of the ICP. However, a system is now in place in our laboratory for automated measurement of temperatures and particle densities necessary for such characterization to continue.

## ACKNOWLEDGEMENTS

I would like to acknowledge the love and encouragement offered by my wife Lex during the course of my graduate studies. My cats Bear, Scooter and even the ponderous Rascal also deserve honourable mention.

Thanks is directed to Gary Horlick, my supervisor for (among many things) his help and guidance. The expert work and advice of those in the Machine Shop, Glass Shop and Electronics Shop (in no particular order) along with the life skills advice patiently provided by Bruce Todd, are gratefully acknowledged.

Annabelle Wiseman is commended for reading my writing and subsequently typing this thesis.

Lastly, thank you to NSERC for four years of financial support, and thank you to my parents for all those other years of support.

## TABLE OF CONTENTS

CHAPTER	PAGE
1. INTRODUCTION.....	1
A. Characterization of the ICP.....	1
B. Atomic Absorption/Fluorescence Overview.....	11
C. Atomic Absorption Literature Review.....	16
D. Atomic Fluorescence Literature Review.....	19
2. ATOMIC ABSORPTION STUDY.....	22
A. Introduction.....	22
B. Experimental.....	26
B.1 Optical Configuration.....	26
B.2 Construction and Operation of Controller/Lamp Driver.....	28
B.3 Experimental Outline.....	33
B.4 Test of the System.....	36
C. Results and Discussion.....	41
D. Conclusion.....	44
3. AFS EXPERIMENTAL SYSTEM.....	46
A. Introduction.....	46
B. System Overview.....	46
C. Optics.....	50
D. Lasers.....	54
E. Torch Translation System.....	54
F. Electronics and Measurement Procedure.....	58

CHAPTER	PAGE
4. FLUORESCENCE RESULTS: FASSEL TORCH.....	66
A. Introduction.....	66
B. Effect of Power at 1 lpm Flowrate.....	67
B.1 Overview of Ca Ion Fluorescence.....	67
B.2 Ca Atom Fluorescence Overview.....	71
B.3 Comparison to Strontium Data.....	76
B.4 Discussion.....	79
B.4.1 Inner Filtering Effects.....	81
B.4.2 Effect of Power at Fixed Observation Height (9 and 13 mm ALC).....	82
B.4.2.a Excitation.....	84
B.4.2.b Formation of doubly charged ions.....	90
B.4.2.c Quenching effects.....	92
B.4.3 Effect of Power at Fixed Ob- servation Height (>13 mm ALC)....	94
B.4.4 Effect of Height at Fixed Power..	94
C. Effect of Flowrate.....	95
C.1 Overview: Ca Ion and Atom Fluorescence	95
C.2 Discussion.....	106
D. Comparison of Fluorescence and Absorbance Measurements.....	110
E. Comparison to Other Ground State Studies.....	114
F. Summary and Conclusions.....	116

CHAPTER	PAGE
5. FLUORESCENCE RESULTS: MAK TORCH.....	119
A. Introduction.....	119
B. Ca Ion and Atom Fluorescence.....	121
B.1 Overview.....	121
B.1.1 1 lpm.....	121
B.1.2 .85 lpm.....	128
B.1.3 .65 lpm.....	132
B.2 Discussion.....	138
B.3 Comparison to ICP-MS Results.....	141
C. Lateral Emission Profiles.....	143
C.1 Overview of Emission Results.....	144
C.1.1 Ion Emission (1 lpm).....	144
C.1.2 Atom Emission (1 lpm).....	147
C.1.3 Ion Emission (.65 lpm).....	150
C.1.4 Atom Emission (.65 lpm).....	153
C.2 Discussion.....	153
D. Excited State Fluorescence.....	162
E. Molybdenum Results.....	166
F. Summary and Conclusions.....	174
6. EASILY IONIZABLE ELEMENT INTERFERENCE STUDY:	
MAK TORCH.....	177
A. Introduction.....	177
B. Experimental.....	179
C. Discussion.....	180
C.1 1 lpm.....	180

CHAPTER	PAGE
C.2 .85 and .65 lpm.....	188
D. Conclusion.....	192
7. CLOSING REMARKS .....	193

\*\*\*\*\*

REFERENCES.....	196
APPENDIX A.....	202
APPENDIX B.....	205
APPENDIX C.....	220
APPENDIX D.....	225



# LIST OF TABLES

TABLE	PAGE
1. Details of experimental set-up for atomic absorption.....	34
2. Plasma operating conditions, wavelength of observation and analyte concentrations for absorbance and emission measurements.....	35
3. Comparison of measured and nominal transmittances of neutral density filters.....	37
4. Details of fluorescence experimental system....	49
5. Wavelengths and laser dyes employed for atomic fluorescence.....	55
6. Experimental details for fluorescence studies..	68
7. Comparison of excitation and ionization energies of Sr and Ca.....	80
8. Experimental details for MAK torch studies.....	122

# LIST OF FIGURES

FIGURE	PAGE
1. Schematic illustration of ICP discharge and torch.....	2
2. Illustration of vertical emission profile concept.....	4
3. Radial emission profile concept: (a) schematic illustration, (b) actual radial emission profiles.....	5
4. Schematic illustration of: (a) absorption, (b) fluorescence.....	12
5. Schematic illustration of thermally assisted fluorescence.....	15
6. ICP in typical flame A.A. optical configuration.....	24
7. Schematic representation of opto-electronic absorbance measurement system.....	27
8. Timing of lamp pulses in "intermittent mode".....	29
9. Schematic diagram of controller and driver.....	31
10. Electronic waveforms relevant to Figure 9.....	32
11. Calcium absorbance working curves. "H" and "L" denote high and low current levels. Solid curves are for the ion; dashed curves are for the atom.....	38

12. Magnesium absorbance working curves. Legend as for Figure 11..... 39
13. Effect of power and flowrate on calcium atom and ion absorbance and emission. Power increases from left to right in each frame. Absorbance curves are solid and are referred to the axes at the left side of the figure. Emission curves are dashed and are referred to the axes on the right side of the figure. The numbers 1, 2, 3, 4 refer to aerosol carrier flowrates of 1.0, 1.15, 1.3 and 1.45 lpm in any frame. (a) Ca atom, (b) Ca ion..... 42
14. Effect of power and flowrate on magnesium atom and ion absorbance and emission. Details as for Figure 13. (a) Mg atom, (b) Mg ion..... 43
15. Schematic diagram of atomic fluorescence measurement system..... 48
16. Top: Illustration of axes along which ICP can be translated. Bottom: Acquisition of a 3-point fluorescence profile. The plasma is moving from right to left in frames (a) through (c)..... 51

17. Illustration of modification made to commercial plasma unit (a) unmodified, (b) modified.....	57
18. Torchbox and torch translation system.....	59
19. Interconnection of components shown in Figure 15.....	60
20. Time relationship of laser trigger signal, photodiode output and amplifier output.....	62
21. Spatial locations in plasma at which fluorescence and/or emission measurements were made.....	65
22. 393.3 nm $\text{Ca}^+$ fluorescence power study results, 1 lpm. See text for explanation of format.....	69
23. Intensity of 393.3 nm $\text{Ca}^+$ fluorescence in the central channel as a function of power (1 lpm). The numbers in the figure indicate observation height in mm above the load coil.....	70
24. 422.7 Ca atom fluorescence power study results, 1 lpm.....	72
25. Intensity of 422.7 nm Ca atom fluorescence in the central channel as a function of power (1 lpm). The number attached to each curve is observation height as in Figure 23....	73

26.	Area of Ca atom fluorescence profile as a function of height at various powers (1 lpm). The numbers attached to the curves are plasma power in kW.....	75
27.	407.8 nm $\text{Sr}^+$ fluorescence power study results, 1 lpm.....	77
28.	460.7 nm Sr atom fluorescence power study results, 1 lpm.....	78
29.	Ca ion absorbance as a function of power at 3 observation heights (heights in mm above the load coil.....	83
30.	Partial energy level diagram for Ca ion.....	86
31.	$\text{Ca}^+$ vertical profiles (1 lpm). (a) 393.3 nm emission, (b) 393.3 nm fluorescence.....	88
32.	393.3 nm $\text{Ca}^+$ fluorescence power study results, 85 lpm.....	96
33.	Effect of concentration on $\text{Ca}^+$ fluorescence profile at 13 mm ALC, 1 kW, .65 lpm. Solid curve 400 ppm Ca. Dotted curve 40 ppm.....	98
34.	393.3 nm $\text{Ca}^+$ fluorescence power study results, .65 lpm.....	99
35.	Effect of flowrate on $\text{Ca}^+$ fluorescence profile at fixed power (19 mm ALC/ 1 kW).....	100

36.	Effect of flowrate on $\text{Ca}^+$ fluorescence at fixed power (19 mm ALC/.5 kW).....	101
37.	422.7 nm $\text{Ca}$ atom fluorescence power study results, .85 lpm.....	102
38.	422.7 nm $\text{Ca}$ atom fluorescence power study results, .65 lpm.....	104
39.	$\text{Ca}$ ion and atom fluorescence as a function of power at 3 flowrates. Flowrates are labelled in each frame. Heights in mm above the load coil are attached to each curve.....	105
40.	$\text{Ca}$ ion fluorescence and absorbance results (393.3 nm) at 3 observation heights. H, I and L denote high, intermediate and low carrier flowrates. See text for further description of format.....	111
41.	$\text{Ca}$ atom fluorescence and absorbance results (422.7 nm) at 3 observation heights. The format is identical to Figure 40.....	113
42.	ICP torches: (a) MAK, (b) FASSEL.....	120
43.	393.3 nm $\text{Ca}^+$ fluorescence power study results, 1 lpm - MAK torch.....	123
44.	Normalized $\text{Ca}^+$ fluorescence profiles, 1.25 kW/1 lpm/19 mm ALC. Solid curve: Fassel Torch. Dotted curve: MAK Torch.....	124

45.	422.7 nm Ca atom fluorescence power study results, 1 lpm - MAK torch.....	126
46.	Magnified view of a portion of Figure 45.....	127
47.	393.3 nm Ca <sup>+</sup> fluorescence power study results, .85 lpm - MAK torch.....	129
48.	Dependence of Ca <sup>+</sup> fluorescence intensity (13 mm ALC, .85 lpm/ 1.25 kW) on laser channel , electrode voltage. Straight line is a least-squares best fit to the experimental results.....	131
49.	422.7 nm Ca atom fluorescence power study results - .85 lpm - MAK torch.....	133
50.	Magnified view of a portion of Figure 49.....	134
51.	393.3 nm Ca <sup>+</sup> fluorescence power study results, .65 lpm - MAK torch.....	135
52.	422.7 nm Ca atom fluorescence map, .65 lpm/.75 kW - MAK torch.....	136
53.	Results of partial power study of 422.7 nm Ca atom fluorescence (40 ppm/1000 $\mu$ slit) .65 lpm - MAK torch.....	137
54.	Ca ion and atom fluorescence as a function of power at 3 flowrates (same format as Figure 39) - MAK torch.....	139
55.	Results of a study of the response of ground state Sr <sup>+</sup> behavior to changes in carrier	

flowrate in the zone 17 to 19 mm ALC (MAK torch). (a) $\text{Sr}^+$ fluorescence intensity in the central channel - 17 mm ALC, (b) $\text{Sr}^+$ count rate - 19 mm ALC.....	142
56. 393.3 $\text{Ca}^+$ emission power study results at 1 lpm - MAK torch.....	145
57. $\text{Ca}^+$ vertical profiles (1 lpm). (a) 393.3 nm fluorescence, (b) 393.3 nm emission - MAK torch.....	146
58. $\text{Ca}^+$ fluorescence and emission profiles at 393.3 nm for 4 powers at an observation height of 19 mm ALC (1 lpm) - MAK torch.....	148
59. 422.7 nm Ca atom emission power study results, 1 lpm - MAK torch.....	149
60. 393.3 nm Ca ion emission power study results, .65 lpm - MAK torch.....	151
61. Response of $\text{Ca}^+$ fluorescence and emission to a decrease in flowrate at 19 mm ALC, 4 powers - MAK torch.....	153
62. 422.7 nm Ca atom emission power study results, .65 lpm - MAK torch.....	154
63. 422.7 nm Ca atom emission profiles and 393.3 nm $\text{Ca}^+$ fluorescence profiles as a function of power at 10 mm ALC, .65 lpm - MAK torch.....	160



64.	373.7 nm $\text{Ca}^+$ fluorescence power study results, 1 lpm - MAK torch.....	163
65.	373.7 nm $\text{Ca}^+$ fluorescence power study results, .65 lpm - MAK torch.....	164
66.	390.3 nm Mo atom fluorescence power study results, 1 lpm - MAK torch.....	167
67.	Vertical fluorescence profiles (1 lpm): (a) Mo atom, (b) Ca atom - MAK torch.....	169
68.	390.3 nm Mo atom emission power study results, 1 lpm - MAK torch.....	170
69.	390.3 nm Mo atom fluorescence power study results, .65 lpm - MAK torch.....	172
70.	390.3 nm Mo atom emission power study results, .65 lpm - MAK torch.....	173
71.	Effect of EIE (100-fold molar excess of Na) on 393.3 nm $\text{Ca}^+$ fluorescence profiles as a function of power and observation height (1 lpm - MAK torch). Profiles obtained in the presence of Na are represented by dashed curves.....	181
72.	Normalized fluorescence and emission profiles with and without EIE at 10 mm ALC/1.25 kW/1 lpm. Dashed curves denote the presence of the EIE - Mak torch.....	183

# FIGURE

PAGE

73. Response of: Ca ion emission (a) and Ca atom fluorescence (b) profiles at 19 mm ALC/1 kW/1 lpm to presence of an EIE..... 185
74. Effect of increased concentration of EIE on Ca<sup>+</sup> fluorescence at 25 mm ALC/.75 kW/1 lpm - MAK torch. (1) 4 ppm Ca, (2) 4 ppm Ca/240 ppm Na, (3) 4 ppm Ca/2400 ppm Na..... 186
75. Ca atom fluorescence profiles at 31 mm ALC, 1.25 kW, 1 lpm, MAK torch with (dashed curve) and without (solid curve) excess Na..... 187
76. Schematic representation of effect of excess Na on Ca<sup>+</sup> fluorescence at 3 flowrates. See text for description..... 189
77. Effect of increasing concentration of EIE on Ca<sup>+</sup> fluorescence profile at 31 mm ALC, .75 kW, .65 lpm, MAK torch. Numbering of the curves as in Figure 74..... 191
78. (a) Block diagram of photodiode array driving electronics, (b) schematic diagram of unmodified timing circuitry..... 208
79. Clock circuit schematic diagram..... 210
80. Schematic of altered timing circuitry..... 211
81. Relevant electronic waveforms for array circuitry..... 212
82. Video amplifier schematic..... 216

# FIGURE

## PAGE

83. Block diagram of modified array circuitry interfaced to a computer.....	217
84. Front panel of unit housing array driving electronics.....	219
85. Interfacing of stepper motors.....	222
86. Stepper motor wiring diagram.....	223
87. Details of laser pulse counting circuit.....	227

## CHAPTER 1

### INTRODUCTION

#### A. Characterization of the ICP

The inductively coupled plasma (ICP) (Figure 1) is now firmly established as a valuable tool for analytical atomic emission spectroscopy. Its advantages include wide dynamic range, low detection limits and the ability to analyze samples in a variety of physical forms [1] and matrices.

Recently the ICP has attracted even more interest due to its use as an ion source for mass spectrometric determination of trace elements [2-7]. Linear working curves of 5 orders of magnitude extending from the parts per trillion range [5], plus the capability of convenient isotopic analysis, are two of the attributes of this combined technique.

To exact the best possible performance from the ICP either as an emission source or an ion source for analytical spectroscopy, it is necessary to characterize the plasma at both a practical level and a fundamental level. From a discussion of what has been done in these two areas, and the studies that remain to be done, the

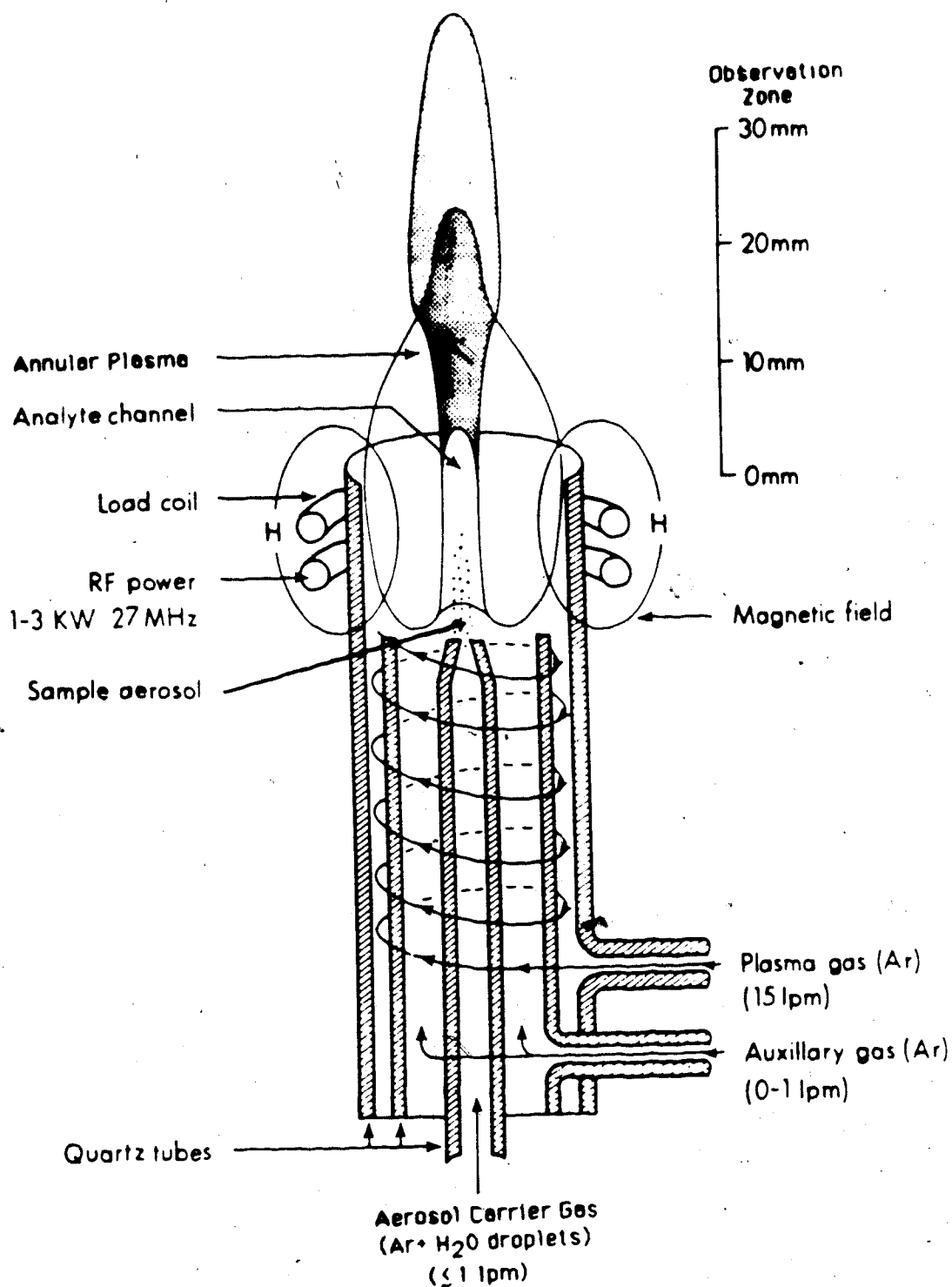


Figure 1. Schematic illustration of ICP discharge and torch.

impetus for the work described in this thesis will emerge.

A practical understanding of the ICP includes knowledge of how the species of interest is distributed within the plasma, how this distribution varies from element to element and how changes in variables such as plasma power and carrier gas flowrate affect the distribution. Knowing these things permits the selection of an optimum observation or sampling zone for example, and facilitates the process of teaching a student or novice user about the ICP. Also, there is an inherent satisfaction in simply having obtained "the big picture" so to speak.

Practical characterization of the ICP for emission spectroscopy has involved the acquisition of, not surprisingly, vertical and radial emission profiles. A vertical emission profile is a plot of the intensity of ion or atom emission in the central channel of the ICP as a function of height above the load coil as illustrated in Figure 2. A radial profile on the other hand, illustrates the variation of emission intensity along any line through the center of a thin cross-section of the plasma. This is shown in Figure 3(a). Obviously a set of radial emission profiles at different heights provides a more accurate picture of the spatial distribution of excited species than a vertical profile. For example, radial profiles

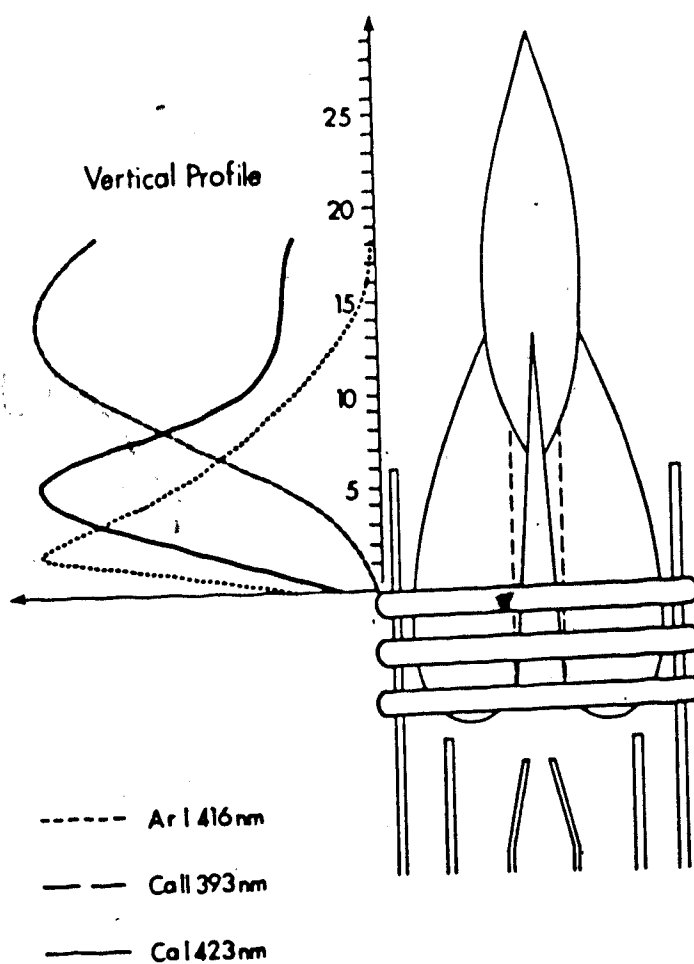


Figure 2. Illustration of vertical emission profile concept.

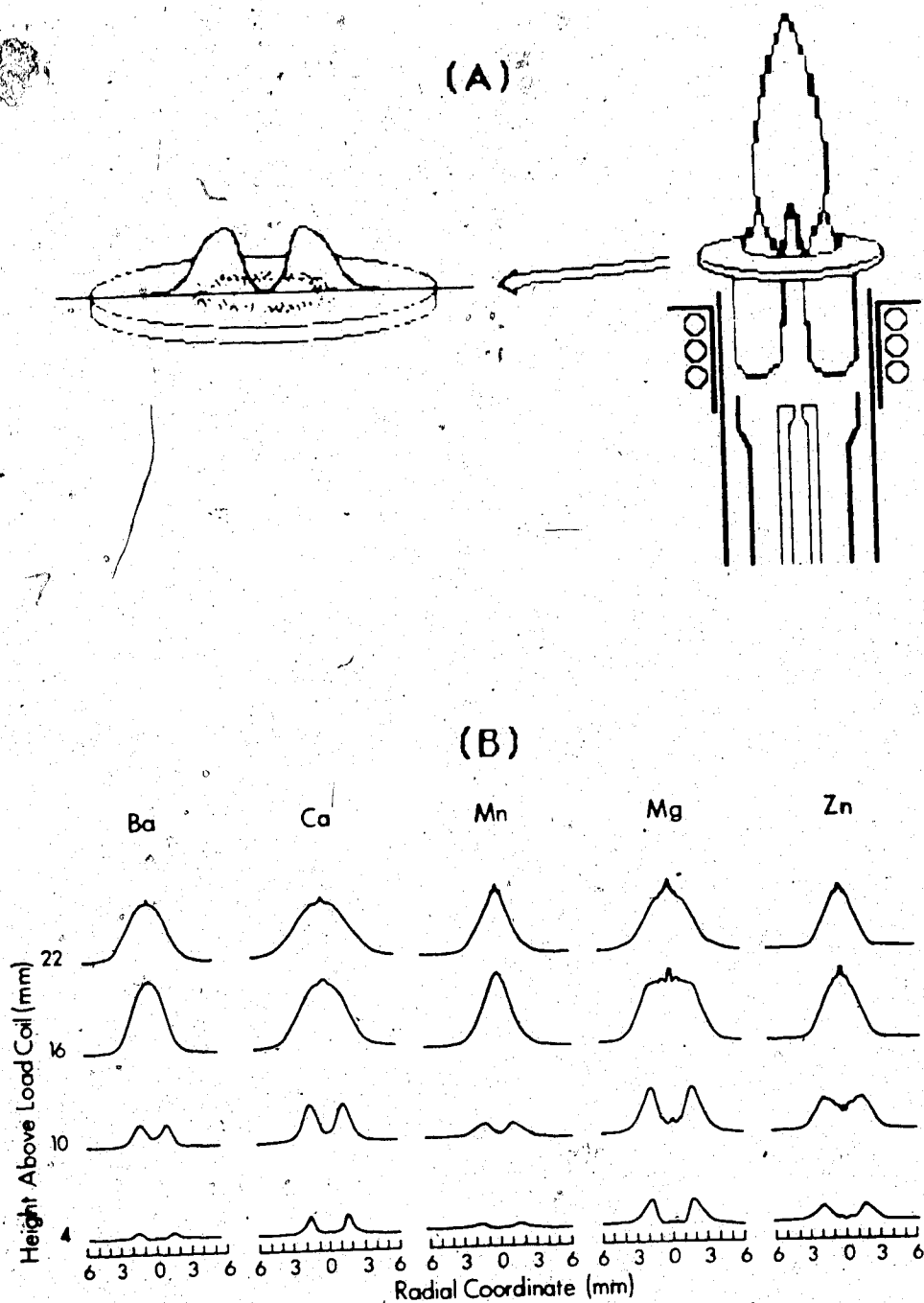


Figure 3. Radial emission profile concept: (a) schematic illustration, (b) actual radial emission profiles from reference [8].



acquired by Furuta [8] seen in Figure 3(b) show that the distribution of excited ions gradually goes from being toroidal to having a central maximum. (The same is true for excited atoms.) This behavior could not have been deduced from the vertical profiles in Figure 2.

The response of emission profiles to changes in operating parameters such as power and carrier flowrate [8-17], element-to-element variations [8,10,13] and the effect of addition of an easily ionizable element (EIE) [9,11,12,15,16,18,19] have all been studied and the utility of these studies has been well-recognized. For example, from Figure 3(b) it is immediately obvious that 4 mm above the load coil (ALC) is not the optimum zone for ion emission whereas 16 mm ALC is a good compromise observation height.

In principle, these profiles should also be useful in a practical sense for inductively coupled plasma mass spectrometry (ICP-MS) since it does not distinguish between ground state and excited ions. However, unless the plasma is highly non-thermal, the majority of the singly-charged ions of some elements should remain in the ground state. Hence a practical characterization of the ICP for mass spectrometry might entail acquisition of ground state ion absorbance or fluorescence profiles of various elements for a variety of observation heights and operating

conditions. Some ground state studies of this type have appeared; they will be discussed later. For now it suffices to say that there is a need for further work in the area.

An understanding of the ICP at a fundamental level includes knowledge of the actual physical processes involved in generating the species of interest in a given situation. If these processes are known, then modifications to the system can be made in an intelligent fashion, i.e. to enhance desirable features or suppress undesirable ones.

However, the physical processes involving analytically important species cannot be considered in isolation from the processes occurring in the plasma as a whole. In fact, in terms of densities, the analyte is a trace impurity in the argon plasma. As a lead-in to the discussion of fundamental studies then, a brief overview of the argon plasma follows.

Some salient features of the typical ICP torch and discharge as well as some nomenclature are presented in Figure 1. The torch described is the standard Fassel-type design [20]. The height scale is referenced to the top of the load coil. The plasma is initiated and sustained in the flow of coolant (see Figure 1) argon. The degree of ionization of Argon is less than 1%. The bulk of the

energy applied to the plasma is dissipated by heating the coolant [21]. The next largest part is dissipated within the load coil and some is used to heat the aerosol carrier gas. Heating of the gases is accomplished by collisions with electrons which, by virtue of their mass, receive energy preferentially from the RF field.

Once a given volume of plasma flows out of the coil region, the electrons within it no longer feel the influence of the RF field and the plasma begins to recombine. The recombination process is slow as shown by electron density measurements [22-24]; the electron density remains high well above the plasma. An interesting observation regarding the electron density ( $n_e$ ) is that if the carrier flowrate is not too high, the  $n_e$  in the central channel is comparable to the value in the annular plasma ( $3 \times 10^{15} \text{ cm}^{-3}$  on average). This is presumed to be due to ambipolar diffusion [25], the (inward) diffusion of electron/ion pairs.

The fact that  $n_e$  is high and reasonably uniform throughout the plasma makes the local thermal equilibrium (LTE) scheme in the sense defined by Alkemade [26] attractive as a framework with which to model the plasma. Accordingly then, a single local temperature has applicability in all the various equilibrium distribution laws such as the Boltzmann or Saha equations with the

exception that it cannot be used in the Planck law to describe the spectral volume density of radiant energy. Verification of the suitability of the LTE approach is conceptually simple. It entails the measurement of various spatially resolved temperatures (e.g. excitation, ionization, translational) which can be derived from relative emission intensities and linewidths.

Much evidence has been provided by spatial temperature measurement demonstrating that an LTE framework is not appropriate to explain many phenomena observed in the ICP [8,10,11,13,16,27-29]. The LTE model need not be abandoned however. The concept of comparing observed emission intensity ratios or degrees of ionization to those expected from a "hypothetical" LTE plasma [24] derived from electron density measurements has proved very effective for quantifying the extent of deviation from LTE in a given region [23,24].

Deviation from LTE can be assessed not only by ion/atom emission intensity ratios but also by a measurement of the ratio of ground state ion density to ground state atom density (or a quantity proportional to this ratio).

Equation (1) is an LTE formulation for this density ratio, ignoring the lowering of the ionization potential by electric field effects.

$$\frac{n_O^i}{n_O^a} = \frac{4.823 \times 10^{15}}{n_e} \frac{g_O^i}{g_O^a} T^{3/2} \exp(-E_i/kT) \quad (1)$$

where  $n_O^i$ ,  $n_O^a$  = the density of ground state ion and atom levels ( $\text{cm}^{-3}$ )

$n_e$  = electron density ( $\text{cm}^{-3}$ )

$g_O^i$ ,  $g_O^a$  = the statistical weights of the ground state ion and atom levels

$E_i$  = ionization energy in ev

$k$  =  $8.6 \times 10^{-5}$  ev/K

$T$  = temperature (K)

Measurement of  $n_e$  and calculation of  $T$  as in references [16,23,24,27,30,31] and as outlined in Appendix A would allow an LTE value for  $n_O^i/n_O^a$  to be calculated, and this could be compared to the observed value. It would be interesting to see if deviations revealed by this method exhibit the same trends as those found by emission studies. Also, using measured values of  $n_O^i$ ,  $n_O^a$  and  $n_e$ , an effective ionization temperature could be calculated [16].

If the population densities of ground state atom and ion levels as well as densities of the lowest lying excited atomic and ionic levels are measured, the degree of ionization could be estimated without requiring that the analyte be close to LTE as in [24].

Measurement of both ground state and excited state

level densities will also be necessary as the kinetic approach to ICP modelling gains acceptance. This approach is outlined in references [26] and [32] and has been applied to the ICP in several instances [33-35] although its use is not yet widespread.

Overall, it has been shown that the study of ground state analyte species in the ICP is useful both in a practical sense and also from the standpoint of improving our fundamental understanding of the ICP. The next section discusses methods available for studying ground states and reviews work which has been done in this area.

#### B. Atomic Absorption/Fluorescence Overview

Ground state species, both atoms and ions, may in general be probed by either absorption or fluorescence. For indepth discussions of the theory of atomic absorption and fluorescence, including calculation of absolute densities from absorbance and fluorescence measurements, see references [26,36,37].

These processes are schematically illustrated in Figure 4(a) and (b). The solid arrows denote transition between electronic energy levels and the "squiggles" represent photons.

Absorption is self-explanatory. Fluorescence consists of absorption of a photon followed by spontaneous

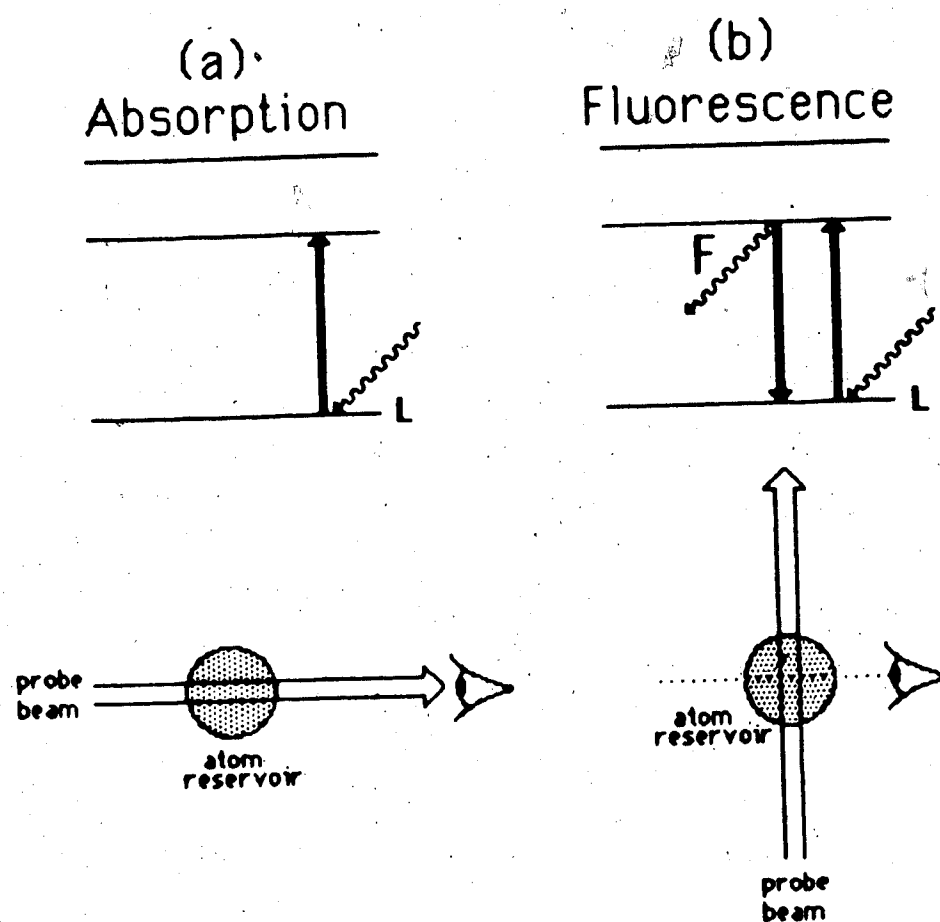


Figure 4. Schematic illustration of: (a) absorption, (b) fluorescence.

emission of a photon (denoted F). In both cases the lower level (denoted L) is not restricted to the ground level but can also be an excited level. For simplicity, only resonance fluorescence, in which the absorbed and emitted photons are of the same frequency, is shown. Many other types of fluorescence are possible [38].

In absorption, the atom reservoir can be thought of as a filter inserted into the path of the probe beam. Fluorescence is generally observed at an angle of  $90^\circ$  to the probe beam although it radiates uniformly from the reservoir in all directions.

Under the condition of high irradiance (generally achievable only with a laser) a phenomenon called saturation occurs in which every absorption is balanced by stimulated emission of a photon (stimulated emission occurs in the same direction and with the same phase as an incident photon). The populations of the upper and lower level of interest become approximately equal.

In absorption this has the effect of "burning a hole" in the atom reservoir; the reservoir appears transparent to the probe beam at the wavelength of interest. Obviously this situation is to be avoided for reliable absorbance measurements. However, when attempting fluorescence, saturation is a desirable state of affairs for several reasons. For example, fluctuations in laser



power will not affect fluorescence intensity if they are not too large. The dependence of saturation on various experimental characteristics such as laser pulse width, pulse power and the characteristics of the level system under consideration have been discussed in detail in references [37] and [39].

At this point, a process characteristic to fluorescence known as quenching should be discussed. Quenching of fluorescence occurs when some non-radiative process, e.g. collisional excitation or de-excitation, is fast enough to compete with radiative depopulation of the upper level of the transition. This results in a reduction of fluorescence from that level and an increase in fluorescence from nearby levels (thermally assisted fluorescence).

Several possible quenching schemes are illustrated in Figure 5. Broken arrows indicate transitions induced by collisions and thermally assisted fluorescence photons are marked by  $F_{Th}$ . Note that under saturated or near-saturated conditions radiative processes become so fast that the effect of collisions is negligible in some cases.

The extent of quenching can be quantified by the quantum efficiency which, for a given excited level, is the ratio of the radiative depopulation rate to the total rate of depopulation (both collisional and radiative

### Thermally Assisted Fluorescence

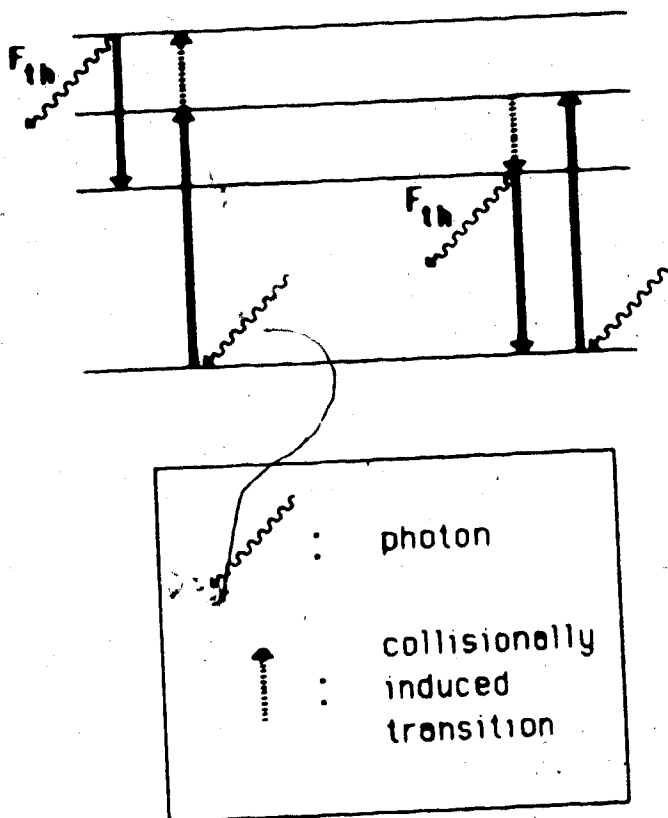


Figure 5. Schematic illustration of thermally assisted fluorescence.

processes). The quantum efficiency can be assessed by studying the fluorescence lifetime, i.e. the decay of fluorescence following a temporally narrow excitation pulse [40].

Finally, a point must be made regarding spatially resolved absorbance or fluorescence measurements. Absorbance, as generally measured, is a line of sight average, and radially resolved absorbances must be derived by Abel inversion [41]. However, the spatial resolution of a fluorescence measurement is determined by the overlap, in the atom reservoir, of the probe beam and the cone of acceptance of the measurement optics [42]. Fluorescence, then, has an advantage over absorption in that spatially resolved measurements can be obtained without Abel inversion [43]. This allows asymmetrical profiles to be accurately mapped, as well as reducing the computational overhead of the measurement. Both techniques have been used to study ground state species in the ICP, and a review of this work follows.

### C. Atomic Absorption Literature Review

Almost 20 years ago, Veillon and Margoshes [44] evaluated an elliptical plasma (one having no central channel) for its possible use as an atom reservoir for atomic absorption. This type of plasma was quickly

supplanted by the toroidal plasma in use today, hence their study is of limited relevance.

In reference [27] Kornblum and DeGalan reported the measurement of excitation temperatures by the so-called emission-absorption method and also calculated ground state calcium atom densities from Abel inverted absorbance measurements. They employed a standard toroidal plasma and made measurements at two aerosol carrier flowrates. However, the lower of the two flowrates was still comparatively higher than that commonly used today.

The same authors [19] also studied the effect of cesium and phosphate on radial density profiles of Ca and Mg atoms and ions, employing the higher of the two carrier flowrates also used in reference [27]. The fact that the approximate degree of ionization of Ca at 15 mm ALC was less than 50% is evidence of the abnormality of their plasma.

Magyar and Aeschbach [45] investigated the possible use of the ICP for analytical atomic absorption measurements and also looked at the effect of power on Cd and Cr atom absorbance. They concluded that the ICP afforded poorer sensitivity and detection limits than the flame. Blades [18] measured Mg atom absorbance in an effort to detect possible ionization equilibrium shifts following the addition of an easily ionizable element

(EIE). (Both these last two examples were not spatial studies.) Rybarczyk et al. [15] measured radial emission and absorbance profiles for several elements (Ca, Mg), in each case doing so for both ion and atom. The plasma was operated at 1.25 kW and 1.1 lpm carrier flow. Besides comparing emission and absorbance profiles they also studied the effect of sample aerosol desolvation and addition of EIE's. However, the zone they studied (0 to 15 mm ALC) is not an analytically useful region of the ICP for emission spectroscopy.

Radial ground state calcium ion and atom absorbance profiles at heights of 7.5, 15 and 25 mm ALC have been reported by Nojiri et al. [16]. They too looked at the effect of an EIE on these profiles. Radial density profiles for ground state Ca atom and ion at a height of 15 mm ALC were also shown and these were used in conjunction with measured  $n_e$  values to calculate effective Ca ionization temperatures.

Details of a technique called saturated absorption spectroscopy have recently been reported by Walters [42]. The relative concentration of ground state species in a small volume can be determined without Abel inversion. Spatial resolution results from the intersection of the probe beam and a modulated saturating beam. They obtained sets of radial ground state Sr atoms

at observation heights ranging from 25 to 90 mm in plasmas optimized for analytical atomic fluorescence (extended torch, low power and high carrier flowrate). Ground state Ba ion profiles at 4 different heights (7, 15, 25 and 40 mm ALC) in a standard 1.25 kW plasma were also shown.

#### D. Atomic Fluorescence Literature Review

The ICP has been more widely used as an atomizer for analytical atomic fluorescence than for atomic absorption. A commercial ICP-AFS system is marketed by the Baird corporation. Papers have appeared on the use of nitrogen [17] and excimer [46] pumped tunable dye lasers and a second ICP [47] as sources for analytical atomic fluorescence. Ionic fluorescence is also included in the general technique of atomic fluorescence.

ICP-LEAFS (Laser Excited Atomic Fluorescence Spectroscopy) compares unfavorably with ICP-OES (OES: optical emission spectroscopy) in that it is a single element technique, although detection limits are comparable [46].

Some characterization of the ICP has been done using LEAFS. Vertical fluorescence profiles of ground state Ca atom and ion at two flowrates in a 1 kW plasma have been published [17]. Radial ground state Ba ion fluorescence profiles have also appeared [43]. In this latter,

profiles were taken as power was varied at a single observation height, and for a single power, profiles at 3 observation heights were taken.

Finally, radial absolute density profiles of ground state calcium atom at various heights for a single (unstated) power appear in reference [33]. These were used to test a kinetic model of Ca ion emission behavior.

From the above review, it is seen that spatial studies of analyte ground state species have not been overlooked. These studies, however, were done at a single power setting with one exception [43] which was not extensive in spatial terms. Several of the studies have limited applicability to analytical optical emission spectroscopy either because the plasma was probed outside the normal observation region for OES [15,42] or the plasma was run with unusual operating conditions [19,27].

The effect of a variation in flowrate over more or less normal values has only been looked at once [17] and here study was restricted to the central channel. In short then, no systematic spatial mapping of ground state analyte ions and atoms has been done for a variety of operating conditions in one ICP. (The difficulty of piecing together sets of data from various laboratories is well recognized [48].) As well, analyte ground state density measurements have not figured prominently in the

overall attempt to rationalize analyte behavior on the basis of a theoretical model.

Thus it was decided to develop an experimental system for both the acquisition of comprehensive spatial maps of ground state analyte species and ultimately, the measurement of their densities. The construction of both hollow cathode lamp and pulsed dye laser based systems for pursuing these ground state studies in the ICP is detailed in this thesis. Experimental results obtained with both systems are presented, discussed in detail, and compared to the results of some of the studies discussed in the literature review.



## CHAPTER 2

### ATOMIC ABSORPTION STUDY

#### A. Introduction

Results of an attempt to develop an experimental system for characterization of analyte ground state atom and ion species in the ICP via hollow cathode lamp based atomic and ionic absorption are presented and discussed in this chapter.

Before attempting an atomic absorption experiment decisions must be made regarding the type of source and the optical configuration in which it will be used. Choices for a source include the hollow cathode lamp, a laser, a continuum source (e.g. Xe lamp) a line source such as an ICP.

Utilization of the plasma as a source gave little success when attempted by Seto [49]. Preliminary experiments indicated that a continuum source gave poor sensitivity. Since a laser was not available at the time, hollow cathode lamps became the only viable option.

In reference [27] Kornblum mentioned that, based on unpublished work, a hollow cathode lamp pulsed at high current was an effective source for ICP-AAS, when combined

with a boxcar integrator. Cordos and Malmstadt [50,51] successfully operated standard commercial hollow cathode lamps in the so-called "intermittent high current mode" for atomic fluorescence spectroscopy in flames. It was decided to implement their approach for pulsing the hollow cathode lamps, utilizing boxcar integration-type signal processing as suggested by Kornblum.

It then remained to choose the optical configuration. The configuration of choice for flame AA has consisted of imaging the source onto the flame, then imaging both source and flame onto the monochromator entrance slit. The implementation of this scheme utilizing an ICP instead of a flame is illustrated in Figure 6. A second approach would be to probe the flame with a collimated beam of light, in which case neither the source nor flame (or plasma) would be imaged onto the entrance slit.

However, since emission, particularly ion emission, is much stronger in the ICP, a basic difficulty occurs in that excessive noise can be introduced if the ICP is imaged onto the entrance slit of a monochromator, even with a lock-in amplifier. This noise is due to random fluctuations in emission intensity having the same frequency as that of the chopper (typically <500 Hz). Particularly strong non-random emission noise components

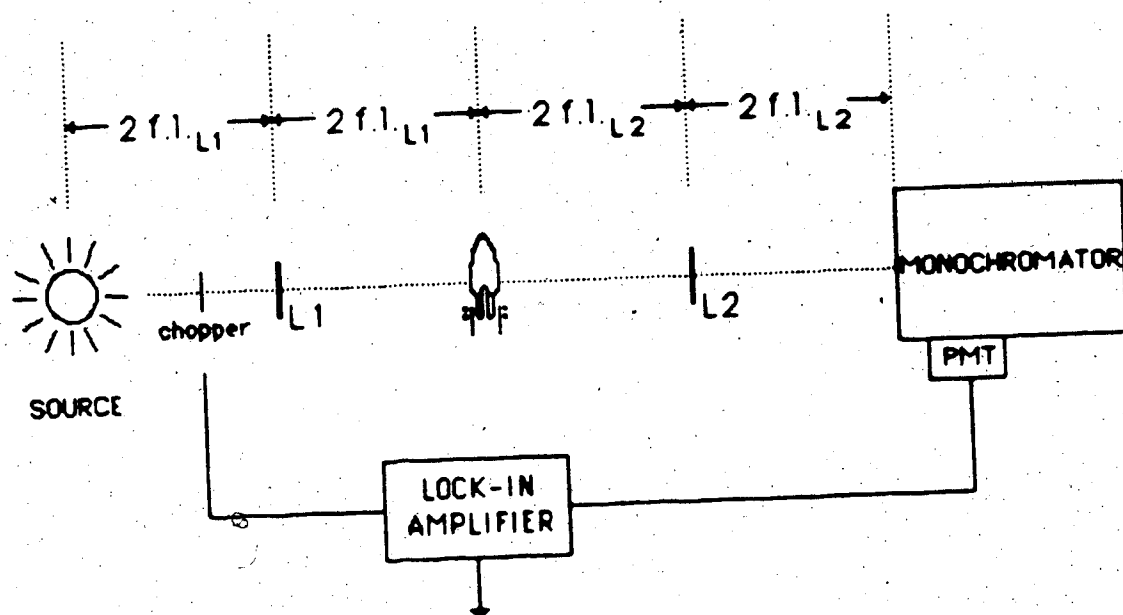


Figure 6. ICP in typical flame A.A. optical configuration.

of frequencies ranging from 200 to 400 Hz are also present in the ICP due to its rotation [52].

Indeed, utilizing the configuration seen in Figure 6, Kornblum [19,27] was able to measure Ca ion and atom absorbance in an ICP only when it was operated with high carrier flowrate. Emission is drastically reduced under this condition. To avoid intense emission, the ion and atom absorbance studies of Rybarczyk et al. [15] were restricted to the region of the plasma close to the load coil although the plasma was operated under normal conditions. This is not the analytically useful region of the ICP. Nojiri et al. [16] reported Ca ion and atom absorbance measurements in the analytical observation zone of a plasma running with normal operating conditions. However, instead of a hollow cathode lamp, another ICP was used as the source for ion absorbance measurements. Again, this was necessary to overcome the strong emission from the "cell" plasma.

In light of the above observations, the second optical configuration mentioned, in conjunction with pulsed hollow cathode lamps, was selected for this work. This approach represented a complete departure from established methods.

In the following sections, the details of construction and operation of the system are presented.

To demonstrate its capabilities, some absorbance measurements obtained for a plasma operated over a wide range of powers and aerosol carrier flowrates will be shown. Discussion of these results however, will be deferred until Chapter 4.

## B. Experimental

### B.1. Optical Configuration

The system employed for this work is illustrated in Figure 7. Collimated light from a hollow cathode lamp is allowed to pass through a circular aperture, the plasma, and another aperture, before being focussed on the entrance slit of the monochromator.

Since the plasma is not imaged onto the entrance slit, considerable discrimination against emission from the plasma is achieved.

In addition, the use of the second aperture, coupled with the long path length from the plasma to lens 2 tends to passively collimate the emission. Thus both absorbance and emission measured with this set-up are values averaged over a cylindrical section of the plasma perpendicular to its long axis, the diameter of the cylinder being 8 mm in this case.

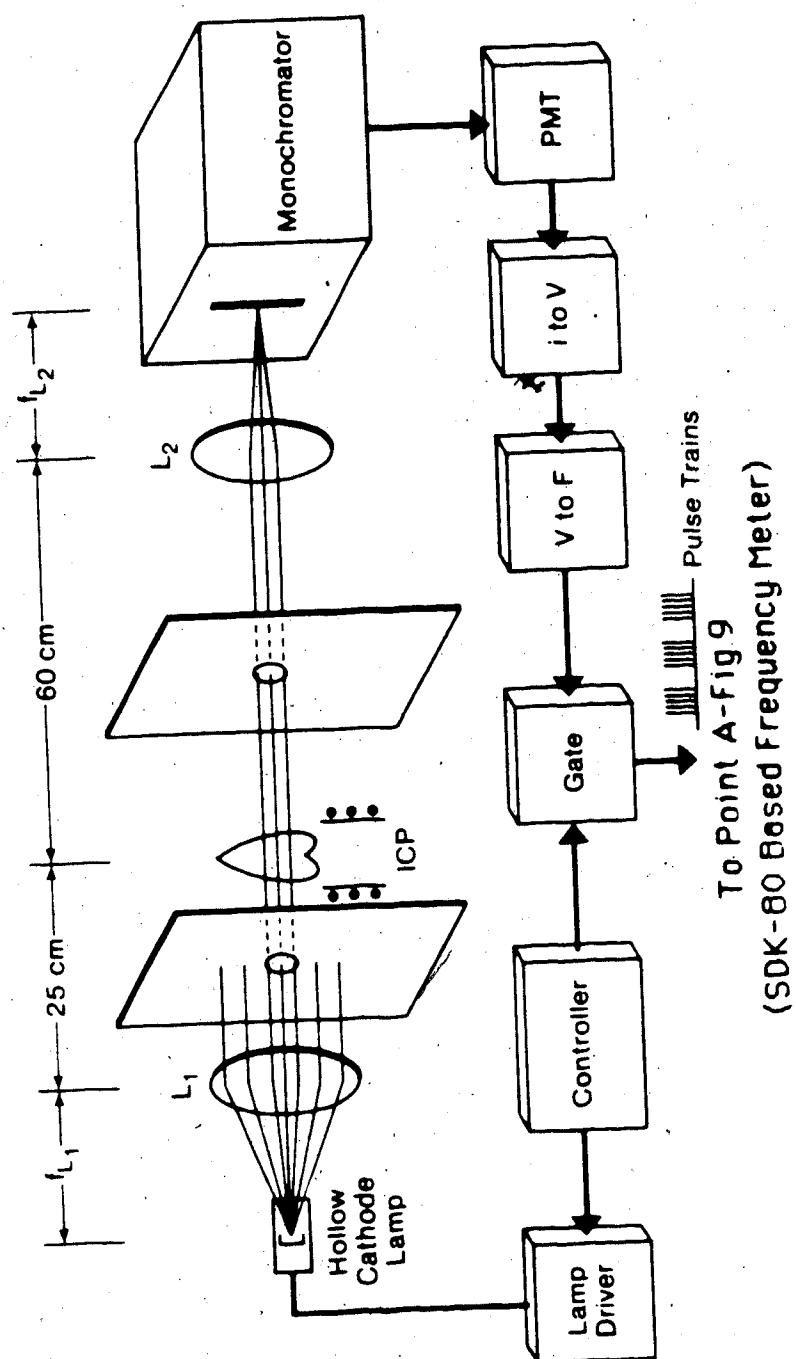


Figure 7. Schematic representation of opto-electronic absorbance measurement system.

## B.2 Construction and Operation of Controller/Lamp Driver

To increase the intensity and improve the stability of the lamps, they were operated in the "high current intermittent mode" [50,51] as mentioned. In this mode, a single measurement cycle consists of a "burst" of twenty, 10 msec wide, lamp pulses spaced 70 msec apart, followed by a wait of 10 to 20 seconds before the next burst (Figure 8).

A controller circuit generates the appropriate sequence of TTL pulses which are fed to a lamp driver (Modified Heath EU-703-70 Hollow Cathode Power Supply). The driver outputs current pulses (variable from 15 ma to 240 ma) having the same phase, frequency and width as the TTL pulses. Details of the operation of the driver can be found in reference [50].

As diagrammed in Figure 7, current pulses from the photomultiplier tube are converted to voltage pulses by a current follower. Any given voltage pulse is converted to a voltage pulse train whose frequency is proportional to the intensity of the HCL source plus any plasma emission. These pulse trains are gated through to a microprocessor controlled frequency meter [53] which counts the pulses and gives the total from 20 pulse trains.

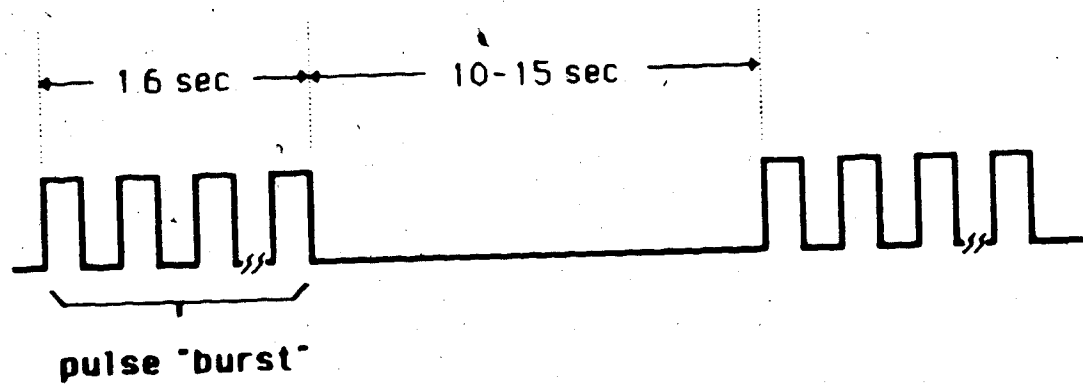


Figure 8. Timing of lamp pulses in "intermittent mode".



In Figure 9 it can be seen that pulses from a free-running 12.5 Hz square wave clock are narrowed by monostable 2 and applied to the clock input of flip flop 2 where, under control of the Enable line, they can be gated through to the driver and the clock input of the modulo-20 counter.

For the following explanation, the waveforms can be seen in Figure 10. When the start count line (from the SDK-80) goes low, mono 1 is triggered and the counter is cleared. On the falling edge of mono 1 (Q output) flip flop 1 toggles, putting the enable line high. The combination of flip flop 2 plus G2 and G3 form an asynchronous waveform gate. If the enable 0→1 transition occurs during a clock pulse, the gate will not open until the next rising edge of the clock. The enable line then remains high until 20 clock pulses have been gated through and counted. The output of the counter is now 10100 which is decoded to a zero by G4, thereby clearing flip flop 1 and disabling the asynchronous waveform gate before the next pulse appears.

Boxcar integration is effected by inserting G5 between the V to F and the frequency meter, and controlling it by the same TTL signal fed to the lamp driver. Thus any emission between lamp pulses is not measured although the total count obtained still reflects

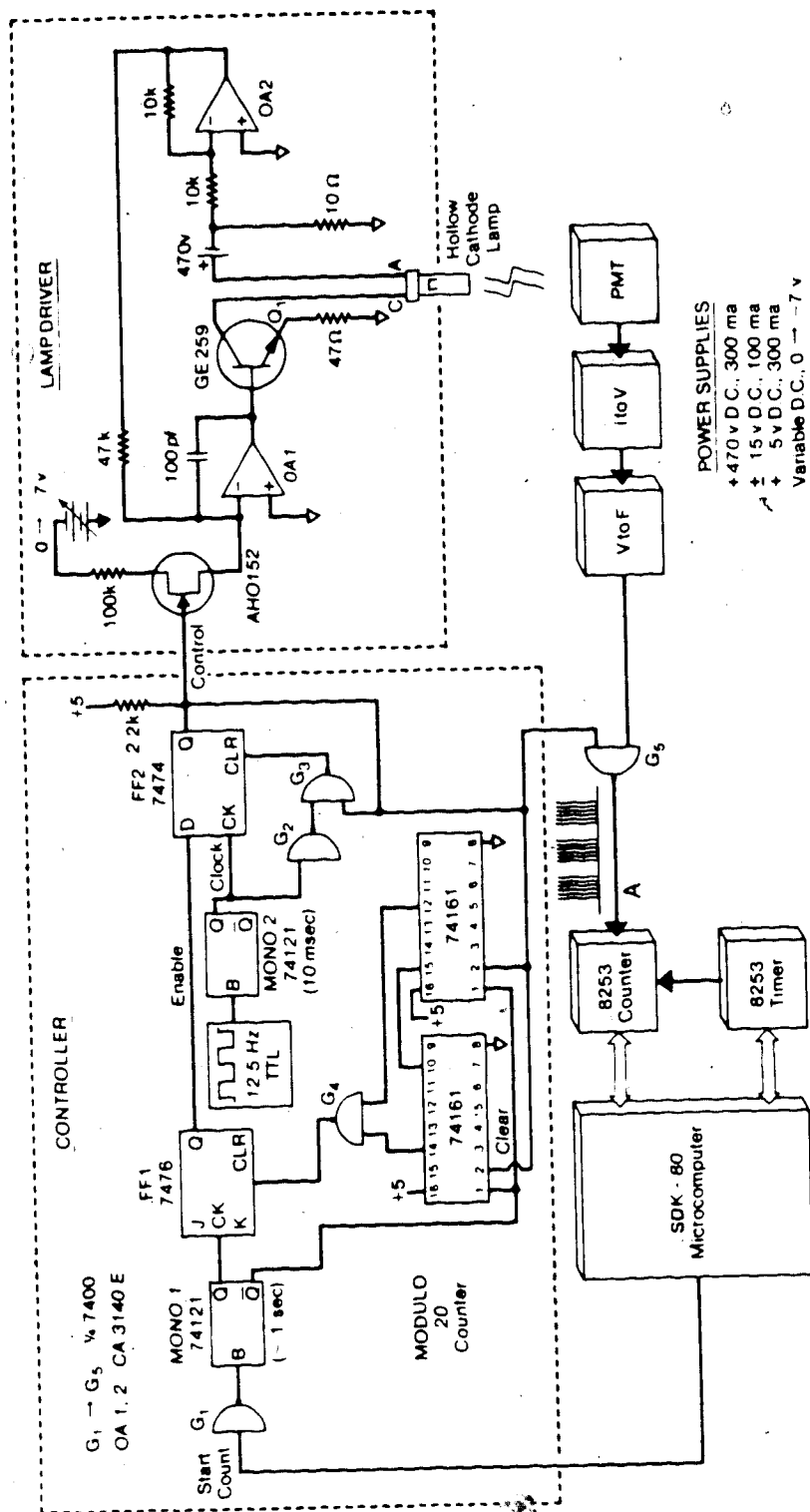


Figure 9. Schematic diagram of controller and driver.

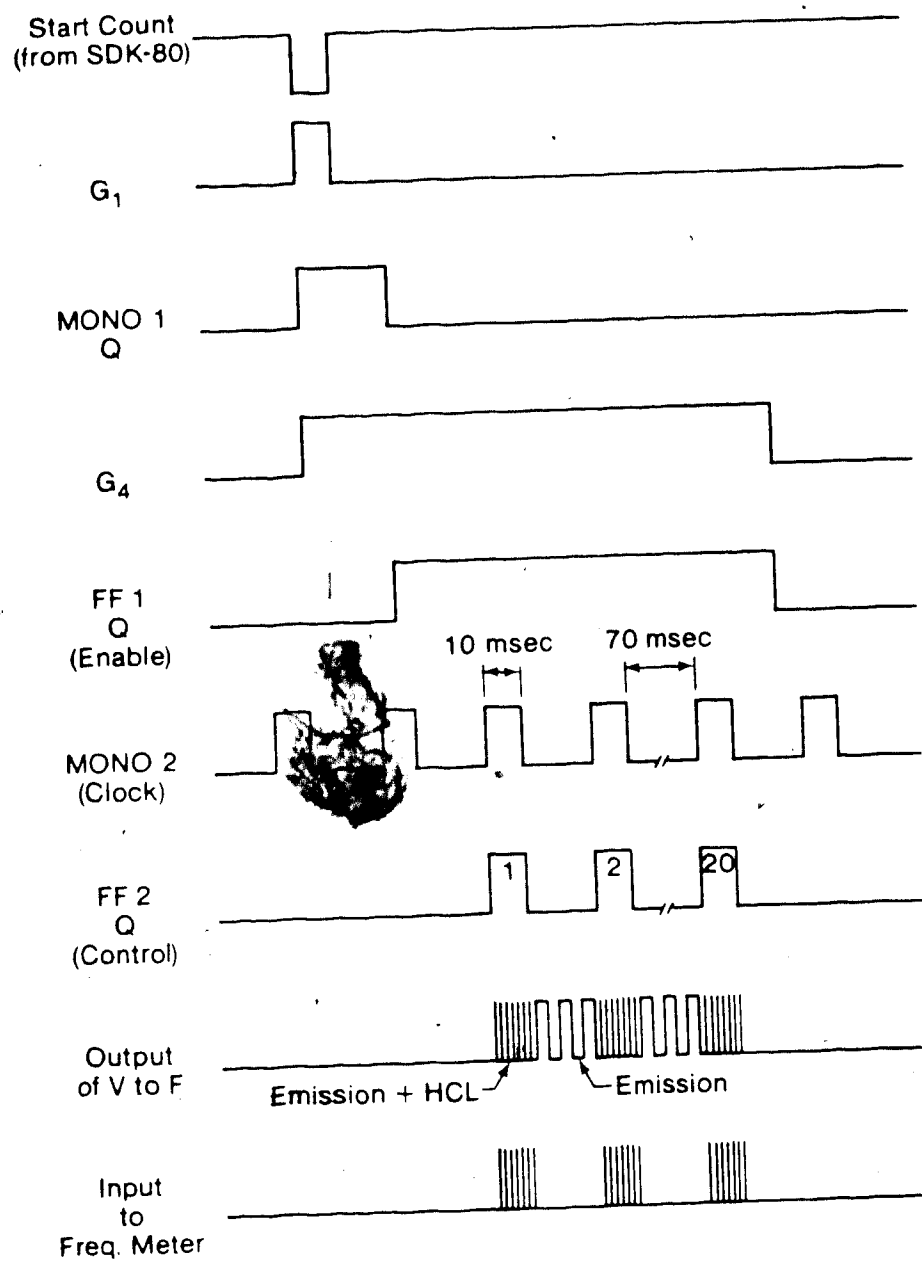


Figure 10. Electronic waveforms relevant to Figure 9.

emission present during the lamp pulses. The count obtained by disconnecting the lamp driver and applying the same sequence of 20 TTL pulses to G5 is a measure of emission only and can be subtracted from the first count to obtain a background subtracted value for  $I_0$  and  $I_T$ . Absorbance is calculated as  $\log_{10}(I_0/I_T)$ .

### B.3 Experimental Outline

A summary of the equipment is presented in Table 1. With the optical system centered at 17 mm ALC, the absorbance and emission of aqueous solutions of Ca and Mg were measured for 20 combinations of power and carrier flowrate as summarized in Table 2. It should be noted here that the torch was positioned so that the tip of the aerosol injector tube was somewhat lower than is normally the case ( $\approx 1$  cm below the bottom of the load coil). This was the configuration which had been employed by the last experimenter to use the system and it was simply left untouched for this work.

A large diameter aperture was chosen because no means of translating the plasma through the probe beam was available at the time these measurements were carried out.

Calcium absorbance was also measured with optics centered at 10 mm and 23 mm ALC. That data will be presented in Chapter 4.

Table 1. Details of experimental set-up.

Hollow Cathode Lamps:	Cathodeon
Power Supply:	Heath EU-703-70 modified as outlined
Pulse Current:	Ca 240 ma Mg 170 ma
Lenses:	L1 Spherical Quartz, 15 cm focal length  L2 Spherical Quartz, 10 cm focal length
Apertures:	8 mm diameter, circular
ICP:	Plasma-Therm 27.12 MHz (operating conditions: see Table 2)
Monochromator:	1 meter, Czerny Turner (minuteman SMP 310), 50 $\mu$ entrance and exit slits
Grating:	1200 lines/mm
Photomultiplier:	1P28
Current Amplifier:	Keithley Model 427
V to F Converter	Analog Devices 537
Frequency Meter:	Microcomputer-based [53]

Table 2. Plasma operating conditions, wavelength of observation and analyte concentrations for absorbance and emission measurements.

Power (kW):	0.5, 0.75, 1.0, 1.5, 2.0
Aerosol Carrier Flow (lpm):	1.0, 1.15, 1.3, 1.45
Auxiliary Gas Flow (lpm):	Only for ignition
Coolant Gas Flow (lpm):	15
Sample uptake (mL/min):	2.5 (1.0 lpm aerosol), 4.0 (1.45 lpm aerosol carrier)

<hr/>		
$\lambda$ (nm)		
<hr/>		
Element	Atom	Ion
<hr/>		
100 ppm Ca	422.7	393.3
300 ppm Mg	285.2	279.5
<hr/>		

#### B.4 Test of the System

Without lighting the plasma, a series of filters having decreasing transmittance were inserted into the beam and their transmittances were measured. A comparison of the measured transmittances to their nominal values is seen in Table 3. These results simply illustrate that basic absorbance measurements can be made with the complete opto-electronic system.

To test for broadband background absorbance, several concentrations of Mg solutions ranging up to 2500 ppm were aspirated into the plasma while an attempt was made to measure the absorbance at wavelengths corresponding to the atom and ion (MgI 2852, MgII 2795 Å). A D<sub>2</sub> hollow cathode lamp and a monochromator bandpass of 2 Å were used for these measurements. No absorbance could be measured indicating that broadband background absorbance is not important. This test could not be done for Ca since the D<sub>2</sub> lamp output was too low at 4000 Å.

At a forward power setting of .75 kW and an aerosol carrier flowrate of 1 lpm, a set of absorbance calibration curves were prepared for each element at high and low pulse currents (high current see Table 1, low current 20-30 ma). The curves are shown in Figures 11 and 12. The relative standard deviation of an absorbance measurement was typically less than 5%.

Table 3. Comparison of measured and nominal transmittances of neutral density filters.

Transmittance (%) <sup>*</sup>	
Nominal	Measured
50	44.6
20	18.3
12	12.1

<sup>\*</sup>422.7 nm



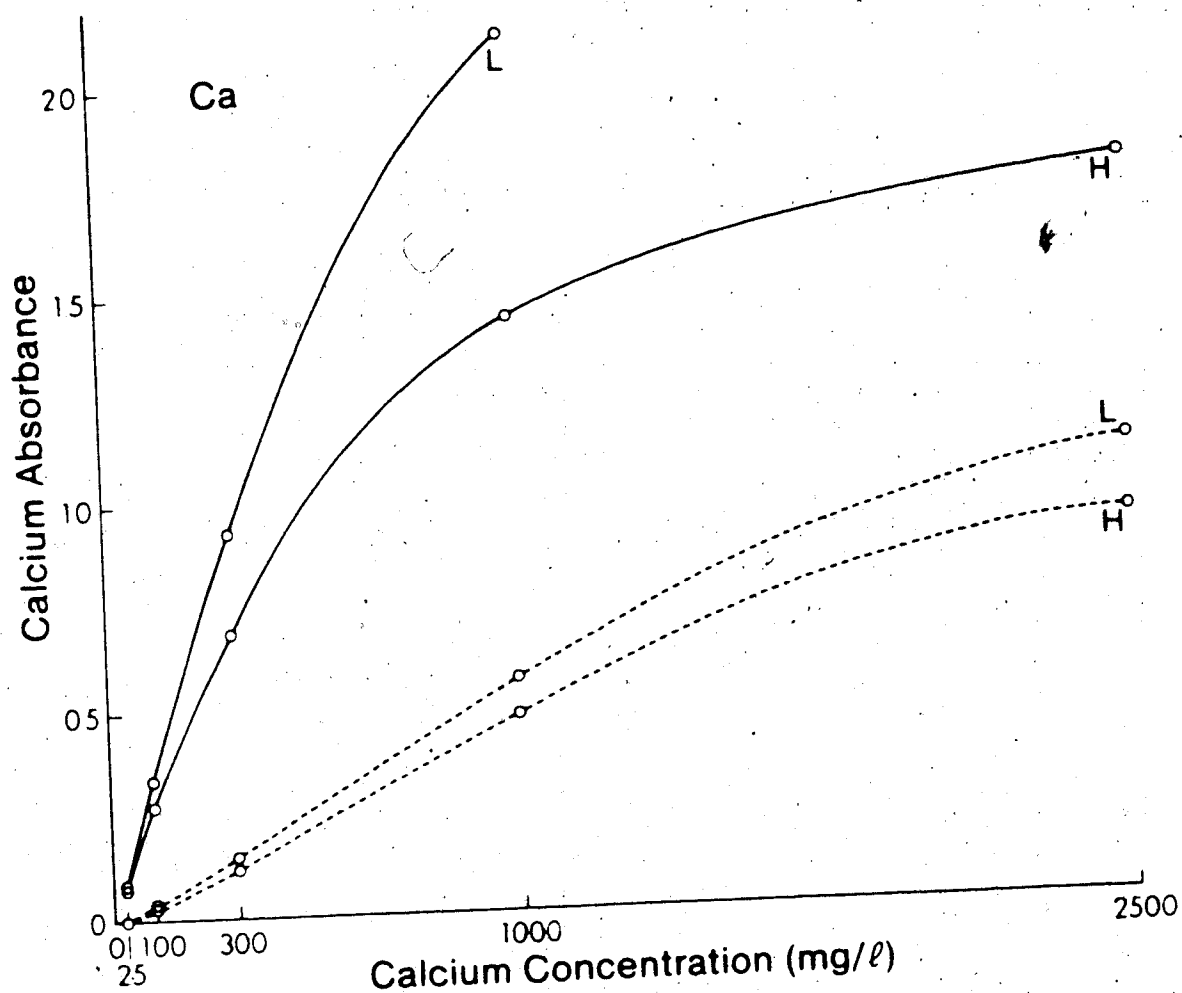


Figure 11. Calcium absorbance working curves. "H" and "L" denote high and low current levels. Solid curves are for the ion; dashed curves are for the atom.

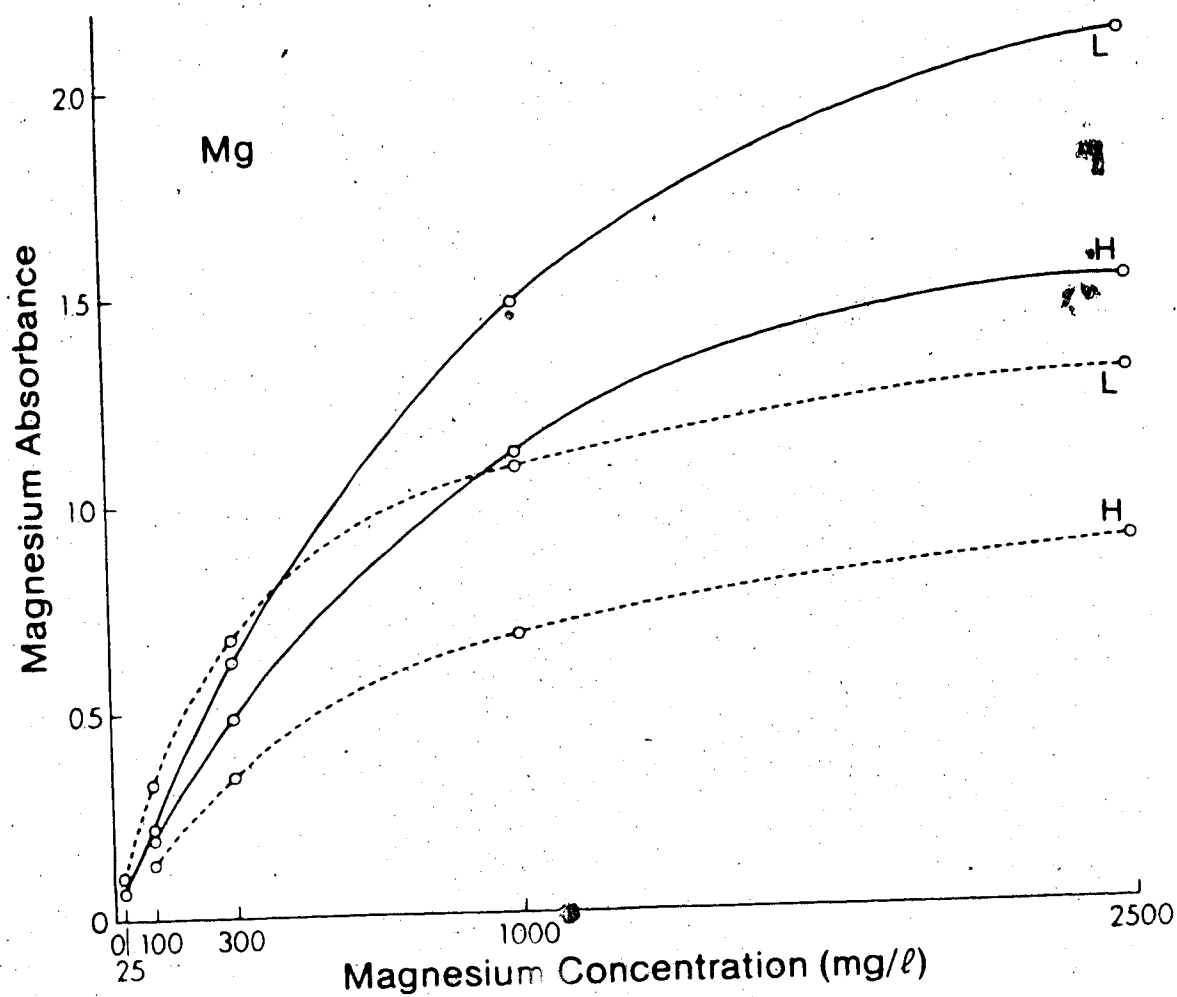


Figure 12. Magnesium absorbance working curves. Legend as for Figure 11.

In general, both the atom and ion curves roll off at high concentration (for example solid line "H" and dashed line "H" in Figure 11).

Some curvature may arise if the beam is not absorbed over its entire cross-section, i.e. if the absorbing region does not fill the beam. However, the majority of the curvature is due to the fact that the source linewidth is not small relative to the linewidth of the absorption profile [54,55], becoming still broader when the lamp is pulsed at high current [56]. Better sensitivity and less roll off are observed at the lower pulse current. Again, in Figure 11 compare solid curve "L" with solid curve "H", and dashed curve "L" with dashed curve "H". These trends are also seen in Figure 12.

However, in cases where emission is strong, one gains by pulsing at higher current and trading a loss of sensitivity for an increase in signal-to-noise ratio. For example, the ion absorbance of 300 ppm Ca at 1.5 kW/1 lpm carrier flow was measured with a S/N of 5 when the lamp was pulsed at 240 ma, but no absorbance above the noise level could be measured when pulsing at 20 ma.

### C. Results and Discussion

Results for Ca and Mg are seen in Figures 13 and 14. The format is explained in the caption for Figure 13. In both Figures 13(a) and 14(a) atom absorbance decreases as power increases whereas ion absorbance (Figures 13(b) and 14(b)) generally peaks at .75 kW. The falloff of Mg ion absorbance as power increases above .75 kW is less noticeable.

From the ion/atom emission intensity ratios at high power (generally  $>10$ ) it is reasonable to assume that the degree of ionization becomes high as power increases. This explains the loss of ground state atoms as power increases (note that if the levels from which 393.3 and 422.7 nm emission originate are equally populated, an ion/atom emission intensity ratio of 1.5 will be seen on the basis of gA values).

An explanation of the decrease in ion absorbance seen as power increases above .75 kW would have to consider increased excitation of ground state ions and formation of doubly charged ions. Recombination does not appear to be significant.

A change in flowrate is also seen to exert a large effect upon ground state atom and ion absorbance. In general, dropping the flowrate (curve 4 to curve 1) causes the solid curves for Figures 13 and 14 to contract back

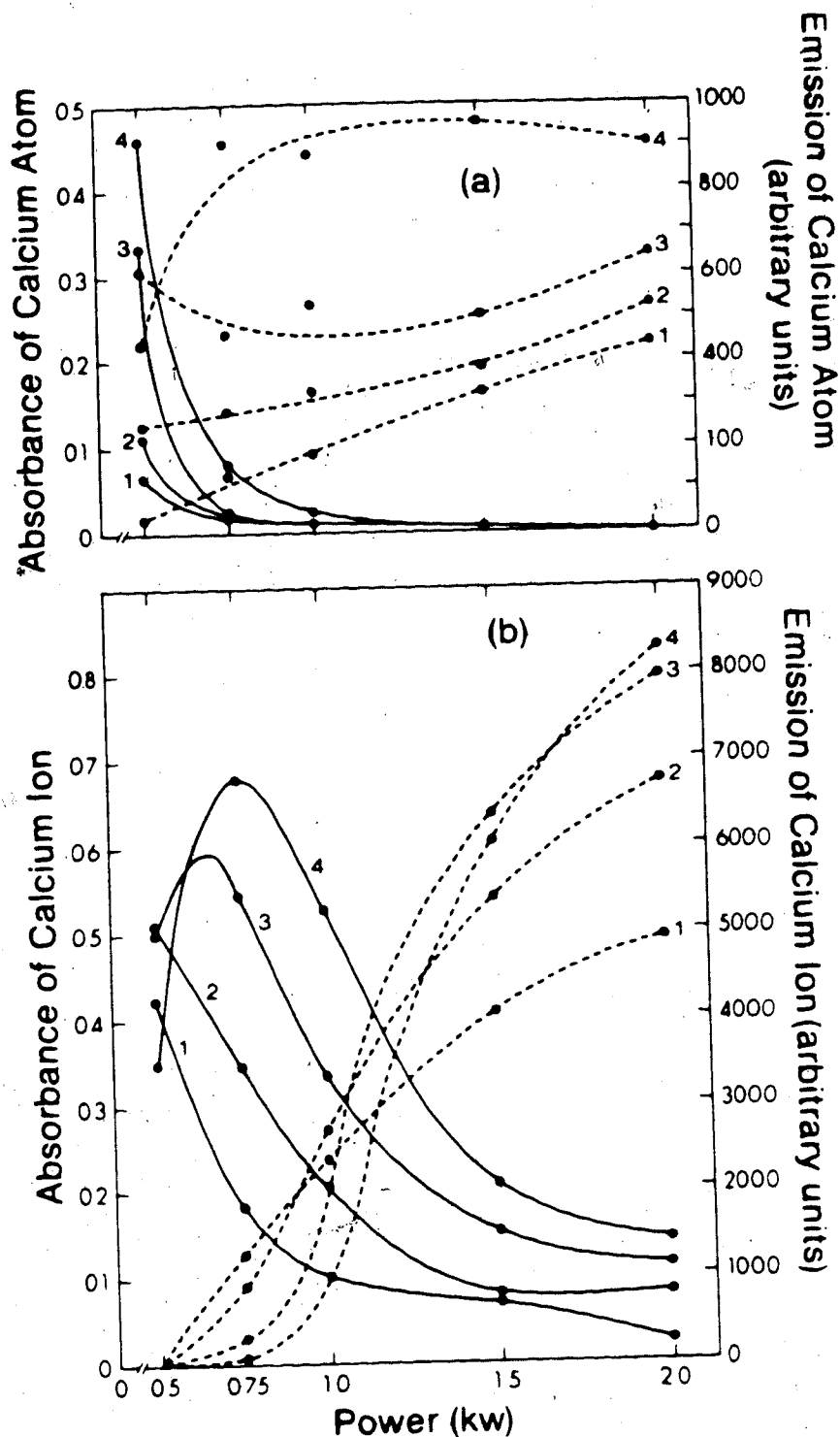


Figure 13. Effect of power and flowrate on calcium atom and ion absorbance and emission. Power increases from left to right in each frame. Absorbance curves are solid and are referred to the axes at the left side of the figure. Emission curves are dashed and are referred to the axes on the right side of the figure. The numbers 1, 2, 3, 4 refer to aerosol carrier flowrates of 1.0, 1.15, 1.3 and 1.45 lpm in any frame. (a) Ca atom, (b) Ca ion.

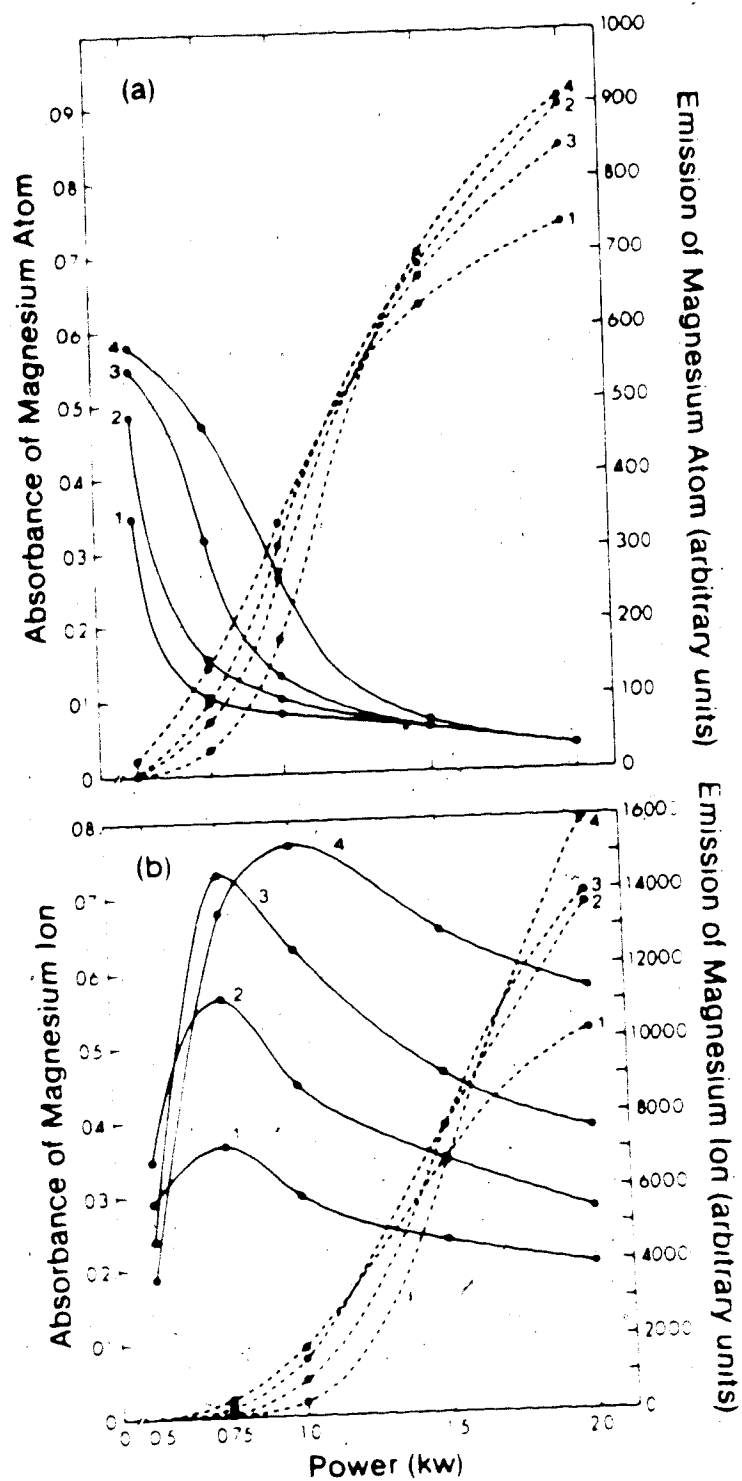


Figure 14. Effect of power and flowrate on magnesium atom and ion absorbance and emission. Details as for Figure 13. (a) Mg atom, (b) Mg ion.

toward the baseline. This is possibly the result of a decrease in overall analyte density and/or a redistribution of analyte amongst its various energy levels due to a change in excitation conditions.

The large increase in  $\text{Ca}^+$  emission intensity as power increases can be modelled with the Boltzmann equation by assuming that the temperature increases from  $\sim 4000$  K at .75 kW to  $\sim 6000$  K at 1.5 kW. (These temperatures are not consistent with those derived from electron densities, as in Appendix A, but are actual measured excitation temperatures.) However, the decrease in Ca ion absorbance seen as power increases is too large to be explained using these same temperatures. (The intensity of emission at 393.3 nm is predicted to increase by a factor of 15 to 20 whereas the ground state ion population is expected to drop by only 10 to 15%.)

Before attaching much significance to the implications of this back-of-the envelope calculation, one has to remember that the absorbance and emission measurements are values averaged over a large spatial region. In light of this, further discussion of the effect of power and flowrate is not warranted until the spatial behavior of the ground state analyte species is known.

#### D. Conclusion

It has been demonstrated that this particular experimental configuration is capable of measuring both atom and ion absorbance over a wide range of operating conditions in the analytically useful region of the ICP.

Radial absorbance profiles could be obtained by Abel inverting lateral absorbance profiles measured using smaller apertures, perhaps in conjunction with boosted output hollow cathode lamps [57] available commercially.

For elements which can be investigated by AFS with a standard dye laser (non frequency doubled) this system does not offer any advantages.

For investigation of other elements such as Mg or Cd it is a cheaper alternative to a system based around a frequency doubled, amplified dye laser or a two plasma configuration.

The results presented in this chapter have not been discussed extensively primarily because of the lack of spatial resolution of the measurements. However basic trends in the response of ground state atoms and ions to changes in plasma operating parameters have been revealed. These results, together with absorbance measurements made at other observation heights in the plasma, will be useful in discussing atomic fluorescence measurements in Chapter 4.



## CHAPTER 3

### AFS EXPERIMENTAL SYSTEM

#### A. Introduction

Following the acquisition of a nitrogen-pumped tunable dye laser it was decided to abandon hollow cathode lamp-based absorbance measurements in favor of attempting photodiode array-based absorbance profiling (analogous to the emission profiling discussed previously).

Toward this end, a one-meter monochromator was modified so that it could be used as a diode array spectrometer. Details of its construction, and operation of the array electronics, can be found in Appendix B.

However, absorbance measurements made with the instrument suffered from poor sensitivity and pulse-to-pulse variation in laser power was also a problem. As a result, absorbance measurements were shelved and characterization of ground state analyte species continued via atomic fluorescence. The experimental set-up used is detailed in the remainder of this chapter.

#### B. System Overview

A schematic diagram of the overall measurement system

is seen in Figure 15. The optical components are mounted on an optical railbed similar to that described by Walters [58]. Details of the equipment can be found in Table 4.

The pulsed dye laser beam (pulse width  $< 1$  ns) is focussed by lens 1, passes through the plasma and into the photodiode array spectrometer mentioned previously. This permits the output of the laser to be centered on the wavelength of interest. A fraction of the beam is diverted to a photodiode and generates a trigger signal.

The optical portion of the detection system consists of a second lens which images the plasma onto the entrance slit of a .35 m monochromator with a magnification of 1.75.

The fluorescence signal after amplification, has a fwhm of  $\approx 10$  ns, (the PMT and amplifier were not optimized for high speed response) hence it is necessary to use a gated integrator detector.

The focussed laser beam diameter and characteristics of the detection optics define a small scattering volume positioned at the intersection of the two optical axes.

Taking the path of least resistance, it was decided to measure profiles by stepping the plasma through this scattering volume, rather than vice versa. To make this procedure as painless as possible, the torch is capable of

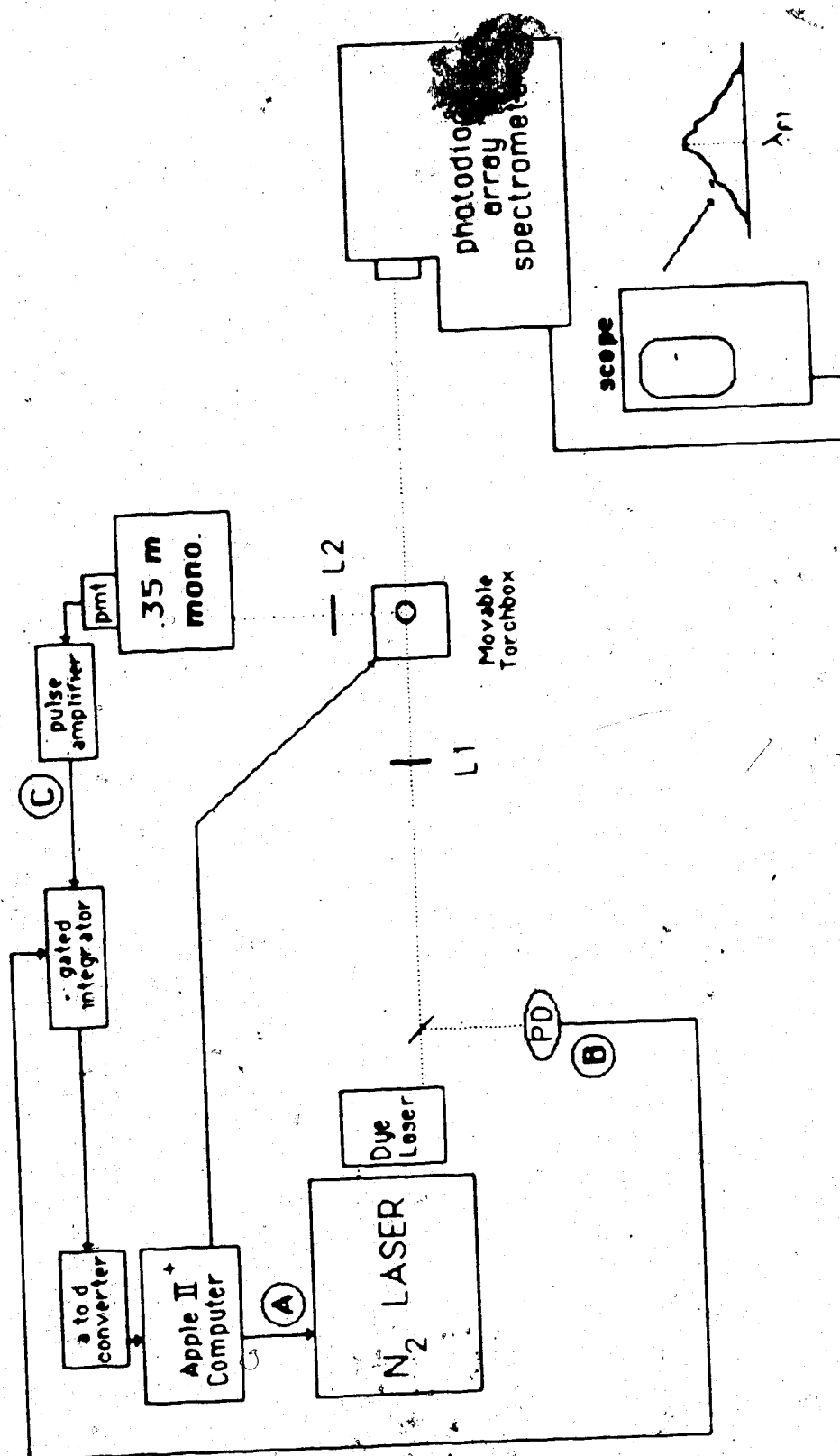


Figure 15. Schematic diagram of atomic fluorescence measurement system.

Table 4. Details of fluorescence experimental system.

Nitrogen Laser:	Photochemical Research Associates Model LN 1000
Tunable Dye Laser:	Photochemical Research Associates Model LN 102
Laser Dyes:	Photochemical Research Associates
Photodiode:	Hewlett-Packard 4220
Lenses:	L1 spherical quartz, 50 cm focal length L2 spherical quartz, 10 cm focal length
Torch:	Standard Fassel Type (Chapter 4) MAK (Chapter 5)
Nebulizer:	Meinhardt, glass concentric
Plasma:	Plasma Therm, 27 MHz
Photodiode Array Spectrometer	Modified 1 meter Czerny Turner (Minuteman SMP 310) Reticon RL 256EC photodiode array
Monochromator:	Heath, .35 m Czerny Turner, stopped by a 3 mm aperture.
Photomultiplier Tube:	RCA 1P28, wired for standard response
Amplifier:	Fluorescence: Hewlett Packard Model 461A, 40 db gain Emission: Keithley Model 427
Gated Integrator:	Stanford Research Systems Model SR-250, 10 ns gate
Analog to Digital Converter:	Interactive Structures model A113
Torch Translation System:	Jack, Oriel #1636 Translator, Oriel #1625 Stepper Motors, Pulsemotor PH42C1, 440 ma/phase Controlling Electronics, Rogers Labs A6T/D, R2D23
Computer:	Apple II+

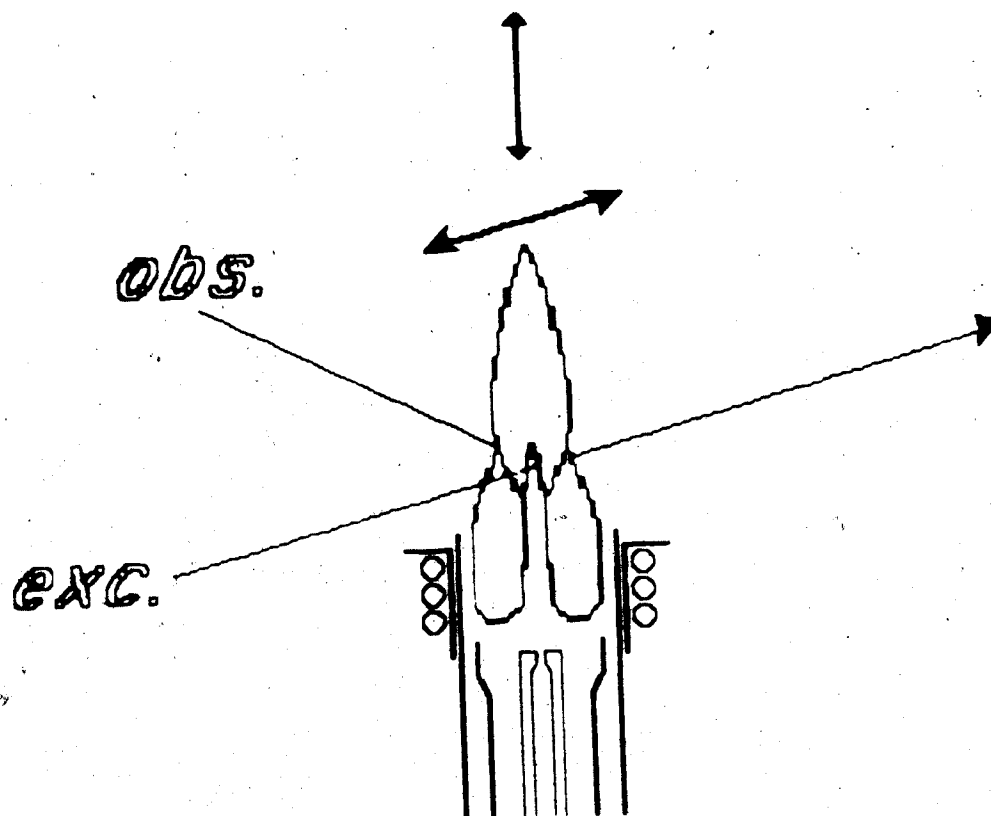
being moved both vertically and horizontally under computer control. The computer, an Apple II+, is responsible for firing the laser, counting pulses, positioning the torch, acquiring the data and outputting it to a printer and plotter.

### C. Optics

To obtain fluorescence profiles, the plasma (in this case) can be translated along the observation axis or the excitation axis (i.e. parallel to the laser beam). Since the mount required to position lens 2 interfered with motion of the torch along the observation axis, profiles were acquired along the excitation axis. This is illustrated in Figure 16; the positioning of the plasma to acquire a 3-point profile for example, is seen at the bottom of the figure.

When profiling along the excitation axis, it is desirable to maintain a uniform probe beam diameter over a distance at least equal to the width of the plasma. This is realized by bringing the laser through the plasma with a long focal length lens. (Note however, that this reduces the power density ( $\text{W/cm}^2$ ) in the focussed beam.) Using such an illumination scheme, other researchers [59] have acquired one-shot fluorescence profiles of a flame with a gated, sensitivity enhanced photodiode array.

The format of Figure 16 is also useful for pointing



### Top View

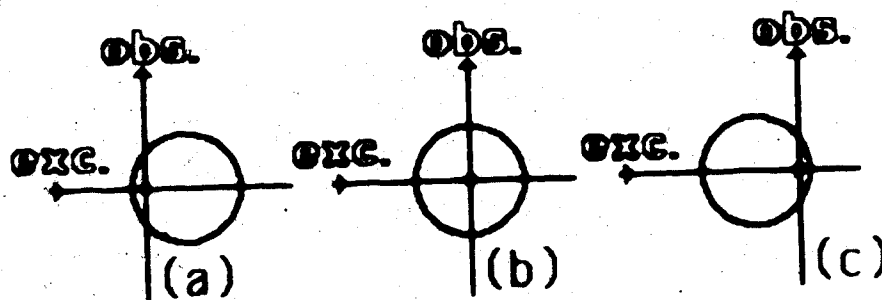


Figure 16. Top: Illustration of axes along which ICP can be translated. Bottom: Acquisition of a 3-point fluorescence profile. The plasma is moving from right to left in frames (a) through (c).

out possible concentration or filtering effects" which include prefiltering (absorption of incoming radiation) and postfiltering (absorption of fluorescence). Referring to Figure 16(a), it is seen that the likelihood of observing either of these effects is small. With reference to frame (b) there is some opportunity for prefiltering, and the path length for postfiltering is maximal. The path length for prefiltering is longest in frame (c), but postfiltering is again minimal. Prefiltering can be avoided by working under saturated conditions where the laser burns a "hole" in the plasma.

As mentioned earlier, the spatial resolution of the measurement is determined by the beam diameter and the collection optics. This is outlined quite well in references [28] and [60]. With a 1000  $\mu$  entrance slit the scattering volume was estimated to be approximately 1 mm<sup>3</sup> and 0.12 mm<sup>3</sup> when a 120  $\mu$  slit was employed. In the case of a 1000  $\mu$  slit, light was collected from a region extending .3 mm on either side of the optical axis (scattering length = .6 mm).

The optics were aligned as follows: The laser and lens 1 were positioned so that the beam waist was 12 inches above the top of the railbed. The .35 m monochromator was then set so that the center of its entrance slit too was 12 inches above the top of the

railbed. It was backlit with a HeNe laser and the .35 m monochromator was then shifted until the HeNe laser intersected the desired region of the dye beam. The tip of an optic fibre was positioned at this intersection point with its face pointing toward the .35 m monochromator. The other end of the fibre was made to intercept the dye laser which was centered on the purple 393.3 nm transition of calcium ion. Lens 2 was then situated so that the end of the fibre was imaged onto the entrance slit of the .35 m monochromator. (A small purple dot would come into sharp focus when the lens was set properly.) Since the range of wavelengths used in these studies was not large, the lens was not repositioned at any time to compensate for chromatic aberration. Finally, the plasma was positioned so that the dye beam passed through its central channel, and the image of the plasma was centered on the entrance slit of the .35 m monochromator.

The .35 m monochromator was set on the wavelength of interest by observing emission from the plasma.

Similarly, a high concentration of the element of interest was aspirated so that the same line appeared on the diode array output which was displayed on an oscilloscope. The scope was adjusted so that the line fell in the center of the graticule. Once the scope had in this sense been



"calibrated", the laser was then adjusted so that the maximum of its spectrum also fell on the center of the graticule. Since the laser output was some 50 Å wide this was not an overly critical procedure.

#### D. Lasers

The lasers were used as received from the manufacturer with the exception that a switch and inverter were installed within the N<sub>2</sub> laser, allowing it to accept both positive and negative going trigger signals.

Some problems with the N<sub>2</sub> laser were experienced after several months of operation. An electrode in the main spark gap had to be rebored and readjusted. Following this, the laser operated quite reliably for the duration of the experiments.

Degradation of the dyes was not found to be a problem. The condition of the dye could be monitored with the photodiode array although an energy meter would be preferable. The dyes used together with the wavelength of interest are listed in Table 5. The numbers in brackets are the suppliers codes.

#### E. Torch Translation System

The commercially built ICP systems used in our laboratories consist of two components: a large power supply and a smaller combination impedance

Table 5. Wavelengths and laser dyes employed for atomic fluorescence.

Species	Wavelength (nm)	Dye <sup>†</sup>
Ca	422.7	BIS-MSB (LN6-2)
Ca <sup>+</sup>	393.3	BBQ (LN3-2)
Ca <sup>++</sup>	373.7	PBD (LN2-2)
CaOH	554.3	C-540 A (LN15-2)
Sr	460.7	C-460 (LN10-2)
Sr <sup>+</sup>	407.8	DPS (LN5-2)
Mo	390.3	BBQ (LN3-2)

<sup>†</sup>Average energy per pulse: 40  $\mu$ J

Supplier: Photochemical Research Associates, 45  
Meg Drive, London, Ontario, Canada,  
N6E 2V2

matching/torchbox unit weighing about 15 kg. The torchbox is firmly attached to the side of the impedance matching unit, so that translation of the plasma torch in that case amounts to translation of the entire assembly (see Figure 17(a)). This is routinely done for spatial work. A milling table [28] for example has been used as a torchbox positioner.

Other researchers have taken a different approach [61], that of separating the torchbox from the impedance matching unit, allowing independent motion of the torchbox, as in Figure 17(b). That approach was adopted for this work.

The load coil, its mounting blocks, and the torch guide were removed from the side of the matching unit and mounted on an L-shaped Plexiglas platform. To shield the torch, a small box was constructed of  $1/4"$   $\times$   $1/4"$  aluminum bars and copper sheeting. The spray chamber was suspended outside this box. Connection back to the matchbox was made via tinned copper braids ( $3/4"$  wide).

In order to get the plasma to light a 50 pf capacitor, which was connected in parallel with the tunable vacuum capacitors, had to be removed from the matching unit. (The 50 pf capacitor actually consisted of two 100 pf, 15 kV capacitors in series.) When this was done, the plasma was actually easier to light than it had been

## Top View

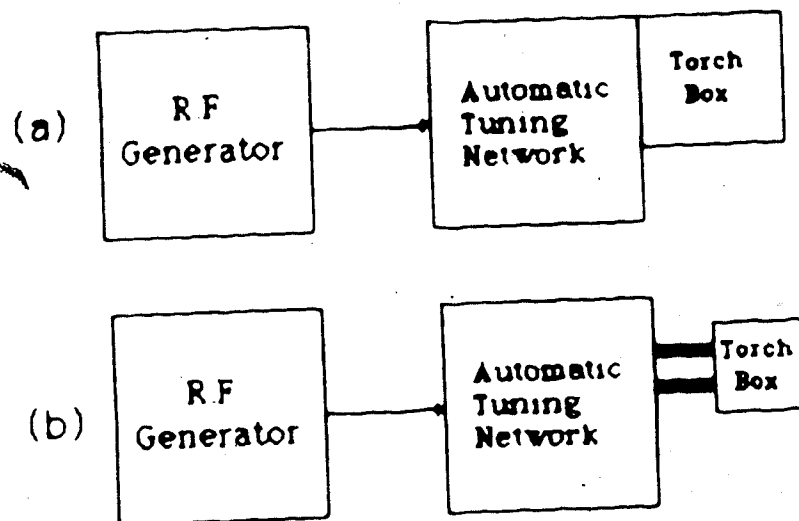


Figure 17. Illustration of modification made to commercial plasma unit (a) unmodified, (b) modified.

previously, the reason being that the three-turn load coil had been taxing the capabilities of the automatic matching network (it was designed for a two-turn load coil).

The platform/torchbox was mounted on a micrometer driven jack/translator combination, the micrometers being geared to small stepper motors. The overall arrangement is depicted in Figure 18 where the stepper motors and gearing have been omitted for simplicity.

The entire assembly sat on a platform slung beneath the rails and was capable of being manually raised or lowered via a 3-point suspension system. This was necessary only during initial set-up of the experiment.

The stepper motors were controlled from the Apple II+ in BASIC using the Rogers Laboratories commercial package including machine code software, a timer/driver board and a motor driver board housing the power transistors. Two external power supplies were required. Further details of the wiring, and other points can be found in Appendix C.

#### F. Electronics and Measurement Procedure

A more detailed interconnection diagram for the various electronic components is seen in Figure 19. Points A, B and C correspond between Figures 19 and 15. The A113 is a multichannel analog-to-digital converter. The time relationship between the input and trigger signals for the laser and gated integrator are illustrated

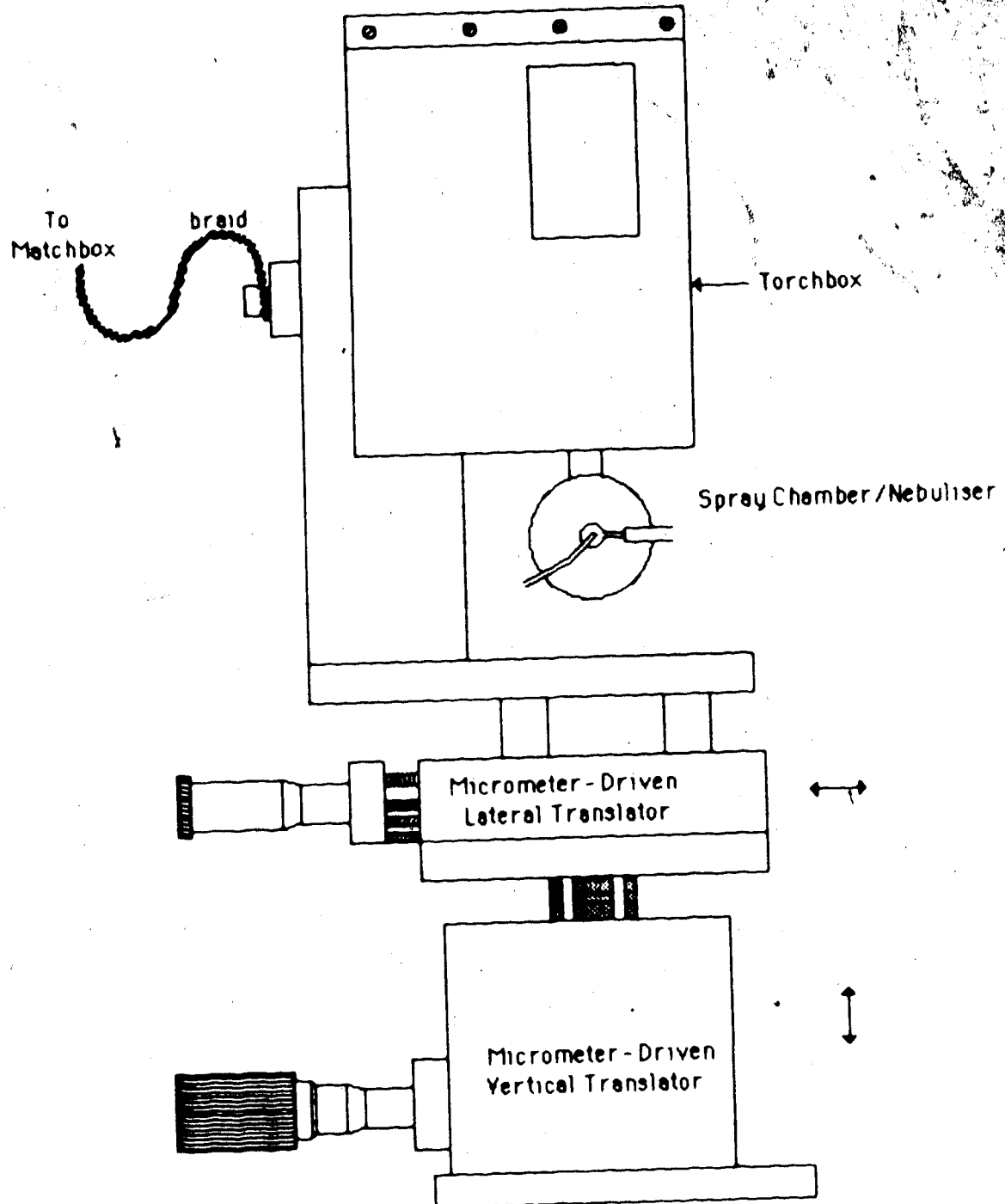


Figure 18. Torchbox and torch translation system

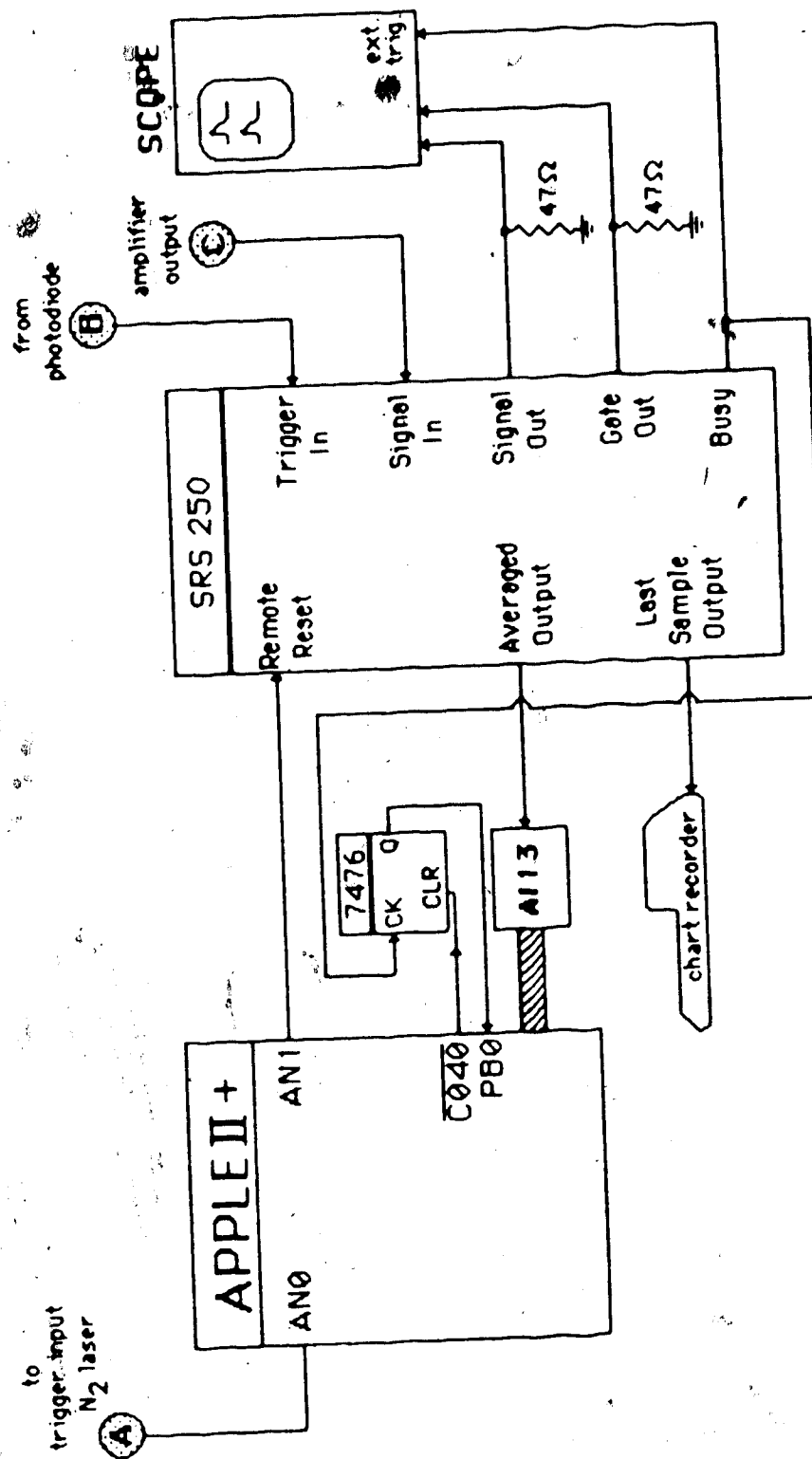


Figure 19. Interconnection of components shown in Figure 15..

in Figure 20. Since lasing jitters by roughly a microsecond from the laser trigger signal, the photodiode provides a reliable trigger for the gated integrator, i.e., the fluorescence signal always arrives at the integrator at a fixed time  $t_d$  after the arrival of the trigger signal from the photodiode (typically 50 ns).

The gated integrator, when it is properly set, waits a time  $t_d$  after it has received a trigger signal, then samples its signal input line. The "last sample" output is proportional to the average value of the input voltage over the time that the sampling window is open, in this case 10 ns.

There are several ways to adjust the gated integrator so that the sampling window and the fluorescence signal coincide. One is to observe both the "signal out" and "gate out" lines on an oscilloscope (triggering from the "Busy" line) and adjust the built-in delay for visual coincidence of the signals. Alternately, the "last sample" output can be displayed on a chart recorder and with the laser pulsing, the delay is slowly increased until the chart recorder output is maximized. Provision is built into the unit to take an exponential moving average of a series of sampling events. This averaged value is available at the "averaged output".

In this work, a "scan" consisted of the issuance of a



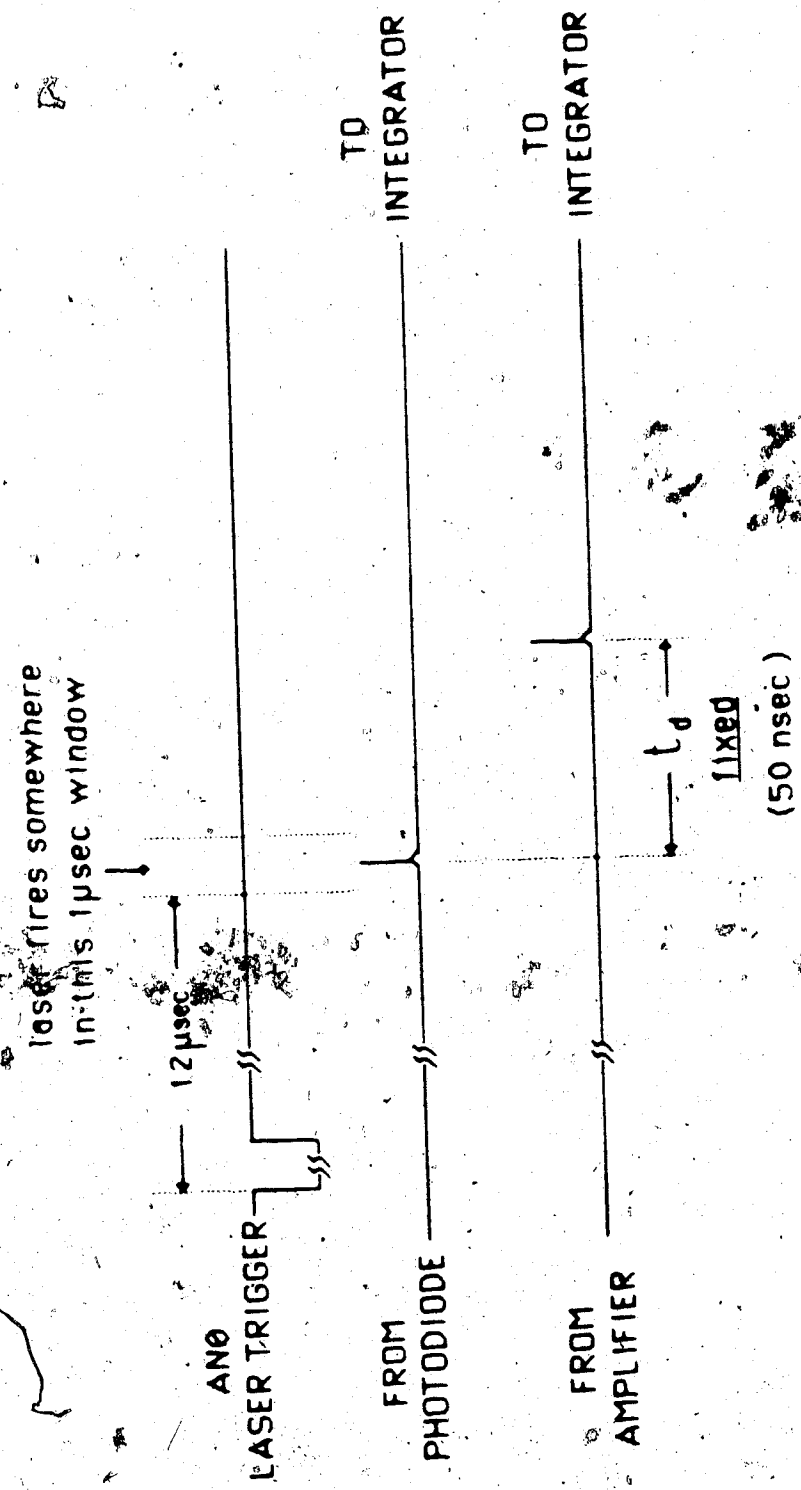


Figure 20. Time relationship of laser trigger signal, photodiode output and amplifier output.

train of 30 laser pulses. Following this, the "averaged output" value was digitized using the A113 and stored. A feedback loop was built in to ensure that 30 dye laser pulses actually occurred. (The  $N_2$  laser would fire weakly on occasion, with insufficient power to make the dye lase. See Appendix 2 for details..

The measurement of fluorescence at a single spatial location consisted typically of two scans of 30 pulses. The results of each scan were averaged. This was sufficient to yield a relative standard deviation of 1% on average. After a complete profile had been acquired it was displayed on the Apple II+ monitor, the results were printed out, and the profile could be plotted if desired.

Lateral emission measurements could also be made with this set-up following a few simple changes. The slit width was reduced and the Hewlett-Packard pulse amplifier was replaced by the Keithley high gain current follower. The gate width was increased to its maximum value of 15  $\mu$ s. The delay setting was unimportant. The "averaged output" was digitized after the integrator had been triggered 100 times. The laser was not triggered.

However, when the system was configured to measure fluorescence, emission did not contribute measurably to the signal. This was tested by blocking the laser and comparing scans aspirating water only and aspirating an

analyte solution.

In the following chapters, fluorescence and/or emission maps of the plasma for a variety of operating conditions will be presented. For a given set of operating conditions, the plasma was mapped by measuring fluorescence or emission of each of the 75 locations shown in Figure 21. A map, then, is comprised of a stack of 5 radial fluorescence profiles (or 5 lateral emission profiles as the case may be) taken at heights of 9, 13, 19, 25 and 31 mm ALC. A profile consists of measurements at 15 points spaced 1 mm apart.

At 9 mm ALC, a component of the measured signal was due to scattering from both the torch collar and from microscopic water droplets [15, 43] (central channel only). The raw profiles at 9 mm ALC were corrected for scattering and DC offset via point-by-point subtraction of a complete background profile ( $H_2O$  only). At other heights the average of background measurements spaced several mm apart (horizontally) was subtracted from the raw profiles to remove DC offset.

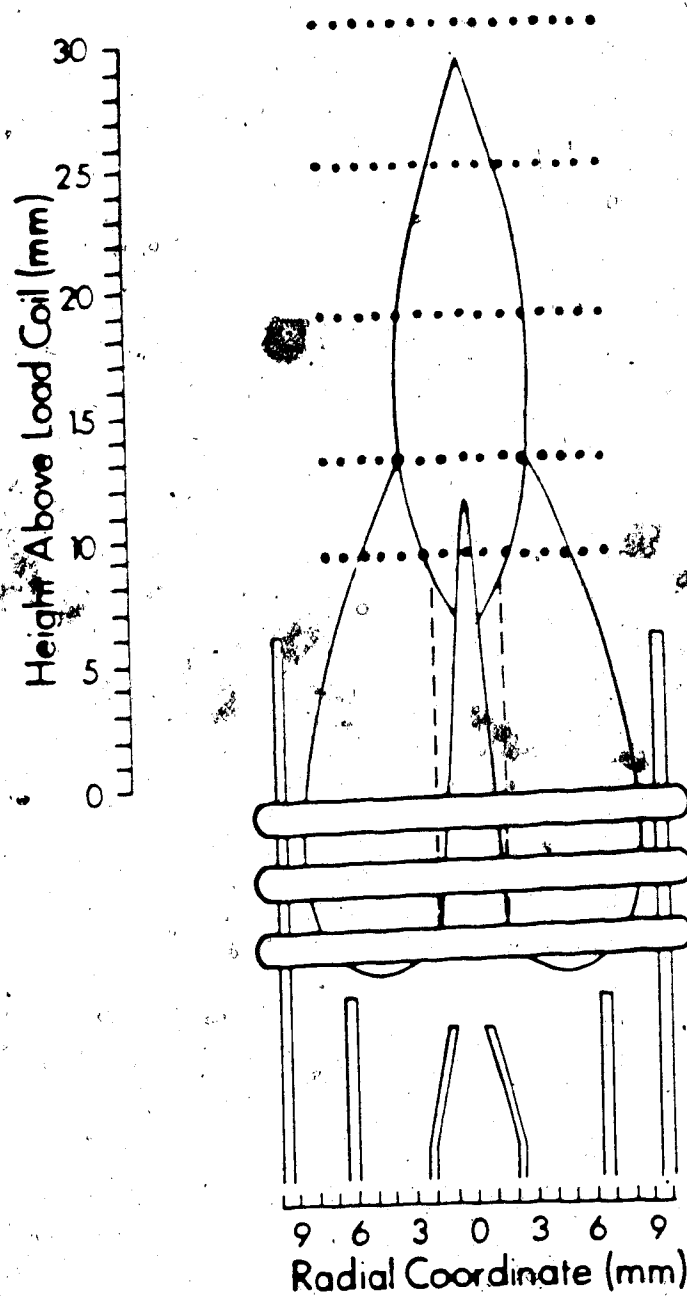


Figure 21. Spatial locations in plasma at which fluorescence and/or emission measurements were made.

## CHAPTER, 4

### FLUORESCENCE RESULTS: FASSEL TORCH

#### A. Introduction

This chapter details an investigation of the effect of power and aerosol carrier flowrate (flowrate) on fluorescence maps of ground state analyte atoms and ions.

The basic study, a power study, consisted of the acquisition of fluorescence maps at powers of .5, .75, 1, 1.25 and 1.5 kw (map being a stack of 5 radial profiles as outlined in Chapter 3). Flowrate was held constant. Each power study then, entailed the acquisition of 25 radial fluorescence profiles.

Power studies were done for ground state Ca atom and ion at flowrates of .65, .85 and 1 lpm. The same procedure was repeated for ground state Sr atom and ion.

The wavelengths employed can be found in Table 5.

Molecular fluorescence profiles of CaOH were also taken.

Additional work such as the effect of concentration, tests for saturation and emission measurements were curtailed by accidental damaging of the torch.

A summary of experimental conditions is given in Table 6. The torch used in Chapter 2 was also employed here, however the nebulizer was replaced by another of the same type, i.e. Meinhardt glass concentric.

## B. Effect of Power at 1 lpm Flowrate

### B.1 Overview of Ca Ion Fluorescence

The results of a power study for ground state  $\text{Ca}^+$  fluorescence at 1 lpm are presented in Figure 22. Power increases from left to right as indicated at the bottom of the figure. The observation height in mm for a given row is labelled at the left side of the figure and increases from bottom to top. All profiles are on the same scale. If one mentally superimposes a picture of the plasma on any given profile, the probe beam enters from the right.

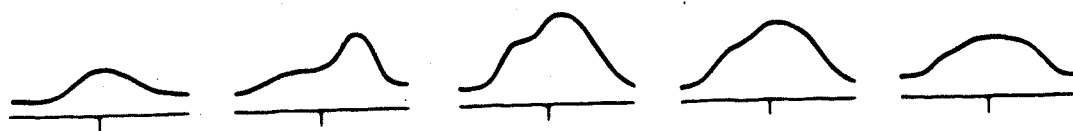
As power is increased, a peaking in either profile area or maximum profile height is seen, regardless of observation height. This can more easily be seen in Figure 23 where fluorescence intensity in the central channel is plotted as a function of power for the 5 observation heights. In this figure, note that low in the plasma a peak appears at .75 kW, shifting to 1 kW higher in the plasma.

Another point to note regarding Figure 22 is that at .5 kW, a broad, uniform column of ions is seen whereas at

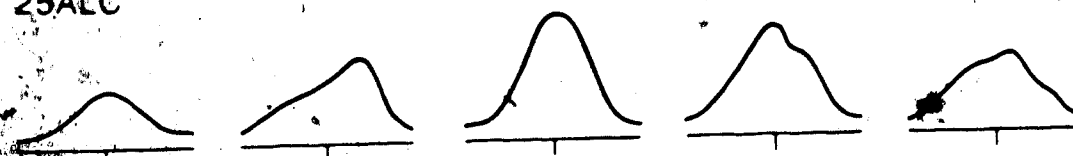
Table 6. Experimental conditions for fluorescence studies.

Power (kW):	.5, .75, 1, 1.25, 1.5
Coolant (lpm):	15
Auxiliary:	(only for ignition)
Aerosol Carrier (lpm):	.65, .85, 1.0
Sample Uptake (mL/min):	2.0 (.65 lpm) 2.3 (.85 lpm) 2.5 (1.0 lpm)
Analyte Concentration:	Ca ion (4 ppm) Ca atom (40 ppm) Sr ion (2 ppm) Sr atom (20 ppm) CaOH (400 ppm)
Slit Width:	1000 $\mu$

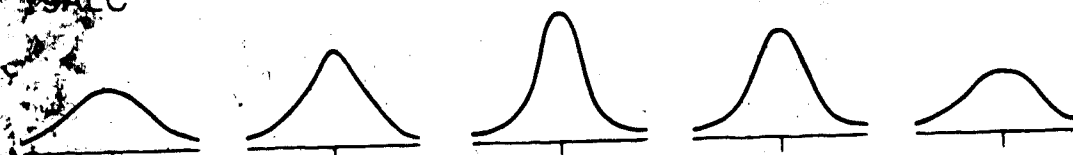
31ALC



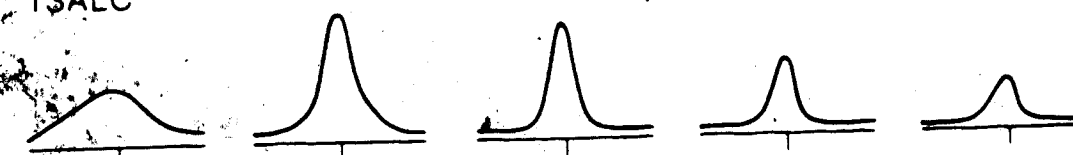
25ALC



19ALC



13ALC



9ALC

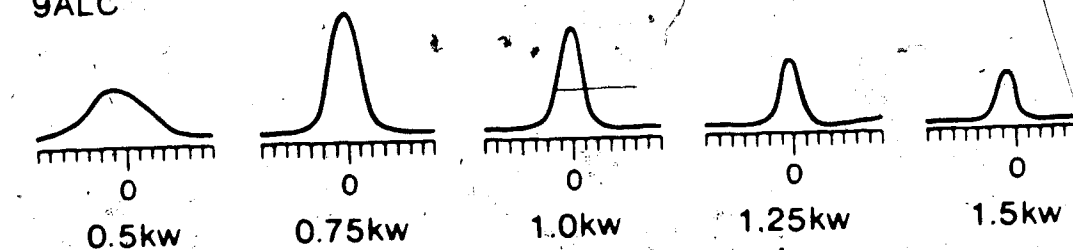


Figure 22. 393.3 nm  $\text{Ca}^+$  fluorescence power study results, 1 lpm.  
See text for explanation of format.



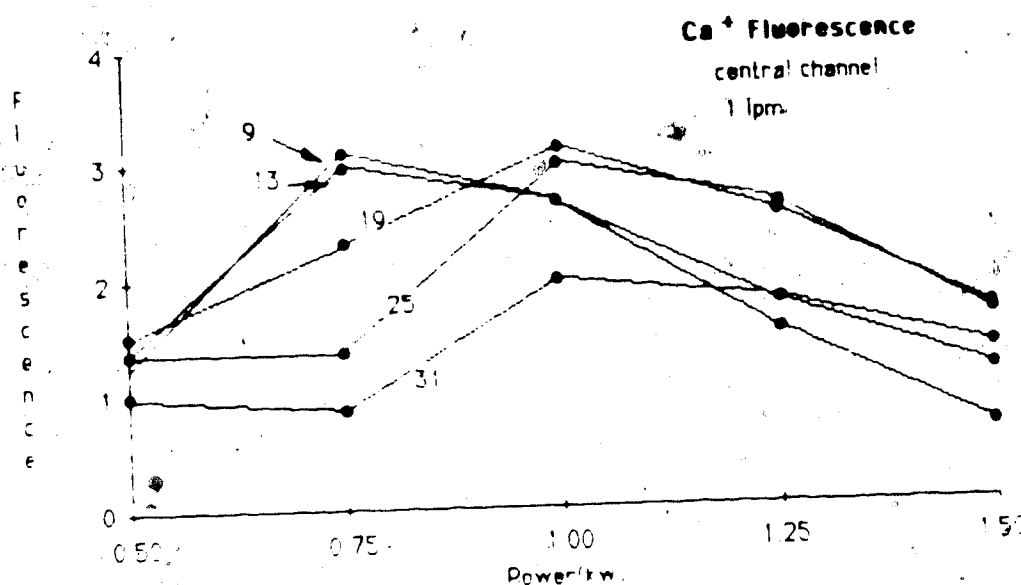


Figure 23. Intensity of 393.3 nm Ca<sup>+</sup> fluorescence in the central channel as a function of power (1 lpm). The numbers in the figure indicate observation height in mm above the load coil.

other powers the profiles are narrow at 9 mm ALC, broadening out as height increases.

The curious asymmetry of the .75 kW profiles at 25 and 31 mm ALC should be pointed out. It is this asymmetry which is responsible for the slight dip at .75 kW appearing in the corresponding curves in Figure 23.

## B.2 Ca Atom Fluorescence Overview

Before trying to rationalize changes in the size and shape of the ion profiles, it is instructive to look at results of a power study of ground state Ca atom fluorescence at 1 lpm. This is presented in Figure 24.

Although all profiles in Figure 24 are on the same scale, no comparison can be made between 22 and 24 on the basis of intensity.

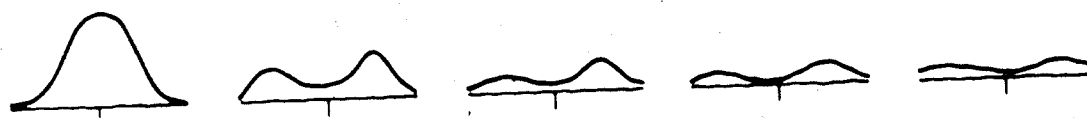
As shown by the data presented in Figure 24, a general disappearance of ground state atoms is seen as power is increased. As for the ions, this is best seen if the height of the profile in the central channel is plotted as a function of power for the various observation heights. This is presented in Figure 25. A loss of ground state atoms as power increases is consistent with a general temperature increase, the atoms becoming excited and ionized.

The atom fluorescence profiles at .5 kW are uniform like their ion counterparts but differ noticeably from the

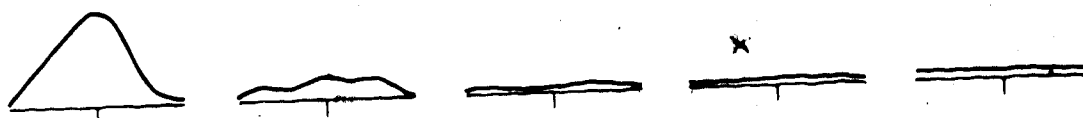
31ALC



25ALC



19ALC



13ALC



9ALC

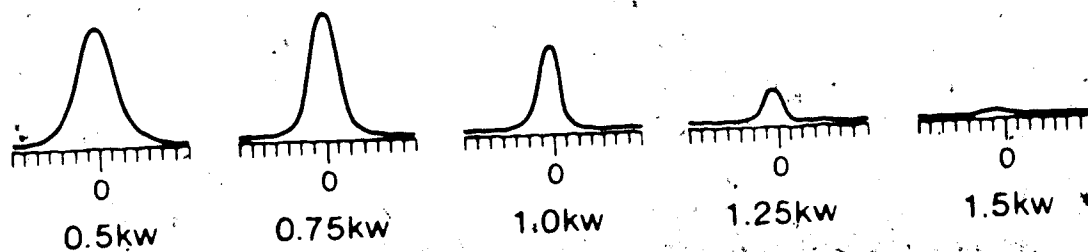


Figure 24. 422.7 Ca atom fluorescence power study results, 1 pm.

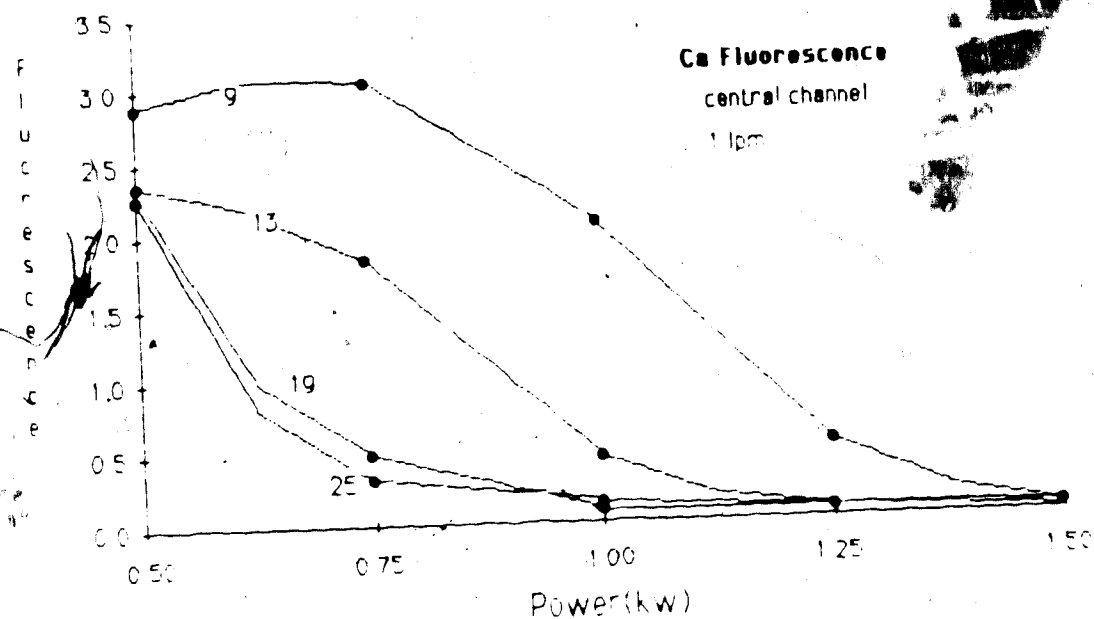


Figure 25. Intensity of 422.7 nm Ca atom fluorescence in the central channel as a function of power (1 lpm). The number attached to each curve is observation height as in Figure 23.

atom profiles at higher powers. At powers above .5 kW, lobes appear at the edges of the plasma at and above the observation height of 25 mm. Note that the presence of these lobes is not reflected by the curves in Figure 25. The general distribution of ground state atoms is not unlike a thick-walled wine goblet. The stem of the goblet then, is eaten away as power increases.

Another way of portraying this is to plot Ca atom profile area as a function of height for the various powers as in Figure 26. At powers above .5 kW, at 19 mm ALC, a zone forms in which the degree of ionization appears to be high; this zone expands downwards as power increases. Of course the degree of ionization cannot be deduced from these profiles alone, but ion/atom emission intensity ratios in this region on the order of 100 to 200 [24] are a good indicator.

As discussed in Chapter 1, electrons enter the central stream of injected gas by ambipolar diffusion, thus establishing a more or less uniform electron density even quite low in the channel. As the electrons diffuse inward, they lose energy by collisions with the injected atoms and molecules. An electron is much more likely to encounter an atom or molecule with which it could combine, hence a situation can be envisioned where the electron density is high, but the electrons are cooler than they

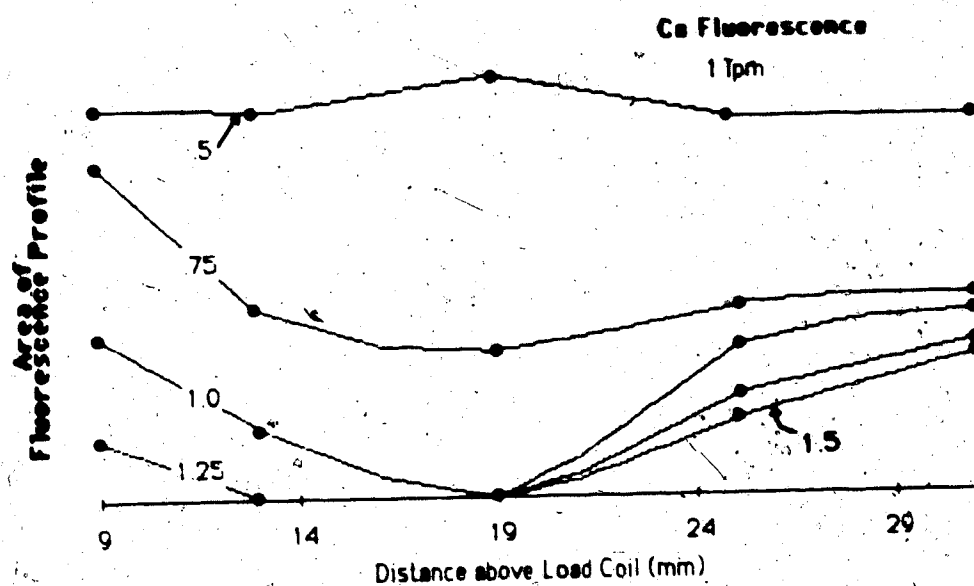


Figure 26. Area of Ca atom fluorescence profile as a function of height at various powers (1 lpm). The numbers attached to the curves are plasma power in kW.

would be if the channel was in LTE. This would result in a degree of ionization of analyte lower than the LTE value.

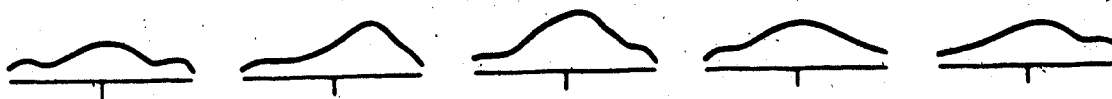
At any given height, the disequilibrium between the electron density and the electron temperature in the central channel should be lessened as power is increased; the annular electrons then start their journey into the channel in greater numbers and with more kinetic energy, yet the same amount of gas is being heated. The average electron then, retains more energy at higher powers, and the degree of analyte ionization should be closer to the LTE value of 100%.

### B.3 Comparison to Strontium Data

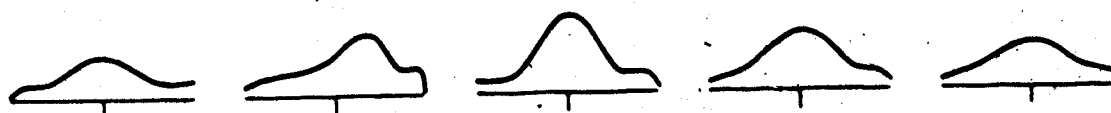
Profiles very similar to those seen in Figures 22 and 23 were also obtained for ground state Sr ion and atom. Figure 27, a power study of Sr ion fluorescence at 1 lpm can be compared to Figure 22. Apart from a slight scale difference, the two figures are almost identical, down to the asymmetry in the profiles at .75 kW high in the plasma.

Scrutiny of Figure 28 (power study of ground state Sr atom fluorescence at 1 lpm) and Figure 24 reveals that the similarity extends to the atom fluorescence profiles as well. Agreement between the response of Sr and Ca was

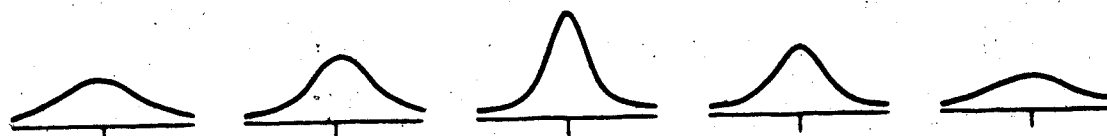
31ALC



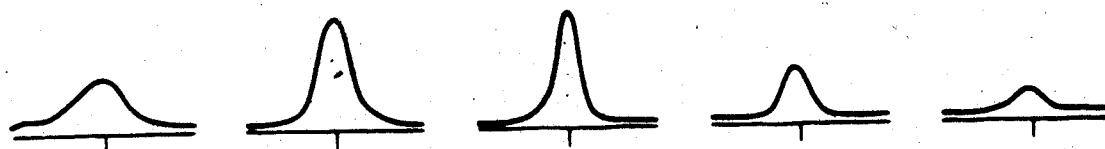
25ALC



19ALC



13ALC



9ALC

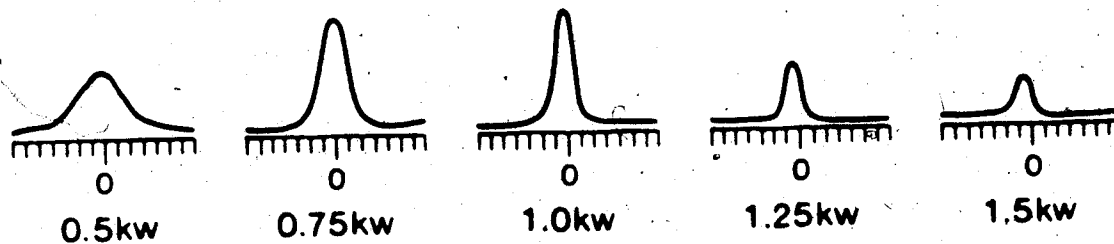
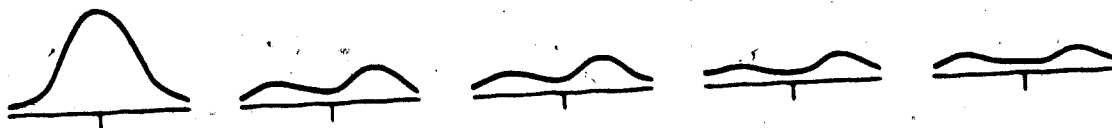


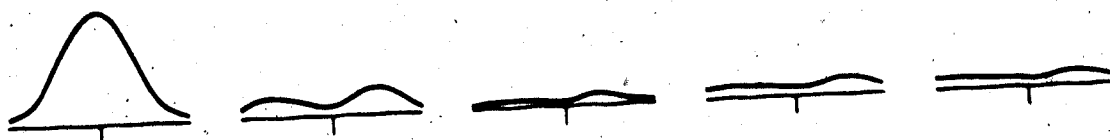
Figure 27. 407.8 nm  $\text{Sr}^+$  fluorescence power study results, 1 lpm.



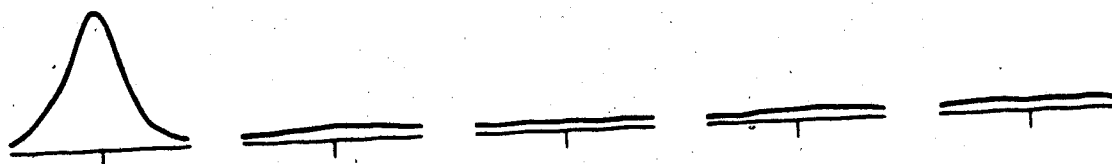
31ALC



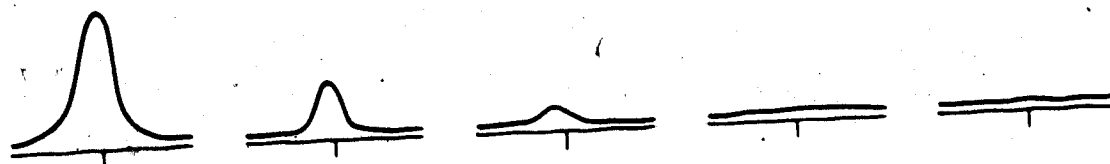
25ALC



19ALC



13ALC



9ALC

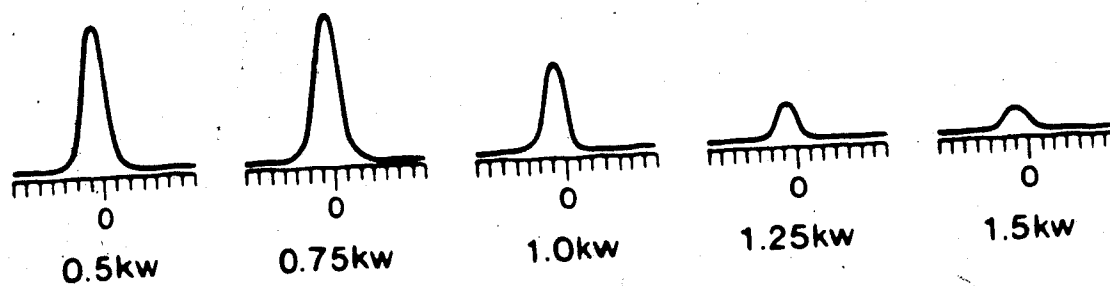


Figure 28. 460.7 nm Sr atom fluorescence power study results, 1 lpm.

also observed at other flowrates.

Strontium, being in the same column as Ca, has similar ionization potentials and its atomic and ionic resonance lines have similar excitation potentials as shown in Table 7. It should not come as any surprise then, that the behavior of Sr resembles that of Ca.

#### B.4 Discussion

Returning now to discuss the Ca results in more detail, it is obvious that the .5 kW plasma is an unusual case. It consists of a uniform, stable jet of ions and atoms. Since the visible .5 kW plasma does not extend out of the coil region, the injected gas receives little energy input once it leaves this region, and expansion is limited. Note that although no visible plasma extends from the load coil, the electron density above the coil should still be relatively high thus some ionization can take place.

The lobes of ground state atoms appearing in Figure 24 are most likely formed by recombination from ions. Recombination does not, however, appear to be responsible for the overall disappearance of ions from high in the plasma as power increases, since the atom lobes also disappear as power increases. Recombination is certainly not responsible for the loss of ions seen low in the plasma as power increases. Atom fluorescence has disappeared at 1.5 kW.

Table 7. Comparison of excitation and ionization energies  
for Sr and Ca.

	First Ionization Potential (eV)	Second Ionization Potential (eV)	Atom Excitation Energy* (eV)	Ion Excitation Energy* (eV)
Ca	6.11	11.9	2.9	3.13
Sr	5.7	11	2.7	3.05

\* Resonance line.

Several points remain to be discussed including the broadening of the profiles as one goes up from the load coil at powers above .5 kW, the general peaking behavior seen in Figure 23 as power increases, and the asymmetry in the profiles at .75 kW. This latter will be considered next.

#### B.4.1 Filtering Effects

Recall that possible concentration effects were discussed in Chapter 3 with the aid of Figure 16. The most likely explanation of the asymmetrical profiles is a prefiltering effect such as might occur in Figure 16(c). By the time the probe beam has reached the far side of the plasma, it has been attenuated, hence fluorescence is attenuated also. Note that the observed asymmetry is consistent with entry of the probe beam at the right hand side of the density profile.

Evidently saturated fluorescence is not being observed although it is difficult to say if this is due to the optics or the shortness of the laser pulse. Had the fluorescence been saturated, this still would not have removed any postfiltering effects. Those can only be removed by working at a lower concentration.

Support for a high ground state ion density high in the plasma at .75 kW (and thus for a prefiltering effect) comes from absorbance measurements made with the system in

Chapter 2. Absorbance as a function of power with the optics centered at 3 different observation heights is shown in Figure 29. Large absorbances are registered at .75 kW and average observation heights of 17 and 23 mm. Absorbances at 1 kW are also high.

In retrospect, fluorescence calibration curves at powers of .75 kW and probably 1 kW should have been obtained at observation heights above 17 mm.

#### B.4.2 Effect of Power at Fixed Observation Height (9 and 13 mm ALC)

Had profiles free of concentration effects been obtained at .75 kW and 1 kW, all the curves in Figure 23 would likely have peaked at .75 kW. A simple explanation for a large increase in ion fluorescence at all observation heights as power increases is that the degree of ionization of the analyte is increasing from say 20% to 80%. If this were the case, then the corresponding atom fluorescence curves should drop markedly as power is increased. This is not what is observed, at least low in the plasma. In Figure 23, the ion fluorescence intensity at 9 mm ALC climbs markedly as power increases whereas in Figure 25, the atom fluorescence intensity at this same height hardly varies at all as power increases.

Invariance of atom fluorescence and an increase in ion fluorescence could be explained by an increase in the

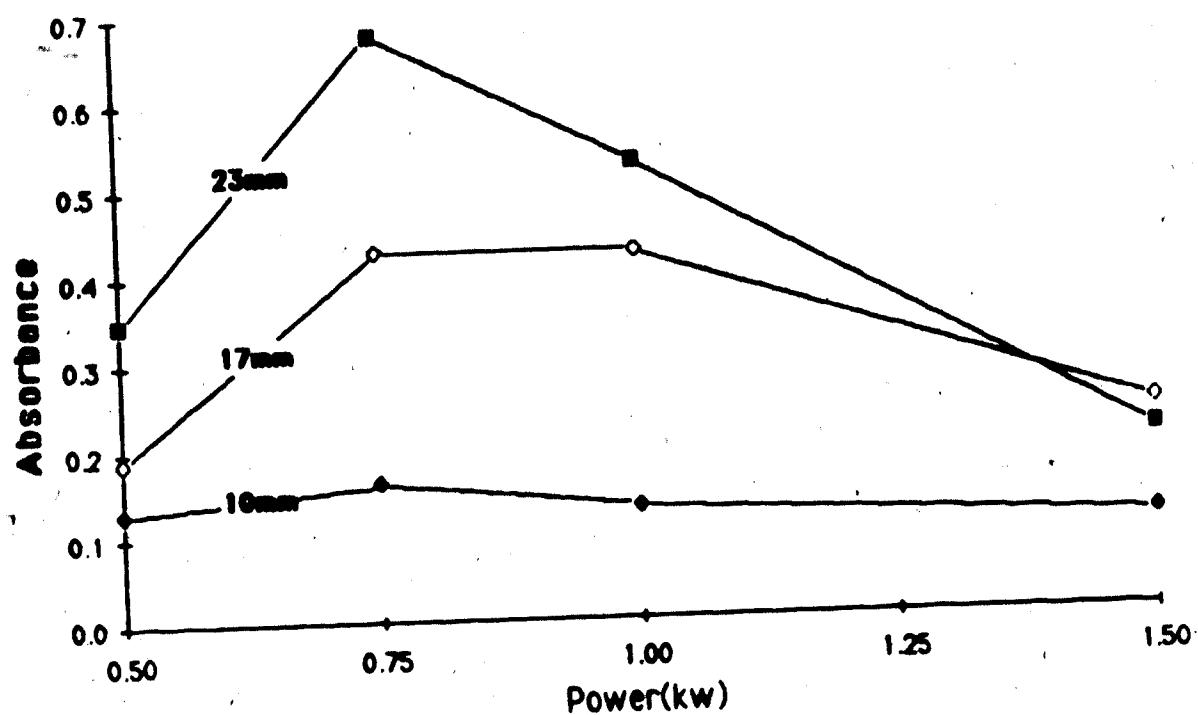


Figure 29. Ca ion absorbance as a function of power at 3 observation heights (heights in mm above the load coil).

dissociation of a molecular species as power increases. A considerable amount of analyte however, could be tied up in the form of  $\text{CaO}^+$  or  $\text{CaO}$  at .5 kW. The trend from mass spectroscopic studies [5] certainly reveals that oxide formation ( $\text{MO}^+$ ) grows worse as power drops. Presence of the uncharged oxide ( $\text{CaO}$ ) might be verified by fluorescence at any one of numerous near-IR wavelengths.

Although the increase of ground state ion fluorescence as power increases to .75 kW has a simple explanation, the same is not true concerning the decrease of fluorescence seen at any height as power increases above .75 kW, or the changes in the width of the profiles at powers above .5 kW.

In order to explain these effects the balance between ground state  $\text{Ca}^+$ , excited  $\text{Ca}^+$  and  $\text{Ca}^{2+}$  as well as any oxide species has to be considered (recombination to atoms is not significant).

For example, in Figure 22 at 9 mm ALC, the ion fluorescence profile at 1.5 kW could be narrower than that at .5 kW because analyte is still present off axis, but in forms other than ground state  $\text{Ca}^+$ , for example excited  $\text{Ca}^+$  ( $\text{Ca}^{*+}$ ) or  $\text{Ca}^{2+}$ . These ideas are discussed in the following sections.

B.4.2.a Excitation. The annular plasma at 9 mm ALC still bears the imprint of the coil region, i.e. it is

hot, relatively dense and may be close to LTE [32] as far as electrons, Argon ions and Ar atoms are concerned.

From an equilibrium calculation using the Saha and Boltzmann equations, it can be shown that analyte entering this region would exist almost entirely as singly charged ions with less than 5% in the form of  $\text{Ca}^{2+}$  (assuming an LTE temperature and electron density of 8350 K and  $2.5 \times 10^{15} \text{ cm}^{-3}$  for a power of 1.5 kW). Of the ions, roughly 60% would remain in the ground state (of the excited ions, almost all would be in a pair of levels at -1.7 eV above ground (see Figure 30)). The same would be true for strontium. The net result is that from an LTE standpoint, the ground state Ca ion profile at 1.5 kW, for example, should be broader than it appears if indeed analyte is present in the annular region at 9 mm ALC.

If Sr is present off-axis, low in the plasma, it too will be highly ionized in an LTE framework. However, due to its differing energy level structure (strontium excited ion levels are closer to ground than their Ca counterparts) a larger fraction of the ions will be in the excited states. One would still expect to see some ground state Sr ions off-axis, but not as many as in the case of Ca.

Recent Thomson scattering experiments [64] measured an electron temperature of 1 eV 3 mm off-axis at 10 mm ALC



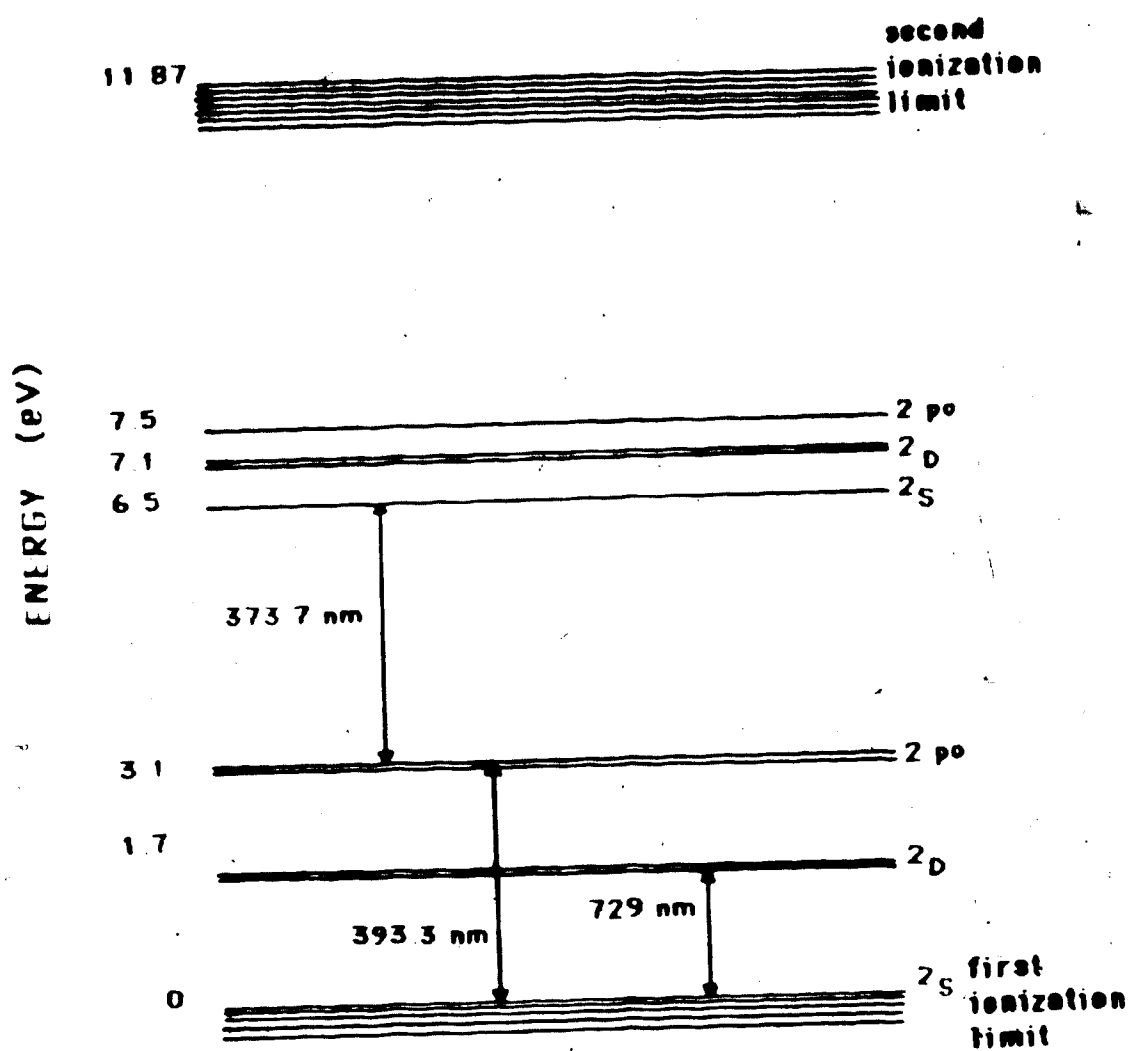


Figure 30. Partial energy level diagram for Ca ion [67].

in a 1 kW plasma whereas an electron temperature of  $\sim 7.5$  eV is predicted from the measured electron density by LTE reasoning. If the electrons off-axis are hotter than their density implies, excited states may be more densely populated than suggested above, particularly so for Sr. This would make the evident lack of ground state ions off-axis low in the plasma less puzzling (but still puzzling!).

Disregarding for the moment the change in the width of the ground state ion profiles at 9 mm ALC as power increases, the possibility remains that increased excitation as power increases is responsible for a decrease in the fluorescence intensity in the central channel.

A set of vertical ion emission profiles (intensity of ion emission in the central channel) at various powers was obtained just prior to melting down the torch. These are shown together with corresponding vertical ground state ion fluorescence profiles in Figure 31.

There is a correlation in that as power increases ion emission increases in Figure 31(a) whereas ground state ion fluorescence decreases in Figure 31(b). However, the magnitudes of the changes do not correlate well. At 13 mm ALC for example, large changes in both emission and fluorescence are seen. At 25 mm ALC large changes in

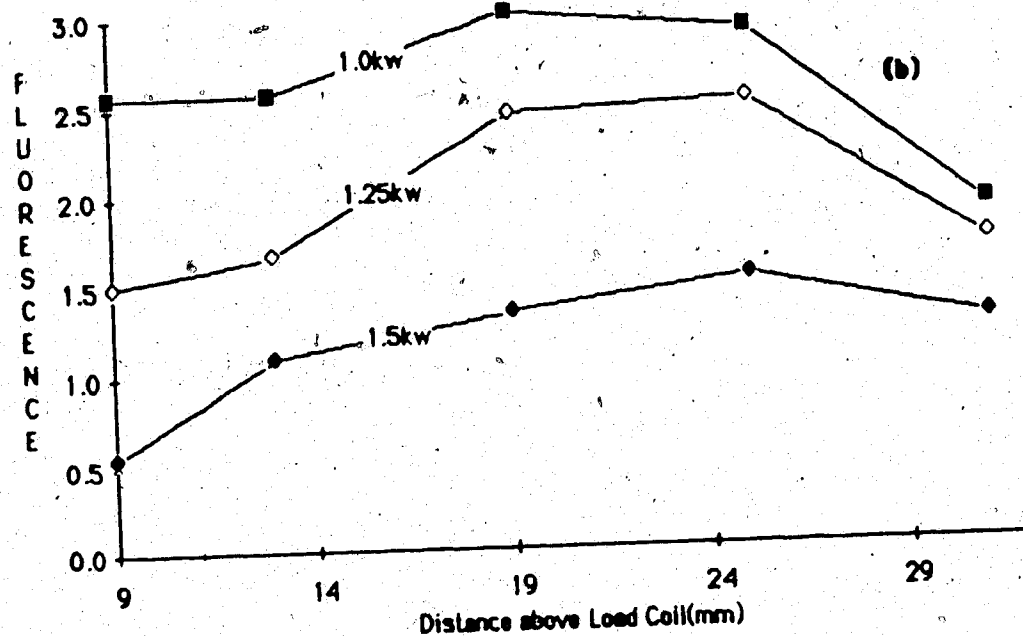
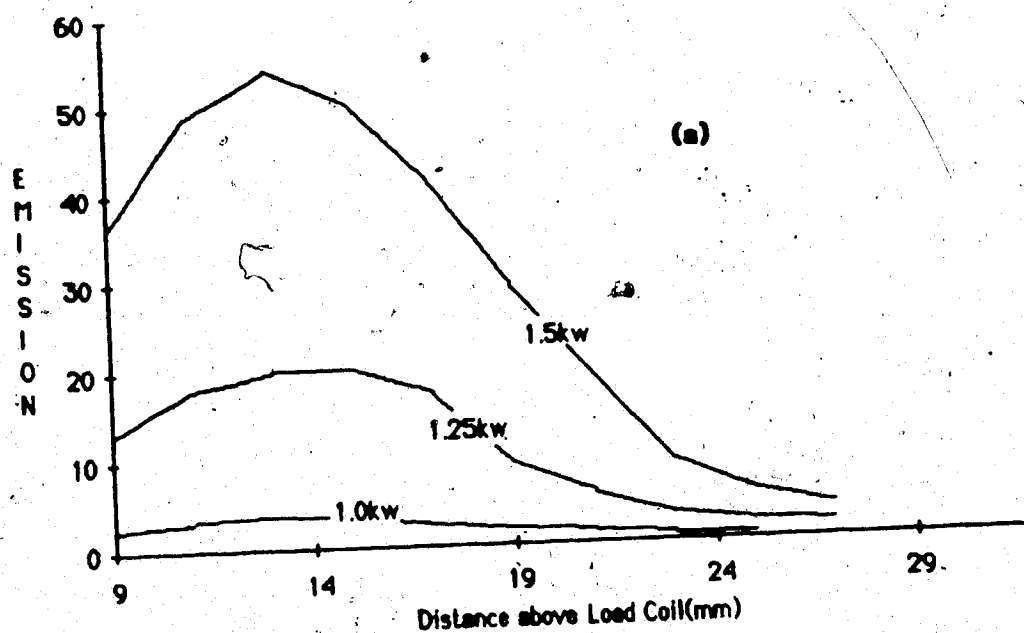


Figure 31.  $\text{Ca}^+$  vertical profiles (1 lpm) (a) 393.3 nm emission, (b) 393.3 nm fluorescence.

fluorescence are still seen but emission has almost disappeared.

Also, by LTE considerations, using temperatures calculated from electron densities [23] and assuming constant total analyte density, it is predicted that at .75 kW, 75% of the Ca ions in a given region of the central channel will be in the ground state and at 1.5 kW, 65% of the ions will remain in the ground state. A change in fluorescence profile height of no more than 10% could be expected on the basis of increased excitation in an LTE framework (of course the assumption of constant total analyte density necessary for the calculation may not be realistic).

Overall, the extent to which increased excitation contributes to the changes in size and shape of the ground state ion fluorescence profiles low in the plasma can really only be determined by measurement of the actual densities of the levels involved, the 1.7 eV levels likely being more important than the 3.1 eV levels in the case of Ca.

B.4.2.b Formation of doubly charged ions. Some idea of the extent of possible involvement of doubly charged ions in the disappearance of ground state Ca or Sr ions as power increases can be had from ICP-MS studies. (Note that ICP-MS is the only method available to probe most ground state doubly ionized species.)

Existence of  $M^{2+}$  in the plasma has been discussed before [15,62]. Doubly ionized La has been observed in emission [28] and ICP-MS studies have detected  $M^{2+}$  as well [4,5,63].

In reference [5], the ratio [counts  $Sr^{2+}$ /counts  $Sr^{+}$ ] at 1 lpm flowrate was  $\approx .03$  at .9 kW, increasing to  $\approx .15$  at 1.5 kW. This was measured with a tall torch at 31 mm ALC observation height. The  $Sr^{+}$  count includes excited ions as well as ground states whereas the  $Sr^{2+}$  count consists of ground states only. The ratio [ $n_{Sr^{2+}}$  ground state/ $n_{Sr^{+}}$  (ground state)] could be larger than .15, depending on the fraction of singly charged ion population which is excited. Note that this ratio is not consistent with an LTE framework which, as mentioned, predicts  $\alpha_{2+}$  on the order of 5% or less.

From the above it is difficult to predict what the situation might be 9 mm ALC for a standard torch. Any over population of  $Sr^{2+}$  seen 31 mm ALC with a long torch might well be even larger at 9 mm ALC with a short torch.

If the electron temperature off-axis close to the load coil is higher than expected, as is suggested by the Thomson scattering measurements mentioned earlier, this might be the cause of the overpopulation of Sr ions. Calcium could be expected to behave similarly although no direct experimental evidence on  $\text{Ca}^{2+}$  has been collected by ICP-MS.

Photoionization of ground state  $\text{Ca}^+$  close to the load coil is a mechanism whereby  $\text{Ca}^{2+}$  might be formed in number over and above that expected in LTE.

With reference again to Figure 30, 11.85 eV Ar atom resonance photons could promote ground state  $\text{Ca}^+$  to within .02 eV of the second ionization limit. The 11.65 eV photon could no doubt also be absorbed since the energy levels are still densely packed within .22 eV of the second ionization limit. This scheme does not depend on any sort of trapping [65,66] mechanism, i.e. it would only apply close to the load coil.

Photoionization of Sr atoms within .85 eV of the first ionization limit (by 11.85 and 11.65 eV Ar resonance photons) might possibly be an important process whereby ground state  $\text{Sr}^+$  could be bled away. (High lying excited levels are generally thought to be collisionally equilibrated with the ground level of the next ionization stage even if LTE does not prevail.)

Further investigation of the  $\text{Sr}^{2+}$  and  $\text{Ca}^{2+}$  species via ICP-MS is certainly warranted. A definitive study would include measurement of the ratio  $\text{Sr}^{2+}/\text{Sr}^+$  as a function of power and flowrate at various observation heights both on and off axis (using a short torch). Ground state  $\text{Sr}^+$  distributions with the same torch could then be studied via fluorescence and compared to the mass spectroscopic studies.

B.4.2.c Quenching effects. The possibility that the size and shape of the ion fluorescence profiles low in the plasma do not reflect the actual distribution of ground state  $\text{Ca}^+$  due to quenching collisions with electrons must also be considered.

In the ICP, the importance of this effect decreases rapidly as the spacing of energy levels in the vicinity of the pumped level increases beyond  $\sim 1$  eV. (This is due to the relatively low ( $< 1$  eV) average energy of the electrons in the ICP.)

For example, Na atom (589 nm) resonance fluorescence in the central channel of the ICP at 10 mm ALC had a quantum efficiency of .99. This was seen to be invariant when both power and flowrate (and hence electron temperature and density) were changed over a wide range [40]. The nearest neighbors to the level of interest in this case were  $\sim 1.1$  eV and 1.5 eV away.

However, off axis low in the plasma, the electron density is high and the electrons are fast. The possibility of electron quenching in this region should be investigated, either by lifetime measurements of fluorescence at various powers, or by looking for thermally assisted fluorescence. Certainly increased quenching as power increases would conveniently explain the changes in size and shape of both Ca and Sr ion fluorescence profiles low in the plasma as power is increased.

With reference again to Figure 30, one might envision that if resonance fluorescence at 373.7 nm were to be attempted, the possibility of electron quenching would be higher due to the closer spacing of the energy levels in the vicinity of the pumped level.

Inspection of the Grotrian diagram for Ca atom (not shown) reveals that there are several close-by levels to which the 2.94 eV excited level (422.7 nm) could be collisionally coupled. The possible effect of quenching on Ca atom fluorescence was not considered. In cases where quenching might tend to be important, Ca atom tends to comprise only a small fraction of the total analyte population anyway, so fluorescence signals are small to start with. Further reduction by quenching will not make a major impact on overall trends observed for ground state Ca atom.



Overall, from these profiles alone, there is not enough information to determine the extent to which the mechanisms discussed (excitation, quenching and  $M^{2+}$  formation) contribute to the decrease in ground state ion population as power increases at 9 and 13 mm ALC.

#### B.4.3 Effect of Power at Fixed Observation Height (>13 mm ALC)

Higher in the plasma, the decrease in area of the profiles and the increase in their FWHM as power increases is most likely due to simple dilution. An increase in oxide formation might be proposed to explain the decrease, however this would run contrary to the trends seen for ICP-MS [5]. Uncharged oxide again might be present and near-IR fluorescence could be used to explore this possibility.

#### B.4.4 Effect of Height at Fixed Power

The apparent broadening of the profiles as observation height increases must be considered in the light of what was discussed previously. At .5 kW the ground state  $Ca^+$  profile at 9 mm ALC in Figure 22 is likely representative of the total analyte distribution. At higher powers, the total analyte density distribution at 9 mm ALC may still be broad, but  $Ca^+$  profiles no longer reflect this for a variety of reasons (excitation,  $Ca^{2+}$ , quenching). Once a given volume of plasma has travelled far enough away from the load coil, however, the

temperature and electron density gradients as one goes off axis reverse direction. Depending on how the situation is viewed then, excited ions would revert to the ground state, doubly charged ions would recombine (or the photon flux responsible for their existence would decrease), and quenching would be reduced. The net result would be a "reappearance" of ground state  $\text{Ca}^+$ . Again, from this study alone there is not enough information to determine the exact situation.

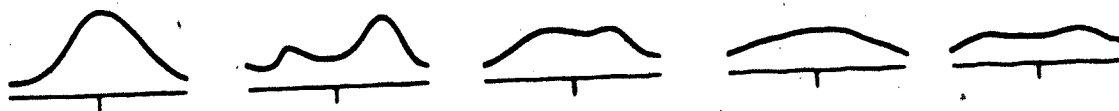
### C. Effect of Flowrate

#### C.1 Overview: Ca Ion and Atom Fluorescence

The results of a power study of  $\text{Ca}^+$  fluorescence at .85 lpm can be seen in Figure 32. Overall no major changes are seen relative to Figure 22. Most of the profiles still exhibit a central maximum although the profiles are somewhat broader overall. A stable jet of ions still appears at .5 kW, however comparing the leftmost columns of Figures 32 and 22 it is seen that there are more ions at .5 kW for .85 lpm. The area of the profiles no longer peaks as power increases, decreasing instead.

High in the plasma at .75 kW, the profiles are again asymmetric as in Figure 22, having a bimodal shape. A study of the effect of concentration on profile shape was

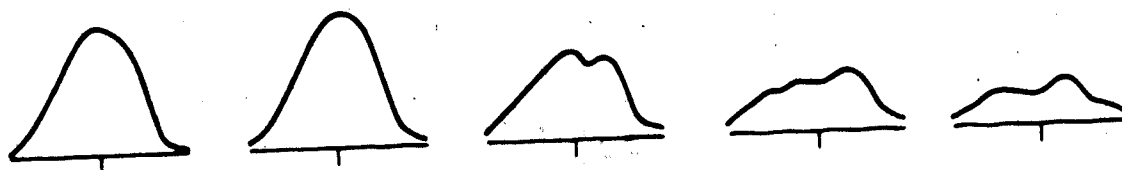
31ALC



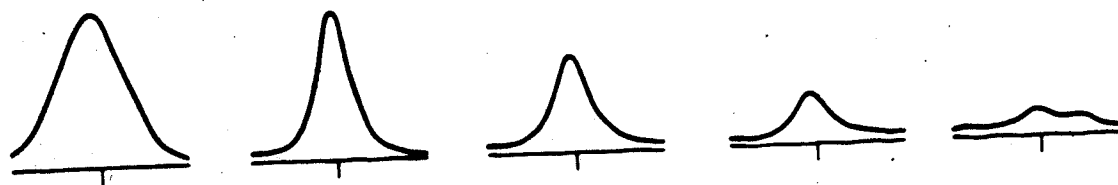
25ALC



19ALC



13ALC



9ALC

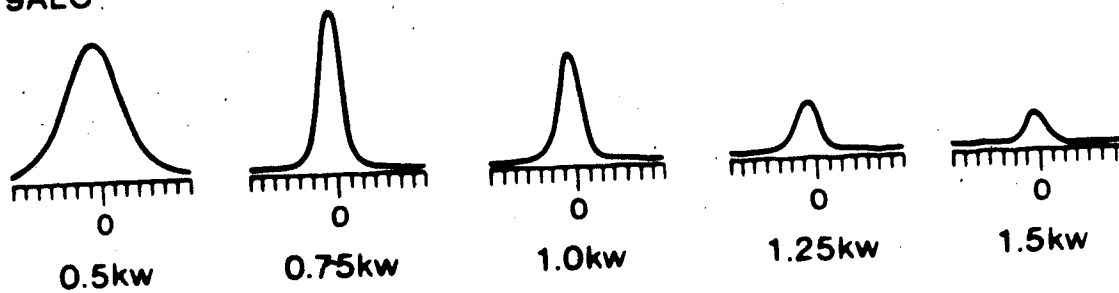


Figure 32. 393.3 nm  $\text{Ca}^+$  fluorescence power study results, 85 lpm.

later carried out and this same bimodal pattern could be generated from an initially Gaussian shaped profile by increasing the concentration. This is shown in Figure 33. Both profiles were taken at 13 mm ALC in a 1 kW plasma operating with .65 lpm flowrate. The solid curve is for a concentration of 400 ppm, the dashed curve 40 ppm. (The fact that these profiles were taken in a different region of the plasma under different operating conditions is not important, the effect of concentration is what is of interest.)

The power study of ground state Ca ion fluorescence at .65 lpm is summarized in Figure 34. Continuing the trend from .85 lpm, the profiles are now generally broad and flat. Overall, dropping the flowrate has apparently resulted in a dramatic loss of ground state ions. Profiles taken 19 mm ALC at 1 kW for the three flowrates are shown together in Figure 35 to illustrate these points. The appearance of a large central depression in the profiles at low power is also evident. This is seen in Figure 36.

The results of the power study of the fluorescence of Ca atoms at .85 lpm flowrate are presented in Figure 37. Figure 37 is basically similar to its counterpart at 1 lpm (Figure 24) as was the case for the ions.

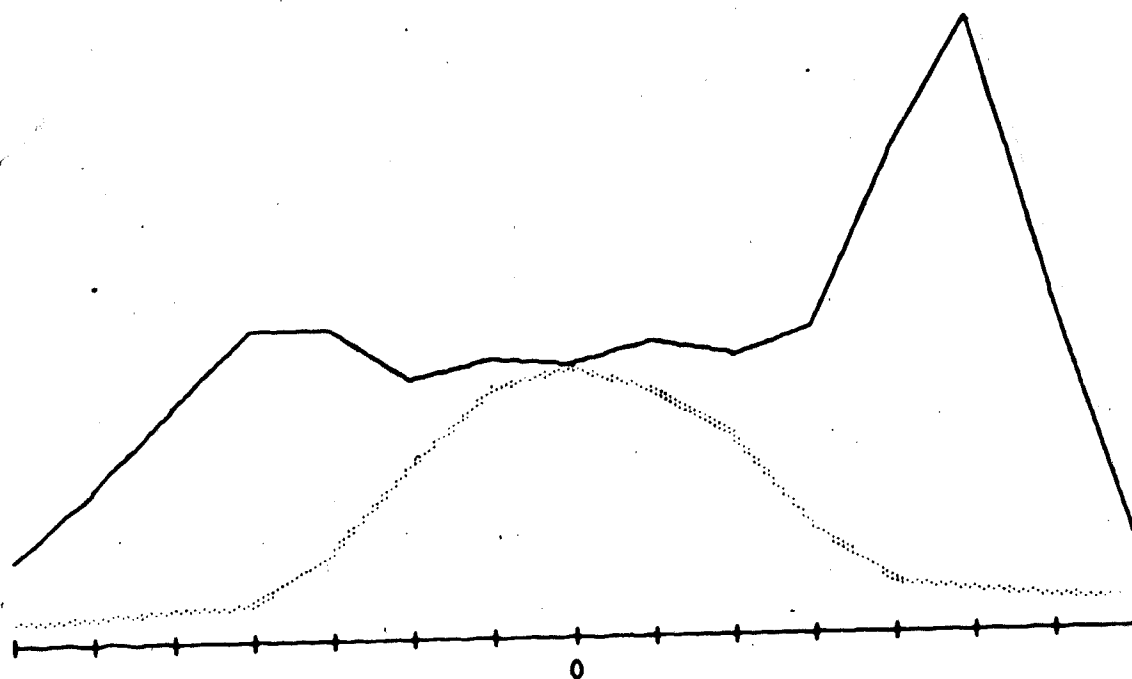


Figure 33. Effect of concentration on  $\text{Ca}^+$  fluorescence profile at 13 mm ALC, 1 kW, .65 lpm. Solid curve 400 ppm Ca. Dotted curve 40 ppm.

31ALC



25ALC



19ALC



13ALC



9ALC

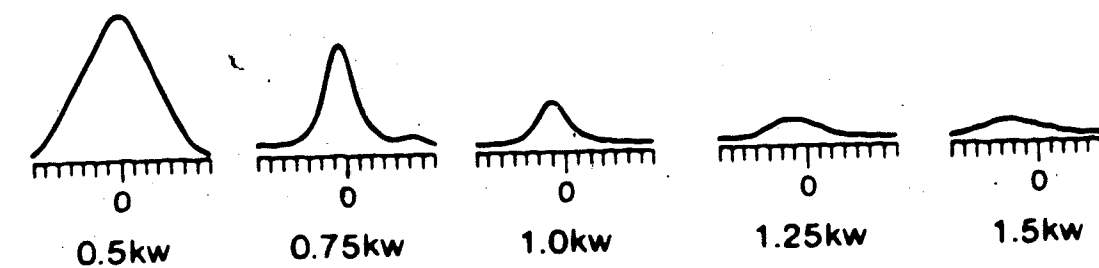


Figure 34. 393.3 nm  $\text{Ca}^+$  fluorescence power study results, .65 lpm.

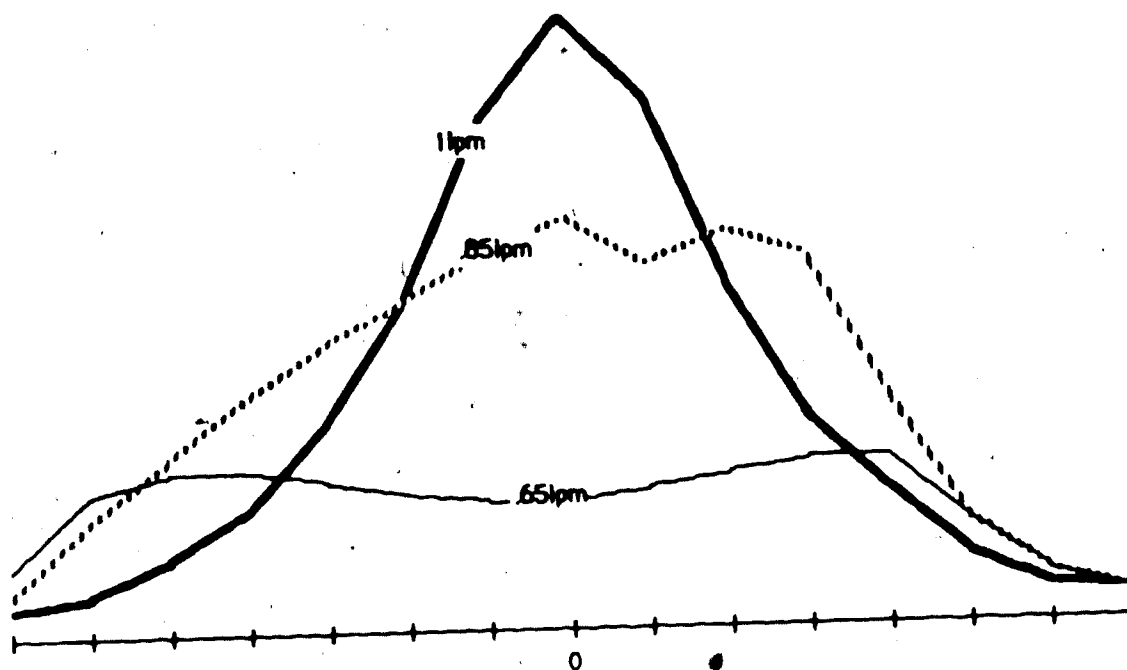


Figure 35. Effect of flowrate on  $\text{Ca}^+$  fluorescence profile at fixed power (19 mm ALC/ 1 kW).

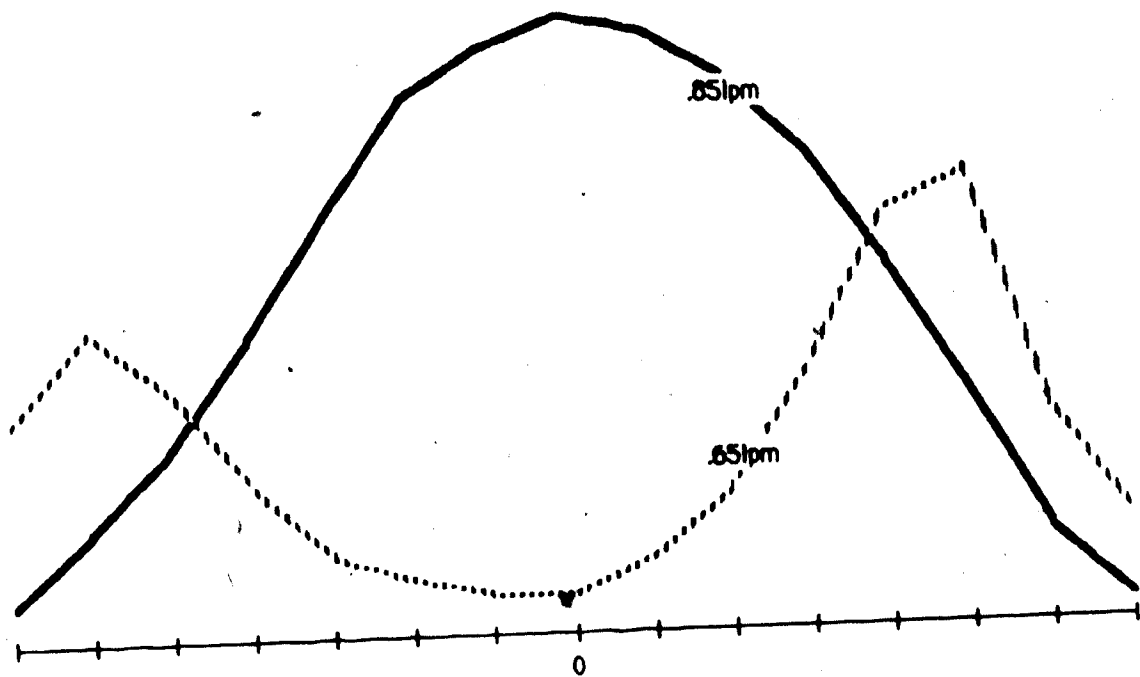
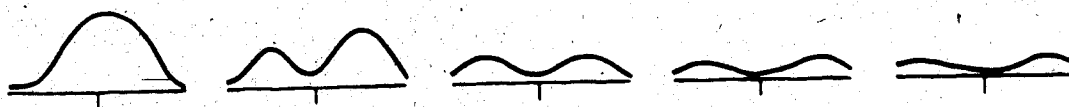


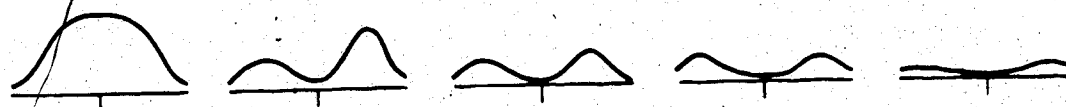
Figure 36. Effect of flowrate on  $\text{Ca}^+$  fluorescence at fixed power (19 mm ALC/.5 kW).



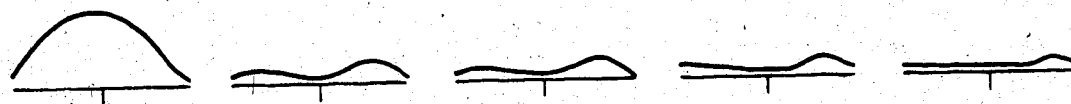
31ALC



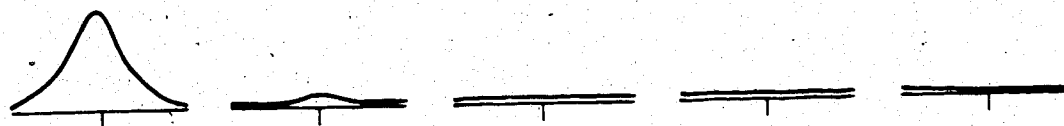
25ALC



19ALC



13ALC



9ALC

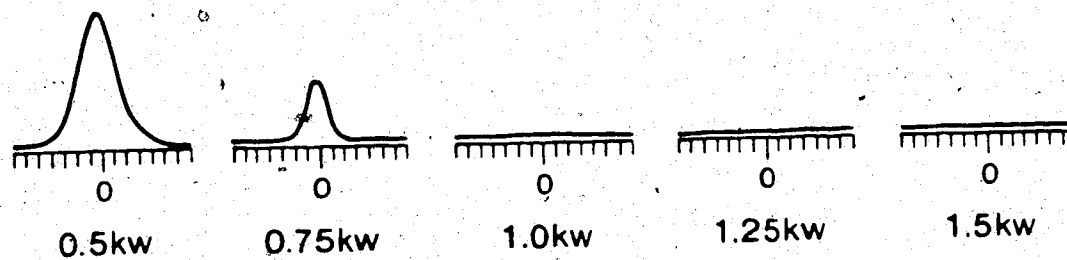


Figure 37. 422.7 nm Ca atom fluorescence power study results, .85 lpm.

At powers above .5 kW, ground state atoms have more or less disappeared from the lowest two rows of the figure. However at 19 mm ALC lobes are present in Figure 37 whereas they were not present in Figure 24. This is probably a reflection of the fact that the ion profiles overall are broader at .85 lpm as pointed out.

Finally, the Ca atom fluorescence power study at .65 lpm is represented in Figure 38. Dropping the flowrate has removed virtually all the atoms from the plasma at 9 mm ALC, including those at .5 kW.

Small lobes now appear at the edges of the plasma at 13 mm ALC again due to the broadening of the ion distribution. A central depression also appears in the profiles at .5 kW as was seen for the ions.

An overall summary of the data presented thus far can be seen in Figure 39. In a given frame the fluorescence intensity (ion or atom) in the central channel is plotted as a function of power for each of the 5 observation heights. Flowrate decreases from top to bottom. Again, note that no comparison can be made between ion and atom fluorescence intensity.

Areas where filtering effects distort the ion fluorescence can be clearly seen in frames (a) and (b) as dips in the curves. The downward turn of the curves in frame (c) for observation heights above 9 mm ALC is due to the central depression at .5 kW.

31ALC



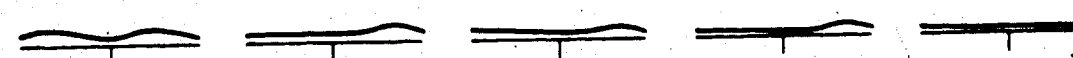
25ALC



19ALC



13ALC



9ALC

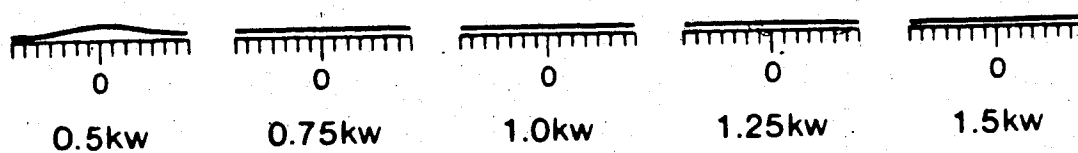


Figure 38. 422.7 nm Ca atom fluorescence power study results, .65 lpm.

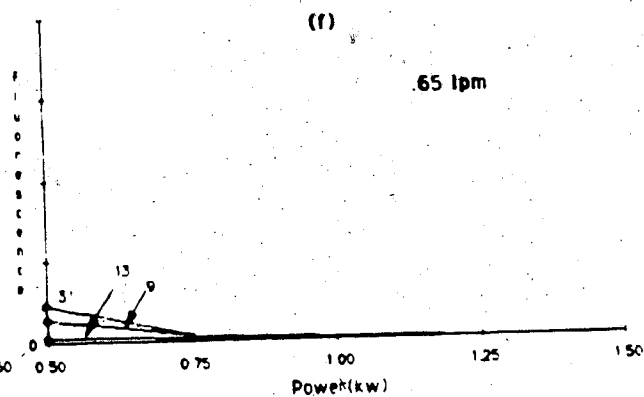
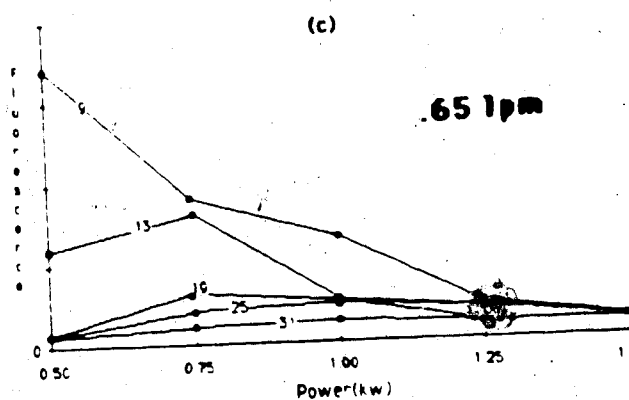
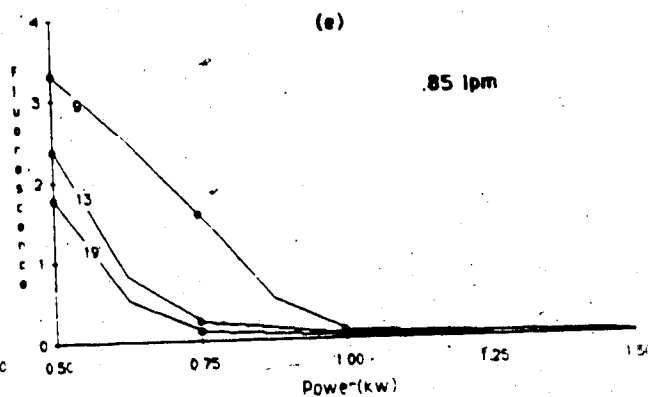
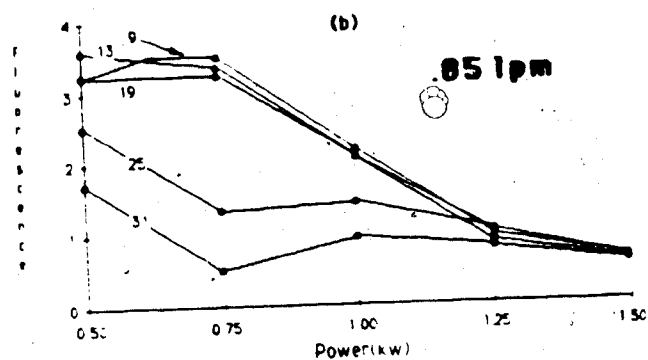
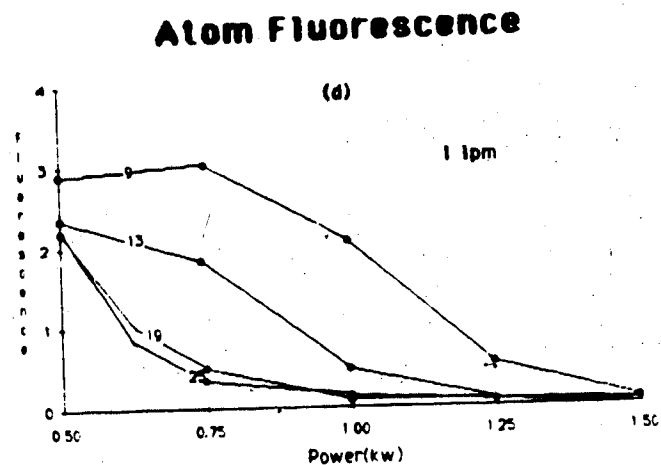
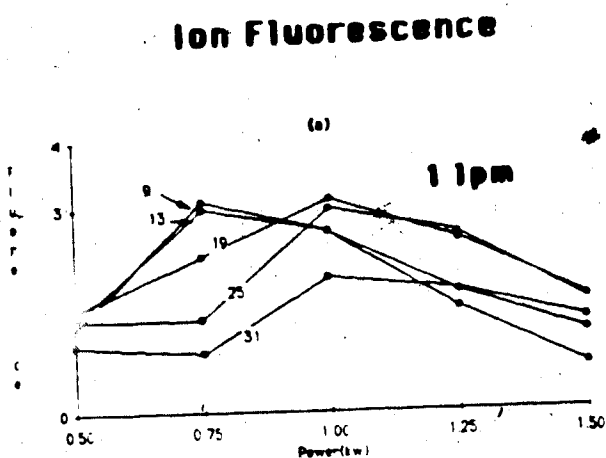


Figure 39. Ca ion and atom fluorescence as a function of power at 3 flowrates. Flowrates are labelled in each frame. Heights in mm above the load coil are attached to each curve.

Taking these points into consideration, the shift from a peaking of fluorescence at 1 lpm as power is increased to a decrease at .65 lpm is clearly seen in frames (a) through (c). A general decrease in fluorescence intensity as flowrate drops is also evident.

Regardless of flowrate, atom fluorescence always disappears as power increases. More noticeable is the disappearance of atoms as flowrate decreases. Again, recombination to atoms evidently cannot explain the disappearance of ions as power increases or flowrate decreases.

It is seen then, from Figure 39, that carrier flowrate exerts as marked an influence on the analyte as does power.

## C.2 Discussion

One result of a drop in flowrate is a drop in sample uptake rate (from 2.5 mL/min to 2.0 mL/min). It might well be imagined that this results in a drop in signal intensity on the basis of a decrease in mass transport. Without knowing how the actual analyte transfer efficiency is changing as flowrate changes, it is hard to tell exactly what effect a change in flowrate will have. (The analyte transfer efficiency is not equal to the nebulizer efficiency because some desolvation might occur in the spray chamber.) If the analyte transfer efficiency stays

constant, then one could expect a 20% decrease in overall signal intensity as flowrate drops from 1 lpm to .65.

A drop in flowrate also affects both the argon plasma as a whole, and how the analyte interacts with the plasma. As flowrate drops, the entire plasma becomes hotter. Less gas and water are injected and so less heat is carried out of the plasma by convection.

Support for a temperature increase comes from measurements of electron density [24] at 1.25 kW for 3 flowrates. The temperature calculated from  $n_e$  (assuming LTE) 8 mm ALC and 3 mm off axis is seen to increase from 8350 K to 8600 K. The magnitude of this change is in agreement with the fact that the ratio [carrier gas flow/total gas flow] drops from 6.25% to 4%. In this work, as flowrate dropped, a decrease in both scattering from microscopic water droplets and CaOH molecular fluorescence at 554.3 nm was seen in the central channel. These observations also point to a hotter plasma at the lower flowrate.

From the viewpoint of the analyte, faster entry of electrons into the central channel is facilitated by a drop in flowrate as pointed out in reference [24]. The analyte channel at a given height becomes hotter as flowrate drops because the injected gas mixes more efficiently with an overall hotter annular gas.

From the above then, it is reasonable to expect that as flowrate drops, the degree of dissociation of molecular species should increase, and the degree of ionization of the analyte should increase, particularly low in the plasma. Analyte dilution will also become more significant. The interplay between these effects has to be considered when looking at Figure 39.

At .65 lpm, the channel is hottest, so the degree of ionization is high even at low power; relatively few atoms are seen in frame (f). An increase in power results in rapid dilution of the analyte as it leaves the coil region, hence the ion population too is relatively low as seen in frame (c).

At an intermediate flowrate (.85 lpm) and at low power the channel is not as hot as it was at .65 lpm, nor is dilution as extensive, hence there are more atoms in frame (e), and ions do not disappear as fast with increasing power or height in frame (b).

The temperature of the central channel continues to drop as flowrate increases to 1 lpm so the trend toward decreasing degree of ionization low in the plasma and at low power continues. This is accompanied by oxide formation.

High in the plasma, dilution is still responsible for the drop-off of the curves in frame (a) as power increases, although it is slower in onset.

The appearance of a central minimum in the ion profile at .5 kW when flowrate drops was seen earlier. That the profiles are symmetric tends to rule out a possible inner filtering effect.

It was mentioned earlier that the plasma is macroscopically rotating at a frequency of several hundred Hz. Presumably this originates due to the tangentially introduced coolant gas although it is not known if spin is imparted to the plasma only close to the coil or if the plasma is surrounded by an actual vortex of gas extending several centimetres out of the torch. This latter is more likely at low power.

If an actual vortex exists at low power it may be able to entrain analyte once the flowrate drops low enough, for several reasons. Firstly, the analyte would have more tendency to disperse rather than remain as a jet. Also, since the temperature of the plasma increases as flowrate drops, the plasma probably spins faster. Rotation frequency was observed to be directly proportional to power (and hence temperature) in reference [52]. Particle track photographs of the plasma at .5 kW running with different flowrates may prove useful to resolve this point.

Quenching effects have not been considered in explaining some of the changes seen as flowrate drops.



One type of quenching not considered earlier which might be important high in the plasma arises from collisions with entrained air molecules. This was postulated to exert a large effect on the quantum efficiency of Na fluorescence in the ICP at observation heights above 10 or 15 mm ALC [38].

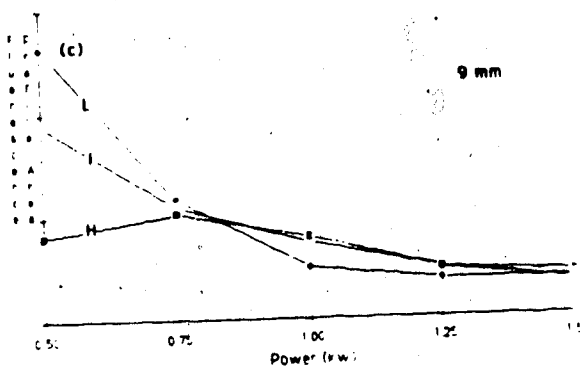
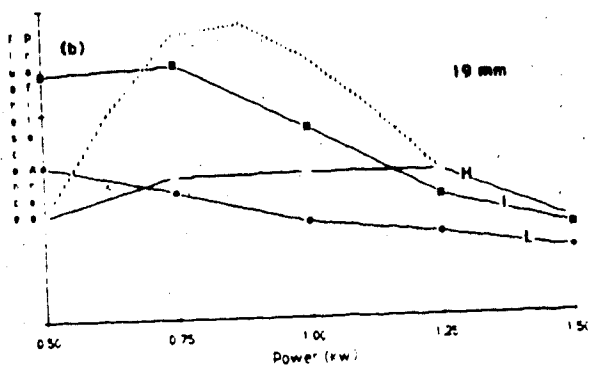
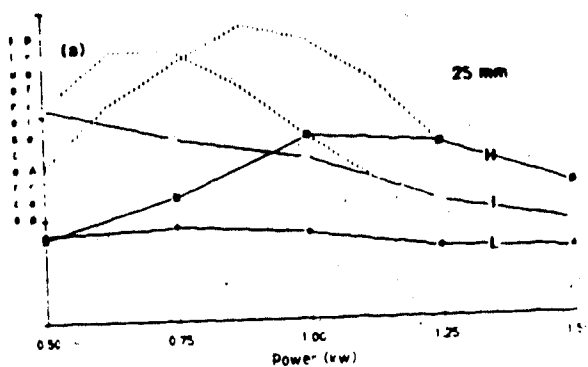
However, considerable support that fluorescence has given an undistorted (except by inner filtering) picture of the behavior of ground state Ca species comes from absorbance measurements.

#### D. Comparison of Fluorescence and Absorbance Measurements

Average absorbance measurements at 3 different heights (mentioned in Chapter 2) are presented in Figure 40 along with fluorescence results from comparable heights. To facilitate comparison, the area of the fluorescence profiles is plotted. In any frame absorbance or area of fluorescence profile is plotted as a function of power for 3 different flowrates denoted L, I, and H (low, intermediate, and high). Observation height increases from the bottom of the figure.

The dotted lines in frames (a) and (b) are an attempt to remove filtering effects. When this is done, good agreement is seen between the curves in the two columns in terms of their general shape and ordering with respect to

## Ion Fluorescence



## Ion Absorbance

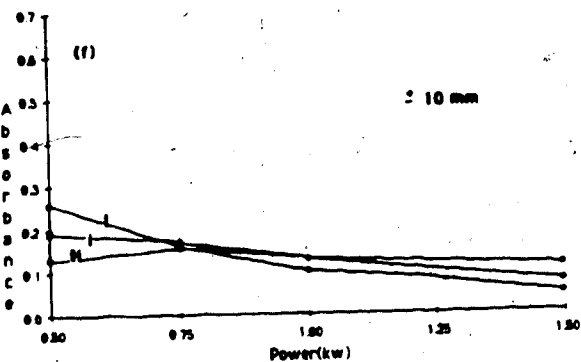
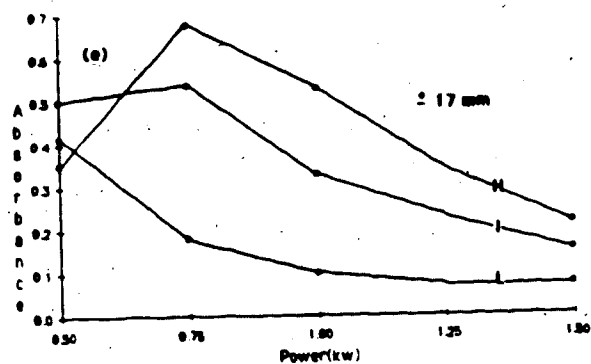
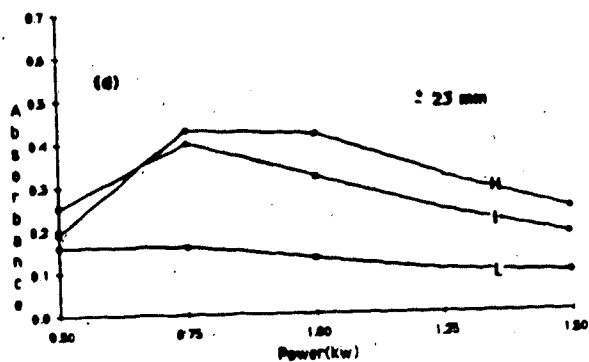


Figure 40. Ca ion fluorescence and absorbance results (393.3 nm) at 3 observation heights. H, I and L denote high, intermediate and low carrier flowrates. See text for further description of format.

flowrate. This is despite the fact that although the nebulizer backpressures were comparable in both studies, the sample uptake rates and aerosol carrier volume flowrates differed somewhat.

The absorbance measurements in Figure 40 include contributions from regions up to 4 mm above and below the stated observation height. It is known from other absorbance profiles in the literature [15] that  $\text{Ca}^+$  absorbance drops off rapidly below 10 mm ALC. Perhaps then, the absorbances at .5 kW in frame (F) are somewhat low relative to their fluorescence counterparts because of the larger (empty) spatial region being viewed for absorbance.

A comparison of ground state atom absorbance and fluorescence is presented in Figure 41. The format of the figure is identical to Figure 40. In frame (b), the curves at .85 and .65 lpm level off above the baseline whereas the curves in frame (e) do not. This is most likely due to the fact that the fluorescence curves are more sensitive to contributions beyond a radius of 4 mm. Overall however, the same reasonably good agreement between sets of measurements is seen.

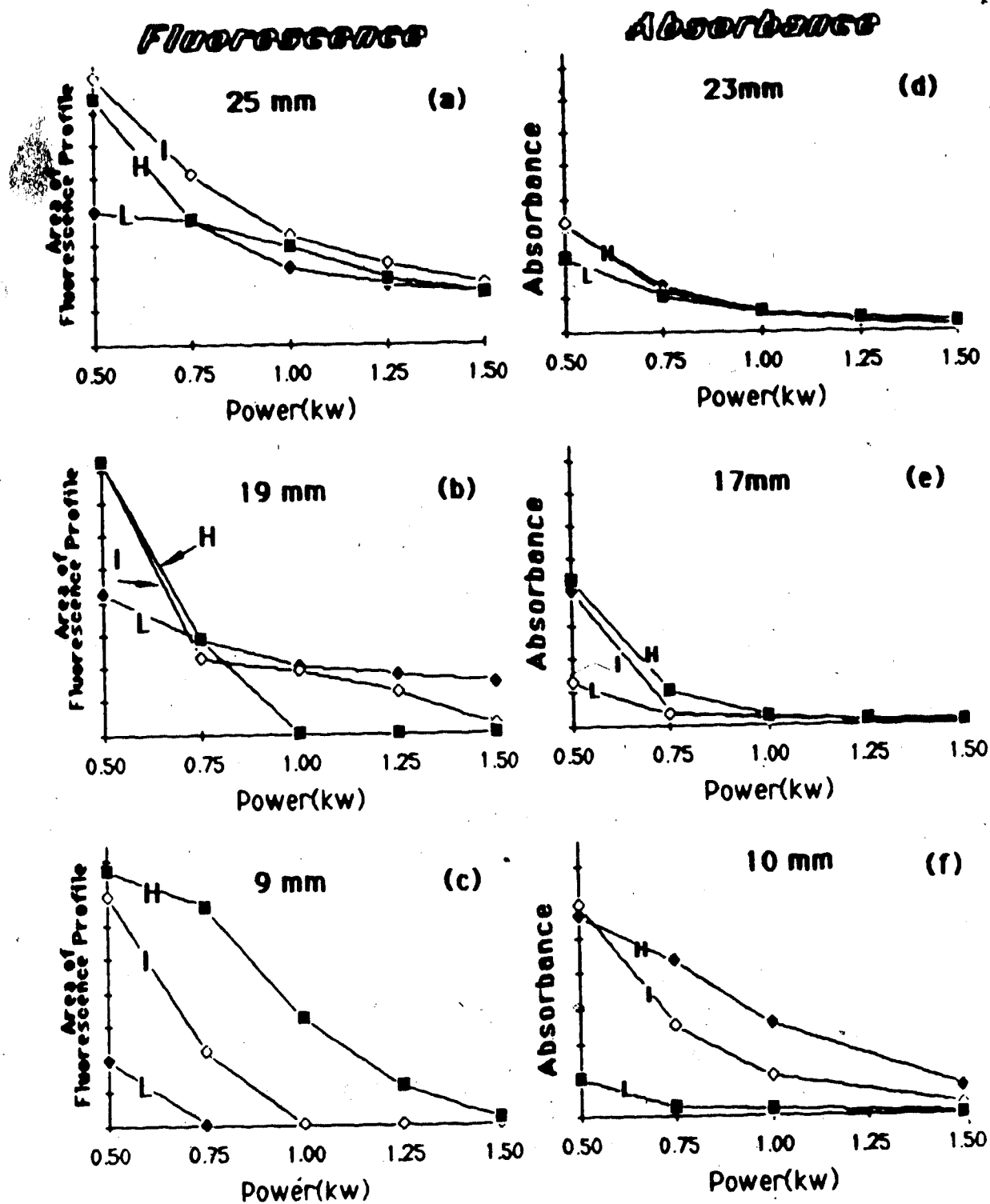


Figure 41. Ca atom fluorescence and absorbance results (422.7 nm) at 3 observation heights. The format is identical to Figure 40.

### E. Comparison to Other Ground State Studies

Another means of cross checking the fluorescence data is to compare it to the results of some of the other ground state studies mentioned in the introductory chapter.

Rybarczyk [15] et al. looked at Ca atom and ion absorbance profiles in the region below 14 mm ALC in a 1.25 kW plasma operated with 1.1 lpm flowrate. From 10 to 12 mm ALC, his ion absorbance profiles appear constant in height. The profiles in Figure 22 also exhibit this constancy although over a slightly extended range. His atom absorbance profiles dwindle in the same fashion as those in Figure 24 going from 9 to 13 mm ALC.

Uchida [17] and co-workers measured vertical atom and ion fluorescence and emission profiles at two different flowrates in a 1 kW plasma.

Their figures, at face value, show ion emission peaking below 5 mm ALC and atom emission peaking at 10 mm ALC. This is contrary to every set of vertical emission profiles ever published. Also, atom emission and fluorescence appear to be a factor of 10 more intense than ion emission and fluorescence. They have evidently mislabelled their figures.

If the labels are reversed, very good agreement with this thesis work is seen. Ground state atoms die out with

a height increase. If the flowrate is increased a gain of atoms, low in the plasma is seen. Ion fluorescence peaks about 20 mm ALC and an increase in flowrate results in a large increase in the population of ground state ions high in the plasma, with less effect lower down.

Nojiri [16] et al. report radially resolved Ca atom and ion absorbance profiles for 3 heights ALC at 1.6 kW and a flowrate of .65 lpm. The atoms are concentrated in the central channel low in the plasma, but the distribution evolves into a bimodal pattern, i.e. lobes are present at the edges of the plasma, at 25 mm ALC exactly as seen in Figure 24. It is somewhat surprising that Nojiri still sees atom absorbance 15 mm ALC at 1.6 kW. This may indicate possible quenching of atom fluorescence in my case.

His ion profiles evolve from a narrow central feature at 7 mm ALC to a broad, flat distribution at 25 mm ALC. Ion density is greatest at 7.5 mm in his case which is different from what is observed both in this work and by Rybarczyk [15]. The discrepancy could be explained by quenching low in the plasma in a fluorescence measurement, but absorbance is not subject to any such effect. Recall that the torch used for the work discussed in this chapter (and in Chapter 2) was positioned somewhat lower with respect to load coil than is normal. It will be seen that

Nojiri's ion results correlate much better with the MAK torch plasma profiles (Chapter 5). Perhaps the difference then, lies in torch design or torch positioning within the load coil.

Kornblum [27] reported Ca atom density profiles at two flowrates. Even at the lower flowrate, his Ca atom profiles retain a single central feature at an observation height of 30 mm. This is contrary to both my results and those in reference [16] and perhaps is symptomatic of the high flowrate employed.

Overall then, nothing in the literature seriously contradicts the results of this work although no other comparable studies of the effect of flowrate exist.

#### F. Summary and Conclusions

At 1 lpm, a clear picture of a spatially extensive, slowly recombining analyte plasma can be painted from the data presented in Figures 22 and 24. Ground state ions are prevalent under a wide range of operating conditions and observation heights compared to ground state atoms. The same is true for both Ca and Sr although given their similar energy level structures this is not too surprising.

From these fluorescence profiles alone it is difficult to deduce the situation on and off axis close to

the load coil (i.e. 9 and 13 mm ALC) regarding the distribution of analyte among its various energy states. There is a possibility that electron quenching colors the fluorescence results in this region, as power increases. Studies necessary to clarify the picture lower in the plasma include various density measurements, ICP-MS investigation and fluorescence lifetime/thermally assisted fluorescence studies.

In any event, higher in the plasma a broad cloud of ground state ions is present at all powers. Ground state atoms, having disappeared close to the load coil, slowly make a comeback higher above the coil, at the edges of the ion cloud. The notion springs to mind that the ICP would be a good ion source for mass spectrometry!

As the flowrate is dropped, the major effect appears to be increased dilution of the analyte (absorbance measurements offer confirmatory evidence that the decrease of fluorescence intensity as flowrate decreases is a real effect). The injected gas expands and mixes with the coolant gas in a more efficient fashion due to an overall increase in the temperature of the plasma and a reduction of the velocity with which aerosol enters the plasma.

Evidently saturated fluorescence was not being observed as illustrated by the presence of prefiltering effects. Future profiling work should be prefaced by an



attempt to saturate the transitions of interest (it may not be possible with the current laser). If density measurements are undertaken, saturated fluorescence is a necessary prerequisite.

As mentioned earlier, further studies with the Fassel-type torch were accidentally curtailed. To assess what if any effects torch design and positioning had on the profiles seen thus far, a replacement torch of a different design was chosen as a successor. Results obtained with this second torch are presented and discussed in the following chapter.

## CHAPTER 5

### FLUORESCENCE RESULTS: MAK TORCH

#### A. Introduction

Following the demise of the Fassel-type torch, fluorescence studies were continued with the widely used Meddings-Anderson-Kaiser (MAK) torch. With this torch the plasma can be sustained at a lower coolant flowrate (4-12 lpm) and hence is less costly to operate. Improved analytical precision is another benefit afforded by use of the "MAK" plasma for emission spectroscopy.

The MAK torch is shown along with a Fassel torch in Figure 42. There is less space between the quartz tubes marked 1 and 2 in the case of the MAK torch, and the injector tube (\*) features a straight bore. The torch was set in the load coil in normal fashion such that the tip of the injector tube was  $\approx 3$  mm below the bottom of the load coil.

The plasma was unstable at powers below .7 kW, hence any power studies done ranged only from .75 to 1.5 kW (in .25 kW increments as before). The same nebulizer was used in both this work and in that detailed in Chapter 4. The range of flowrates remained the same. At an observation

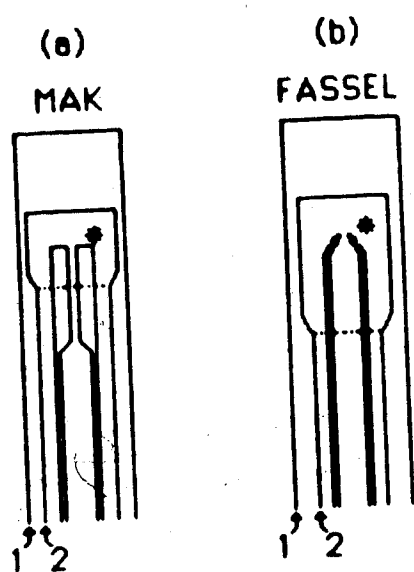


Figure 42. ICP torches: (a) MAK, (b) FASSEL.

height of 9 mm ALC, a strong scattered signal was detected across the width of the torch, even when the plasma was not lit. This was due to reflections off the top of the glass collar used to center the torch within the coil. As a result, the lowest observation height in this work was 10 mm ALC. All other observation heights were the same as in the studies reported in Chapter 4. These and other experimental details are summarized in Table 8.

## B. Ca Ion and Atom Fluorescence

### B.1 Overview

#### B.1.1 1 lpm.

The results of a power study of Ca ion fluorescence at 1 lpm are shown in Figure 43. These profiles on the whole are seen to be narrower than their counterparts shown in Figure 22 (ion fluorescence at 1 lpm, Fassel torch), particularly higher in the plasma. This is illustrated by the plots in Figure 44 where normalized ion fluorescence profiles for the two torches at 19 mm ALC/1.25 kW are presented. Referring back to Figure 43, low in the plasma (10 and 13 mm ALC) at .75 kW, the ions appear to have a toroidal distribution. As power is increased, this "ion doughnut" fills in. This observation was also noted by Rybarczyk in reference [15]. The profiles at 10 and 13 mm ALC grow in size as power

Table 8. Experimental details for Chapter 5.

## Plasma

Coolant (lpm):	12
Auxiliary (1 lpm):	.5
Aerosol Carrier (lpm):	.65, .85, 1
Power (kW):	.75, 1, 1.25, 1.5

Observation Height (mm ALC): 10, 13, 19, 25, 31

## Analyte Concentrations (ppm)

Fluorescence

Ca Atom:	4
Ca Ion:	4
Sr Ion:	2
Ca Excited Ion:	1600

Emission

Ca Ion, Atom:	40
Mo Atom:	100

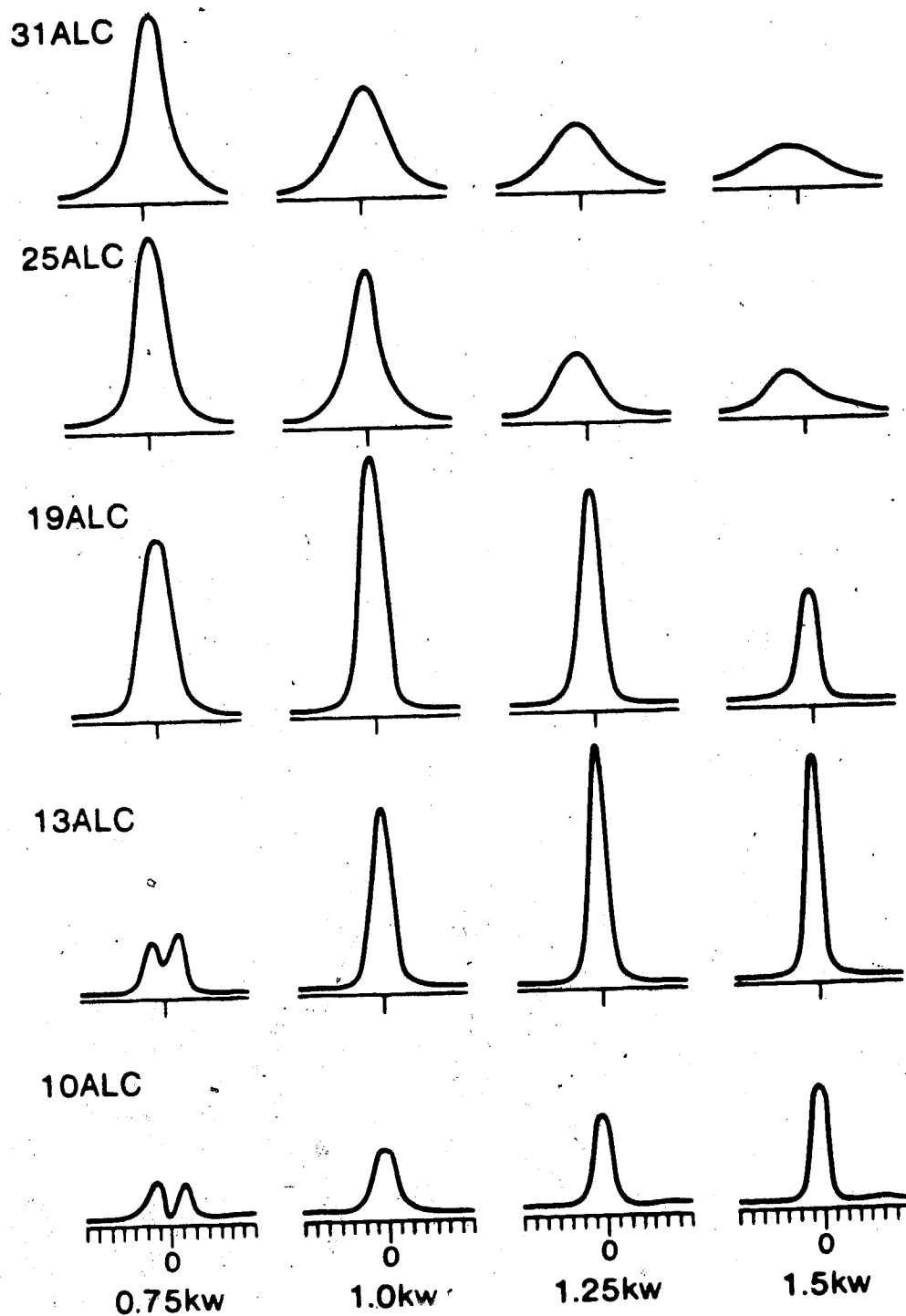


Figure 43. 393.3 nm  $\text{Ca}^+$  fluorescence power study results, 1 lpm - MAK torch.

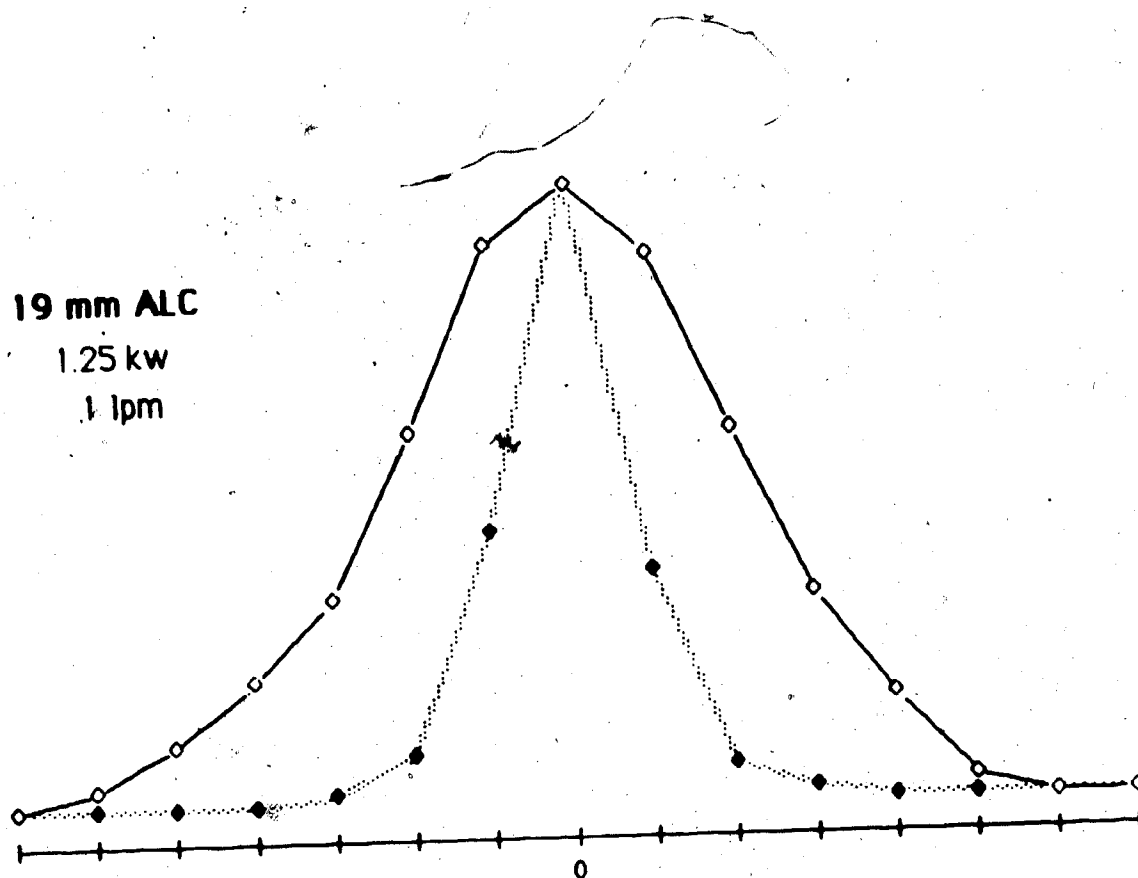


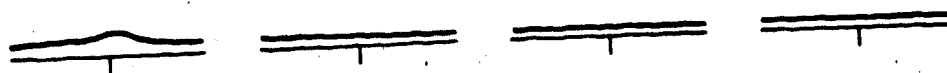
Figure 44. Normalized  $\text{Ca}^+$  fluorescence profiles, 1.25 kW/1 lpm/19 mm ALC. Solid curve: Fassel Torch. Dotted curve: MAK Torch.

increases, in contrast to the trend in behavior exhibited by the corresponding ion profiles taken with the Fassel torch (Figure 22). However, higher in the plasma the profiles decrease in intensity and broaden as power increases, as was seen for the Fassel torch profiles. Finally, high above the load coil, no asymmetry indicative of a possible inner filtering effect is seen at .75 kW. Freedom from inner filtering was verified by determining that fluorescence intensity was linearly dependent on concentration for all the conditions of the 20 frames of Figure 43.

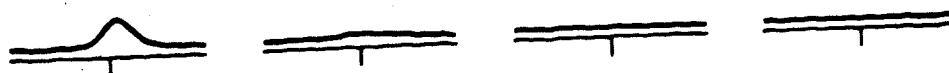
Data from the atom fluorescence power study at 1 lpm is summarized in Figure 45. Evidently the centre of the ion doughnut (.75 kW, 10 and 13 mm ALC, Figure 43) is filled with atoms. A central atom fluorescence feature persists even at 19 mm ALC. The atom lobes which appear higher in the plasma using the Fassel torch (Figure 24) seem to be absent from the data shown in Figure 45. A five-times-magnified view of a portion of the data from Figure 45 appears in Figure 46. As can be seen in this figure, lobes are just appearing at 31 mm ALC. In Chapter 4, the size of the atom lobes was correlated to the width of the corresponding ion profiles. Here as well, the overall narrower ion profiles observed with the MAK torch are most likely responsible for the absence of atom



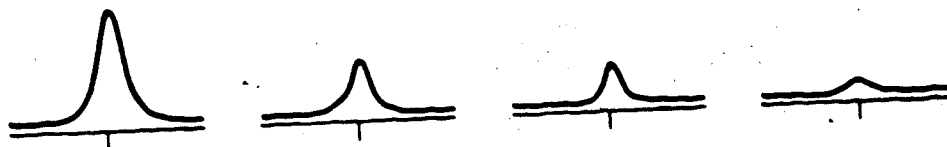
31ALC



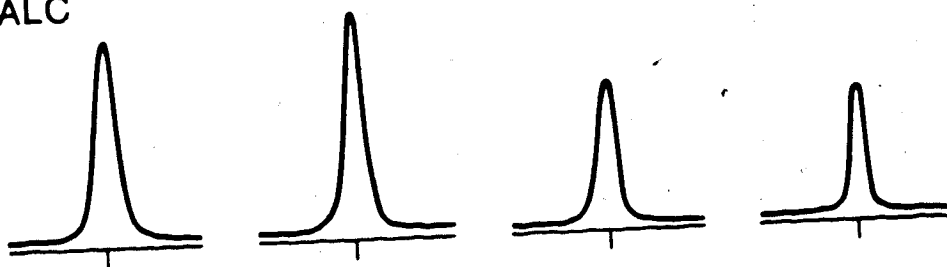
25ALC



19ALC



13ALC



10ALC

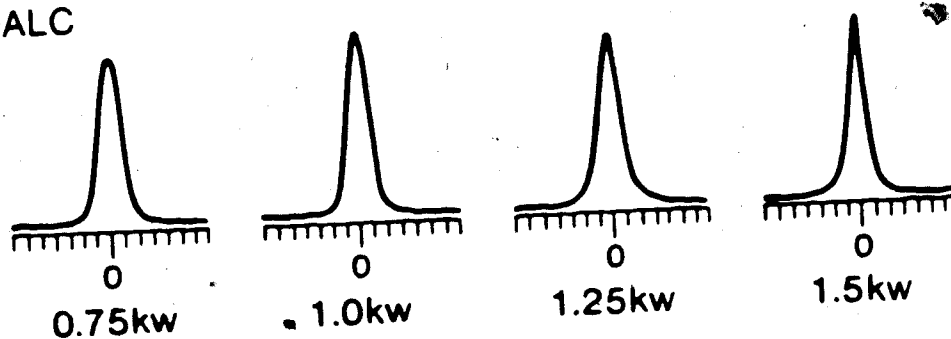


Figure 45. 422.7 nm Ca atom fluorescence power study results, 1 lpm  
- MAK torch.

31ALC



25ALC



19ALC

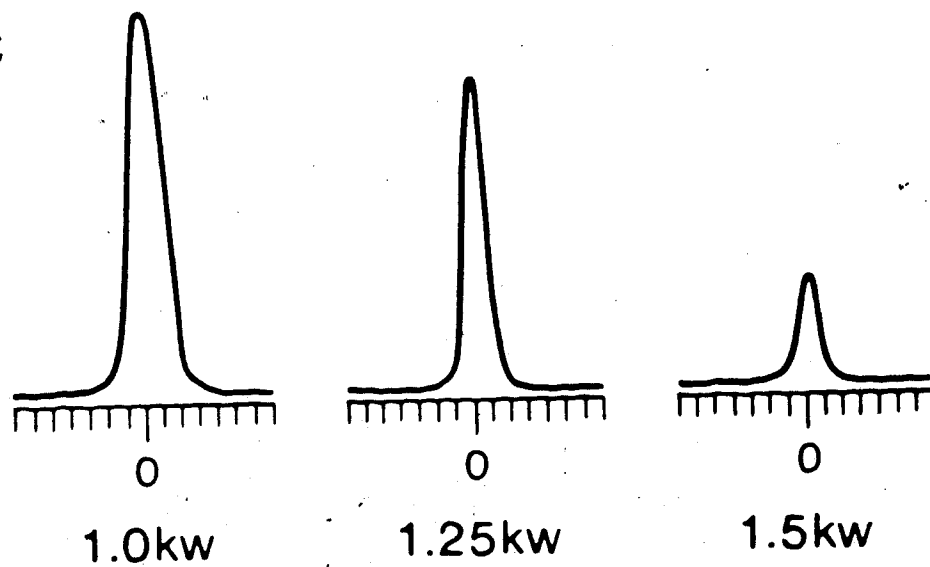


Figure 46. Magnified view of a portion of Figure 45.

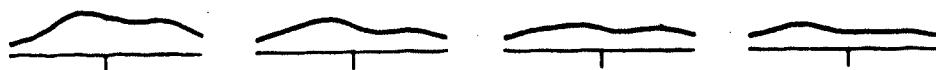
lobes. The fact that the profiles are all roughly the same size at 10 mm ALC (in Figure 45) could be an indication of inner filtering. However, repeat sets of profiles at this height, as well as profiles at a concentration of 1 ppm indicated that while the profile at 1.25 kW should probably be slightly larger than it appears, inner filtering does not appear to be a significant factor.

#### B.1.2 .85 lpm.

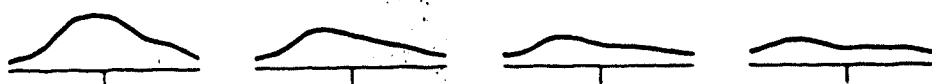
The ion fluorescence profiles above 13 mm ALC broaden and shrink noticeably when the flowrate drops to .85 lpm. This is seen when the data in Figure 47 (ion fluorescence at .85 lpm) is compared back to Figure 43 (ion fluorescence at 1 lpm). The distribution of ions at .75 kW is no longer toroidal. A trend established low in the plasma at 1 lpm reverses itself at .85 lpm, i.e. ions now tend to disappear as power increases.

Nojiri's [16]  $\text{Ca}^+$  absorbance results are duplicated quite closely by the column of  $\text{Ca}^+$  fluorescence profiles at 1.25 kW in Figure 47 (.85 lpm). (Recall that he had seen a narrow ion absorbance profile low in the plasma (7.5 mm ALC) broaden and shrink in height as the observation height increased to 25 mm ALC.) This same type of behavior was also exhibited by  $\text{In}^+$  radial profiles obtained by ICP-MS [4]. Hence these MAK torch profiles

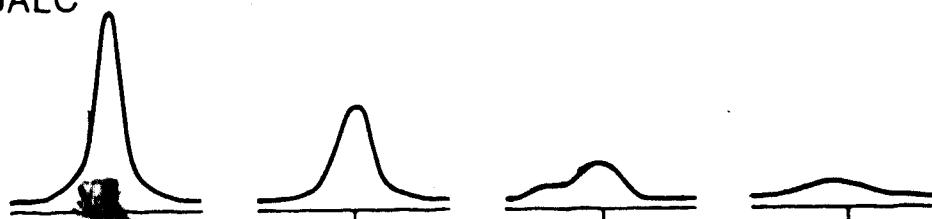
31ALC



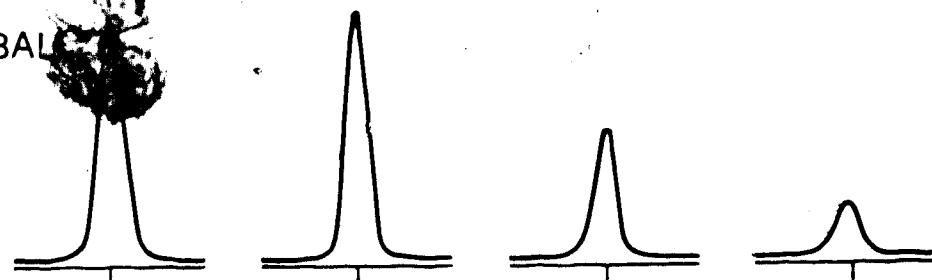
25ALC



19ALC



13ALC



10ALC

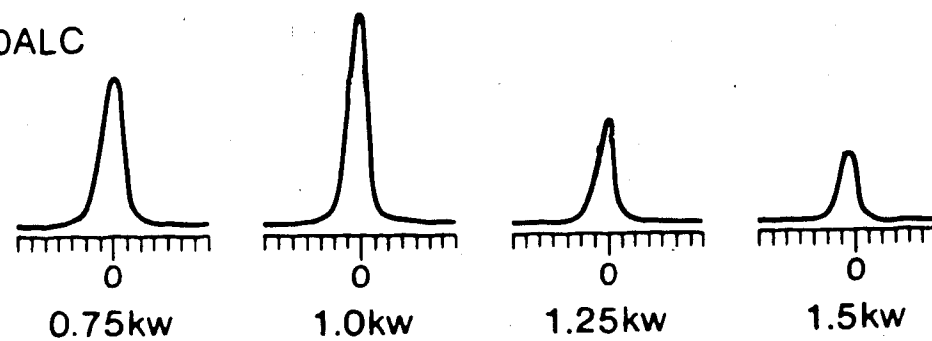


Figure 47. 393.3 nm  $\text{Ca}^+$  fluorescence power study results, .85 lpm - MAK torch.

agree well with what little other data is in the literature.

An experiment done at .85 lpm to assess the extent of saturation of fluorescence at 393.3 nm should be discussed at this point. The variation, with laser power, of fluorescence intensity in the central channel 13 mm ALC at a power of 1.25 kW was observed. The laser power was varied by increasing the potential difference across the lasing channel. As shown by the plot in Figure 48, fluorescence intensity varies linearly over the range of powers used, indicating that the fluorescence is not saturated under these conditions (if one assumes that laser power is a linear function of electrode voltage). The same is probably true overall since plasma conditions have less effect on the phenomenon than the physical and temporal properties of the laser pulse.

If at some point the optical configuration is changed so that the dye beam is more tightly focussed, thereby improving the chances of saturation, a measurement of the incident laser power as a function of channel electrode voltage should be made. If this function is linear and the intensity of fluorescence is observed to roll off as channel voltage is increased, one could be more certain that saturation is occurring. Alternately, a series of filters could be employed to vary the beam power.

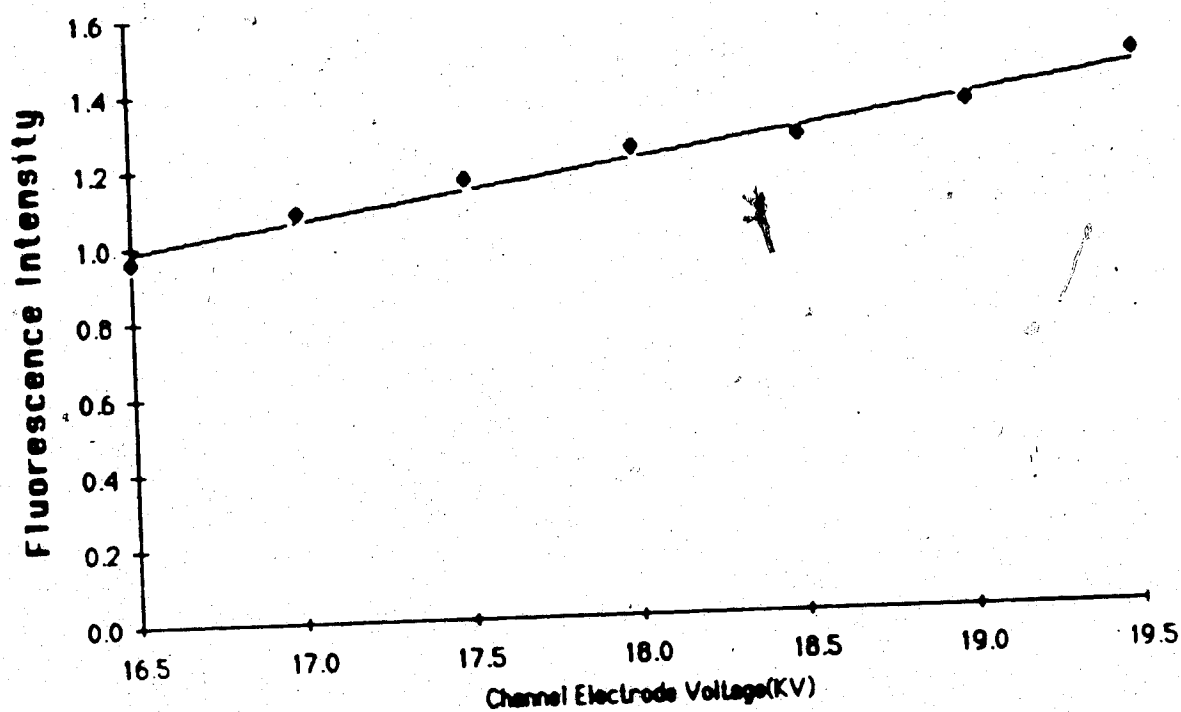


Figure 48. Dependence of  $\text{Ca}^+$  fluorescence intensity (13 mm ALC, .85 lpm/ 1.25 kW) on laser channel electrode voltage. Straight line is a least-squares best fit to the experimental results.

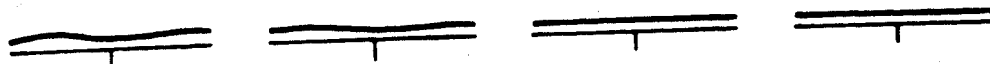
Moving on, the effect of a drop in flowrate (to .85 lpm) on Ca atom fluorescence is illustrated in Figure 49. The atom profiles retain the basic shape shown in Figure 45 (Ca atom fluorescence 1 lpm) although the plasma above 10 mm ALC appears almost devoid of atoms at all powers. A 400 ppm Ca solution gave the profiles shown in Figure 50. The lobes are there, they are just very much smaller in the MAK torch plasma. Note that at 31 mm ALC increasing the power spreads the lobes farther apart.

#### B.1.3 .65 lpm.

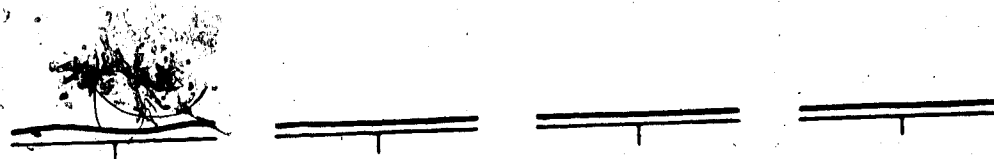
The ion fluorescence power study results at .65 lpm are summarized in Figure 51. For the most part ground state ions have disappeared from the plasma relative to 1 lpm. Curiously, the ion profiles higher in the plasma exhibit faint lobes much as did the other atom profiles when magnified.

A single map of atom fluorescence is shown in Figure 52, containing profiles at .75 kW for a .65 lpm carrier flowrate. Atom fluorescence has virtually disappeared even at this power setting. However, Ca atom fluorescence profiles for a 40 ppm Ca solution and a 1000  $\mu$  slit show that lobes are present (Figure 53).

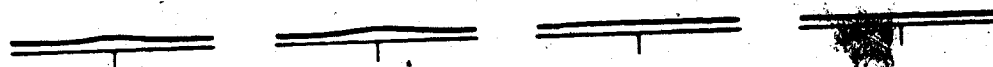
31ALC



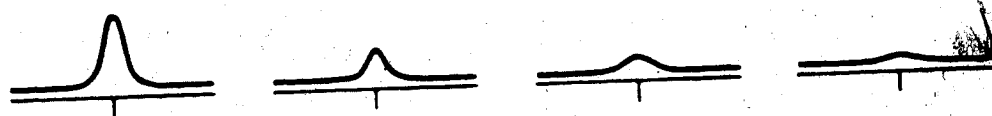
25ALC



19ALC



13ALC



10ALC

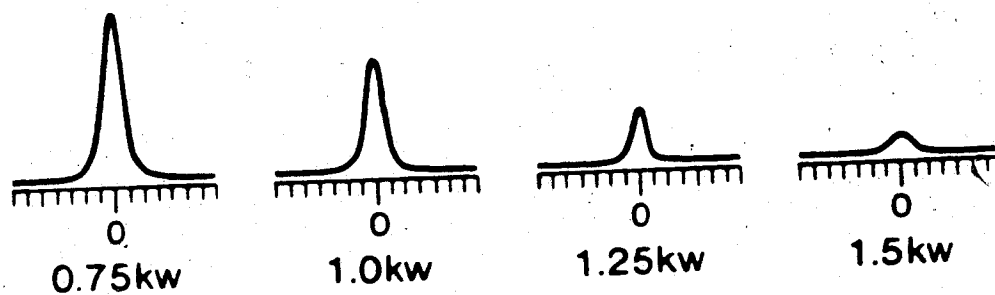
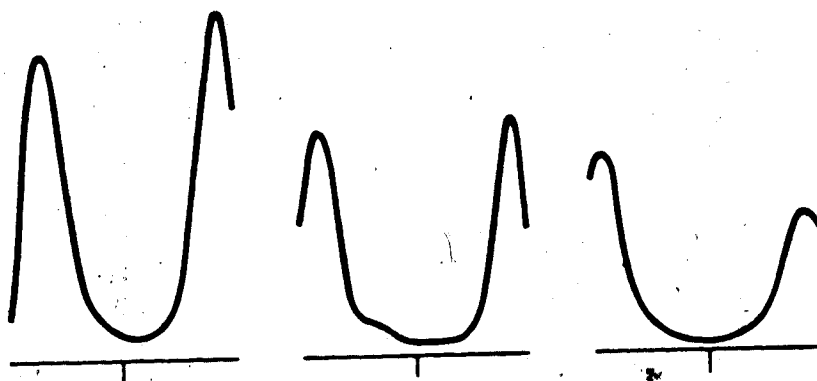


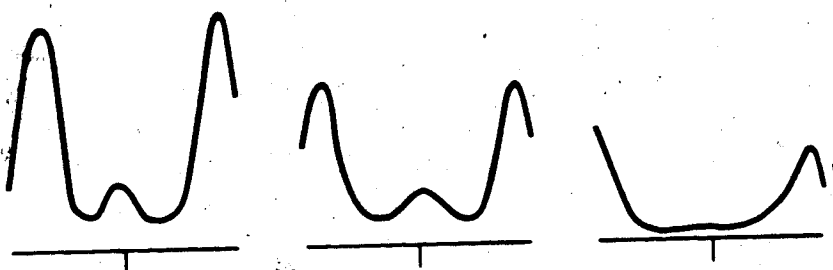
Figure 49. 422.7 nm Ca atom fluorescence power study results - .85 lpm - MAK torch.



31ALC



25ALC



19ALC

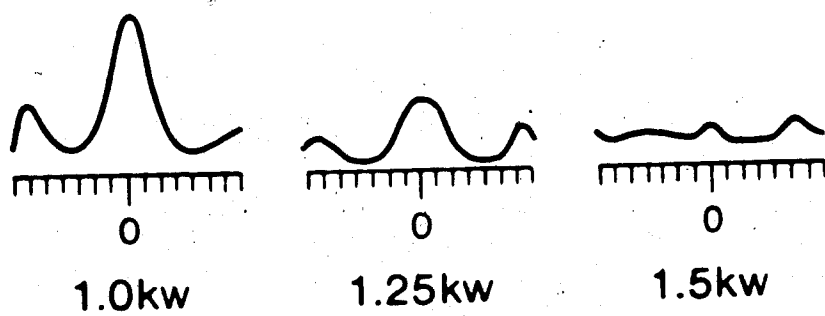
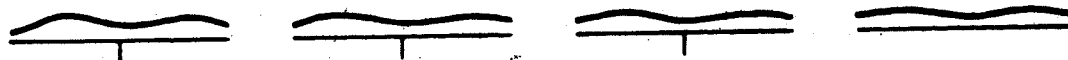


Figure 50. Magnified view of a portion of Figure 49.

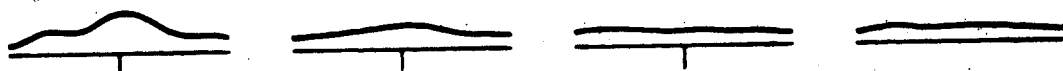
31ALC



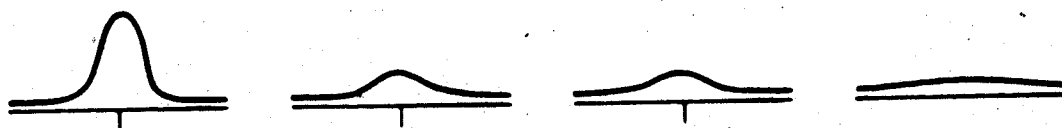
25ALC



19ALC



13ALC



10ALC

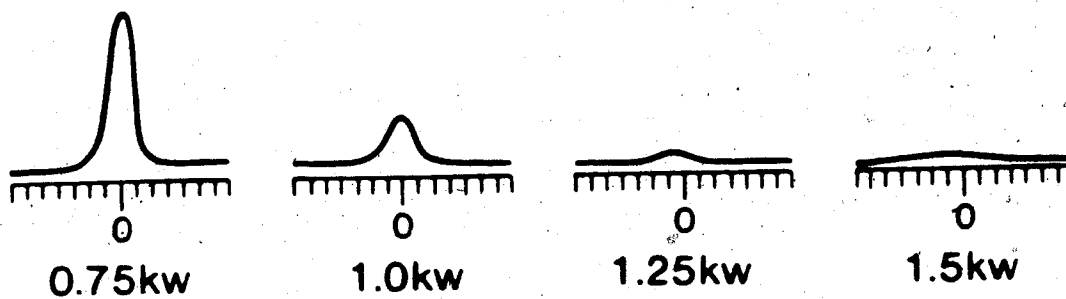
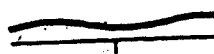


Figure 51. 393.3 nm  $\text{Ca}^+$  fluorescence power study results, .65 lpm - MAX torch.

31ALC



25ALC



19ALC



13ALC



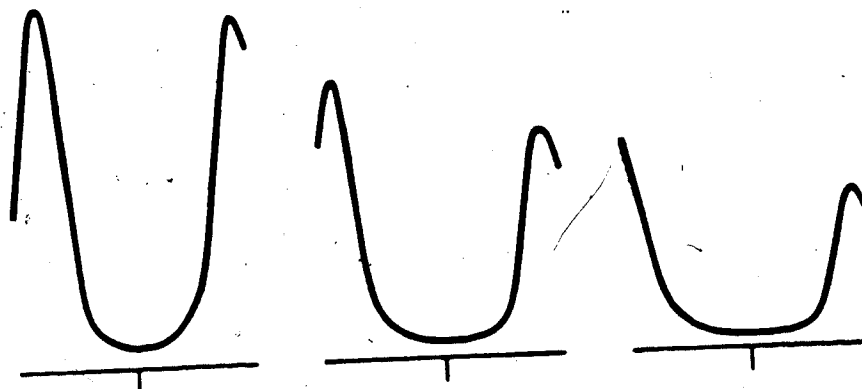
10ALC



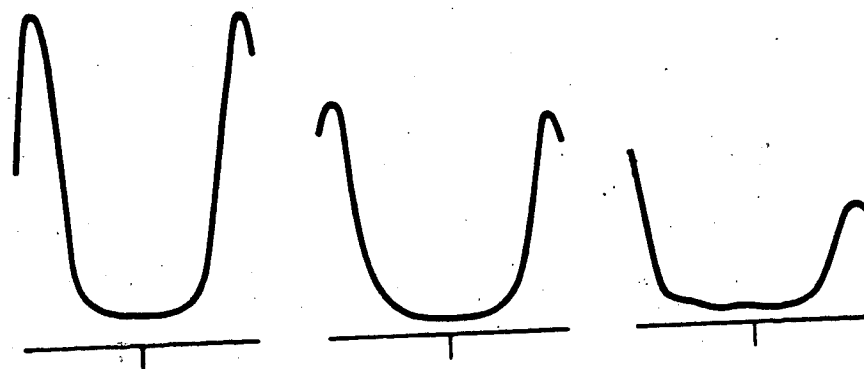
0.75kw

Figure 52. 422.7 nm fluorescence map, .65 lpm/.75 kW - MAX torch.

31ALC



25ALC



19ALC

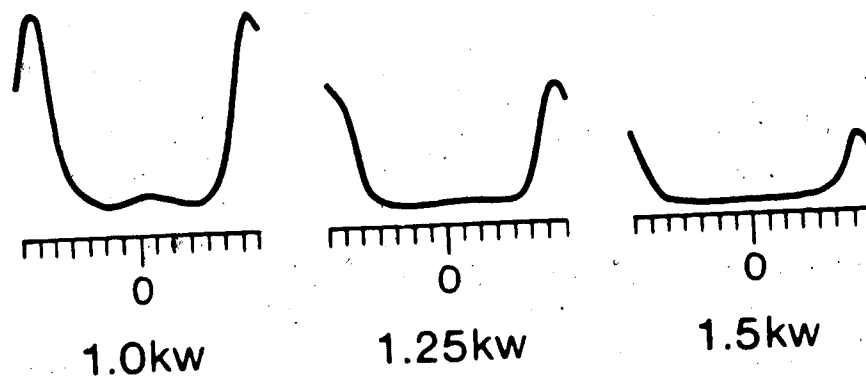


Figure 53. Results of partial power study of 422. nm Ca atom fluorescence (40 ppm/1000  $\mu$  slit) .65 lpm - MAK torch.

## B.2 Discussion

The data presented thus far is summarized in Figure 54. In a given frame, ion or atom fluorescence as a function of power for the 5 observation heights is plotted. Flowrate decreases as one goes down the figure. Ion fluorescence is seen on the left side, atom fluorescence on the right. This figure is directly comparable to Figure 39, which summarizes the results obtained with the Fassel torch. Although the two figures are dissimilar at 1 lpm (compare frames (a) and (d) in each of Figures 39 and 54) they become more similar as flowrate drops. A large decrease in the intensity of both ion and atom fluorescence is seen (relative to 1 lpm) as the flowrate drops.

Focussing on 1 lpm, it is seen that at the lowest observation heights, the atom fluorescence signals for the MAK torch plasma (frame (d) in Figure 54) are much less responsive to an increase in power than the corresponding signals for the Fassel torch plasma (frame (d), Figure 39). Comparing frame (a) in the two figures, the ion fluorescence signal at low observation heights is seen to increase much more slowly as power increases for the MAK torch plasma.

Evidently the lower region of MAK torch plasma at 1 lpm is much cooler than in the other plasma. This is

## Ion Fluorescence

## Atom Fluorescence

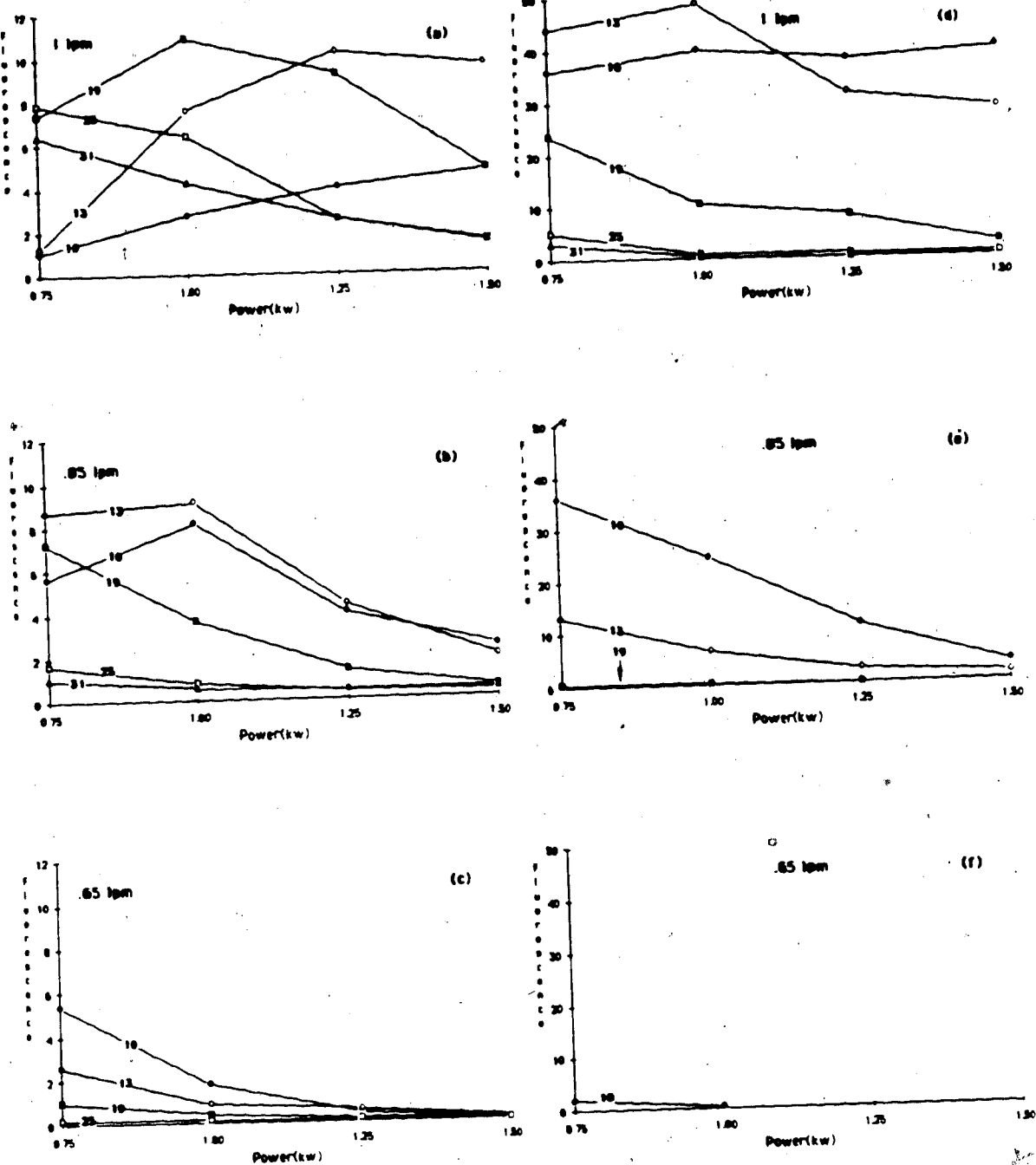


Figure 54. Ca ion and atom fluorescence as a function of power at 3 flowrates (same format as Figure 39) - MAK torch.

supported by the additional observation that the scattering signal obtained from  $H_2O$  in this region at low power was much stronger in the case of the MAK torch plasma. In fact it could be detected at 1.5 kW.

Although there was some difference in the way the torches were positioned within the load coil, the main cause of the different behavior seen with the MAK torch at 1 lpm can likely be ascribed to the straight-bore injector tube. The sample aerosol presumably is injected into the plasma in a collimated stream whereas a more conical spray pattern could be expected to issue from the injector tube on the Fassel torch. Presumably there is less interaction of the injected gas with the interior of the energy addition zone (within the load coil) in the MAK torch plasma, so the overall process of getting the analyte into a "useful" form is delayed.

The MAK torch profiles at 1 lpm are probably narrower because the analyte is still confined in a tight stream, not because of any explanation such as quenching or formation of doubly charged species. Of course eventually the injected gas has to expand and so the profiles higher in the plasma become broader.

As the flowrate drops, the heating of the injected gas must be rapid enough to override any difference between the sample streams for the two torches, so the

same dilution and resultant loss of ion fluorescence occurs. A general loss of ground state ion fluorescence as flowrate drops was independently confirmed by absorbance measurements for the Fassel torch. Absorbance data was not available for the MAK torch, but an experiment was performed whereby a reasonably direct comparison of fluorescence results and mass spectroscopic results could be made.

### B.3 Comparison to ICP-MS Results

The SCIEX-ELAN® ICP-mass spectrometer in our laboratory has limited capability to sample off-axis regions of the discharge, hence the same sort of radial profiling as for fluorescence could not be done with the instrument. Instead, at 19 mm, the  $\text{Sr}^+$  count rate was measured as a function of power and carrier flowrate ( $^{40}\text{Ca}^+$  cannot be measured due to a  $^{40}\text{Ar}^+$  overlap) using a MAK torch. The  $\text{Sr}^+$  fluorescence intensity in the central channel as a function of power and flowrate was then measured for observation heights bracketing 19 mm ALC. The results of the two studies are represented in Figure 55 where fluorescence (a) or ion count (b) as a function of flowrate is plotted for 4 powers. The flowrate axes, though nominally comparable, are not exactly superimposable. It is necessary to slide one plot relative to the other, but the same trends are evident in



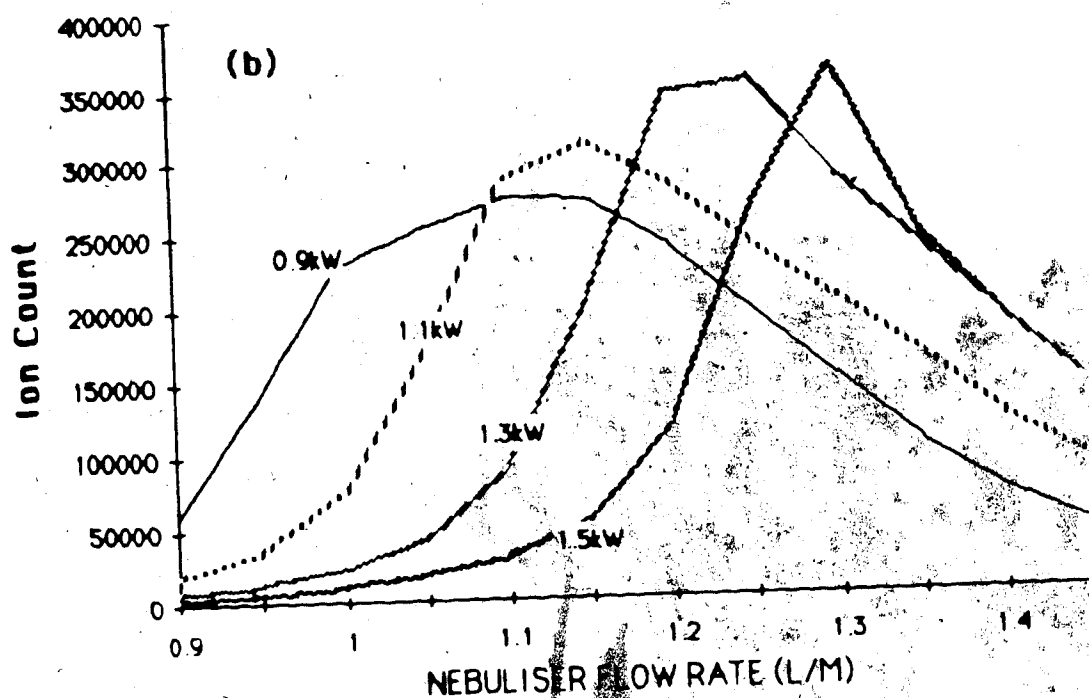
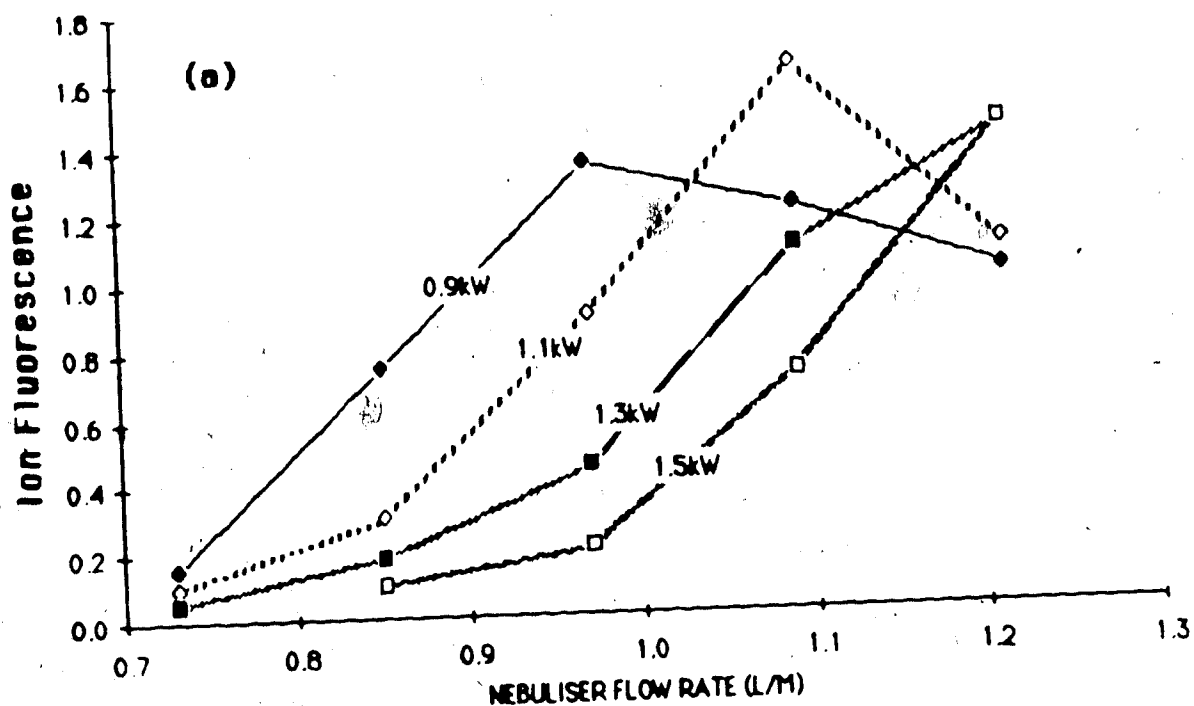


Figure 55. Results of a study of the response of ground state  $\text{Sr}^+$  behavior to changes in carrier flowrate in the zone 17 to 19 mm ALC (MAX torch). (a)  $\text{Sr}^+$  fluorescence intensity in the central channel - 17 mm ALC, (b)  $\text{Sr}^+$  count rate - 19 mm ALC.

both cases. This tends to rule out an apparent loss of ground state  $\text{Ca}^+$  due to fluorescence quenching. Either both techniques are yielding accurate information, or both techniques are in error. If both are in error, it is unlikely that they would err in exactly the same fashion under the wide range of conditions employed. If one supposes that the fluorescence data is accurate (this being backed up by absorbance results) then from the mass spectrometrists' side of the fence, it appears that a representative sample of the plasma is being taken.

### C. Lateral Emission Profiles

Once it was realized that the gated integrator could also be used to measure emission (as outlined in Chapter 3), sets of lateral emission profiles were acquired, although it was seen in Chapter 4 that 393.3 resonance fluorescence did not correlate very well with 393.3 nm emission ( $\text{Ca}^+$  ion). However, the effect of power and flowrate on radial (or lateral) emission profiles has only been looked at in two rather limited studies [11,41] so these results may be useful in their own right.

## C.1 Overview of Emission Results

### C.1.1 Ion Emission (1 lpm)

The results of a power study of  $\text{Ca}^+$  emission at 393.3 nm are portrayed in Figure 56. Any given profile consists of a set of lateral or line-of-sight average values of emission intensity. Abel inversion of these profiles to convert them to radial emission profiles was deemed to be unnecessary for the purposes of this study.

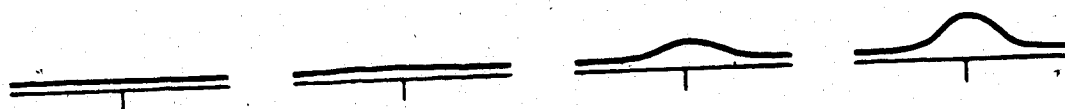
What is most striking about the data shown in Figure 56 is the restriction of ion emission to a rather limited set of conditions whereas ground state ions are prevalent over a much wider range of conditions as shown in Figure 43 (power study of ion fluorescence). This is particularly true higher in the plasma. For example, at or above 19 mm ALC little or no emission is seen at .75 kW and 1 kW in Figure 56 but corresponding ion fluorescence profiles (Figure 43) are large. The lack of correlation between the two figures illustrates the point made in reference [5] that attempts should not be made to draw analogies between optical emission and mass spectrometric studies of the LCP.

The ion emission and fluorescence data shown in Figures 56 and 43 is summarized by presenting vertical ion emission and fluorescence profiles at different powers in Figure 57. The differing power dependencies of the ground

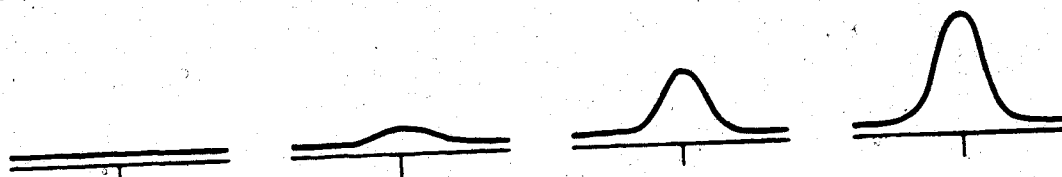
25ALC



19ALC



13ALC



10ALC

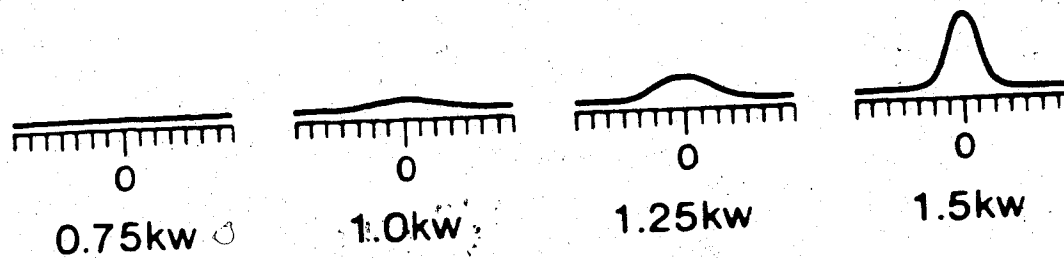


Figure 56.  $393.3 \text{ Ca}^+$  emission power study results at 1 lpm - MAX torch.

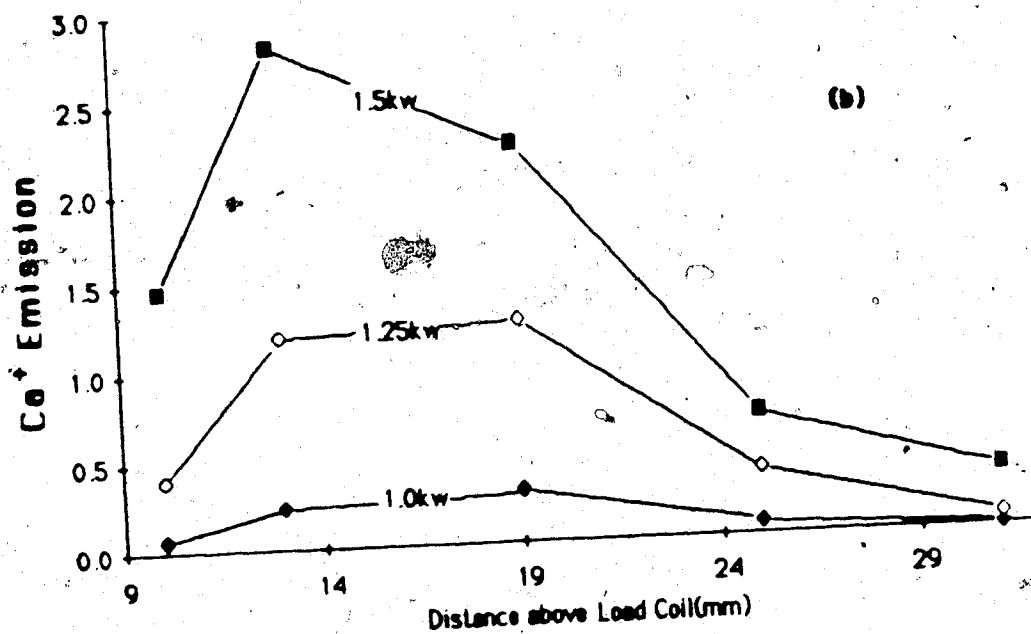
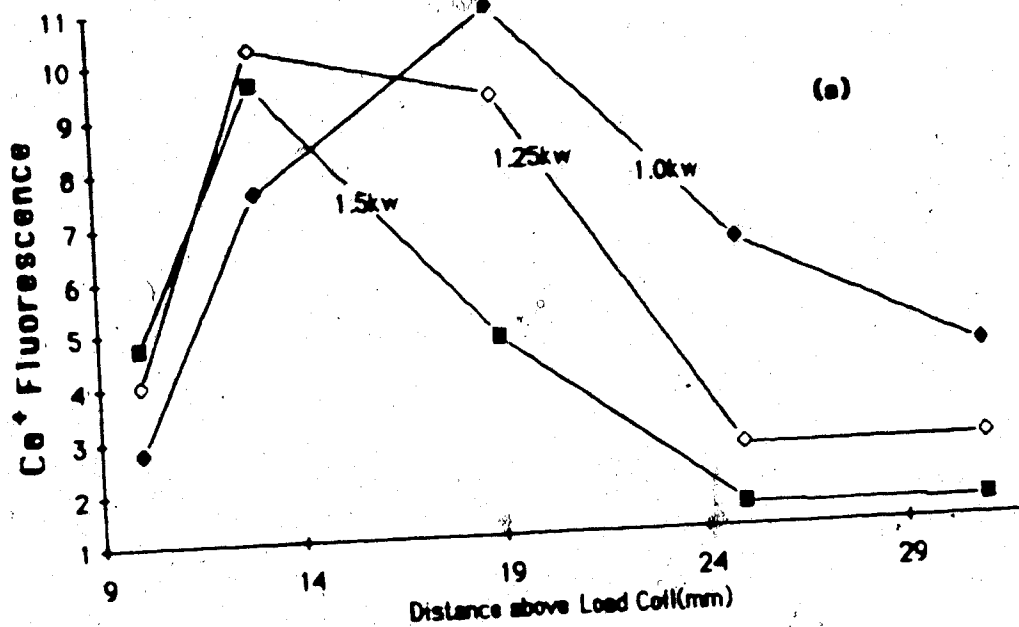


Figure 57.  $\text{Ca}^+$  vertical profiles (1 lpm). (a) 393.3 nm fluorescence, (b) 393.3 nm emission - MAK torch.

state and excited ions are emphasized by these plots. When power is changed, the same fluorescence signal (or close to it) can be recovered by looking in a different zone of the plasma (frame (a)), while emission is simply directly dependent on power at all observation heights (frame (b)).

Some idea of the relative population of the 3.1 eV  $\text{Ca}^+$  level and the ground state ion level can be had from comparing emission and fluorescence profiles as a function of power at an observation height of 19 mm ALC. These profiles are presented in Figure 58. Although a decrease in fluorescence is linked to an increase in emission, the integrated emission increases by several orders of magnitude as power increases whereas the decrease in integrated fluorescence is on the order of a factor of 2. Hence the 3.1 eV excited ion level population is likely small with respect to ground state ion population.

#### C.1.2 Atom Emission (1 lpm)

The results of a power study of Ca atom emission at 422.7 nm are presented in Figure 59. The flat topped profile at .75 kW/10 mm ALC would exhibit a central depression if Abel inverted. These profiles can be compared to the ground state atom fluorescence profiles in Figure 45. At .75 kW the emission profiles are somewhat broader than their fluorescence counterparts, but overall

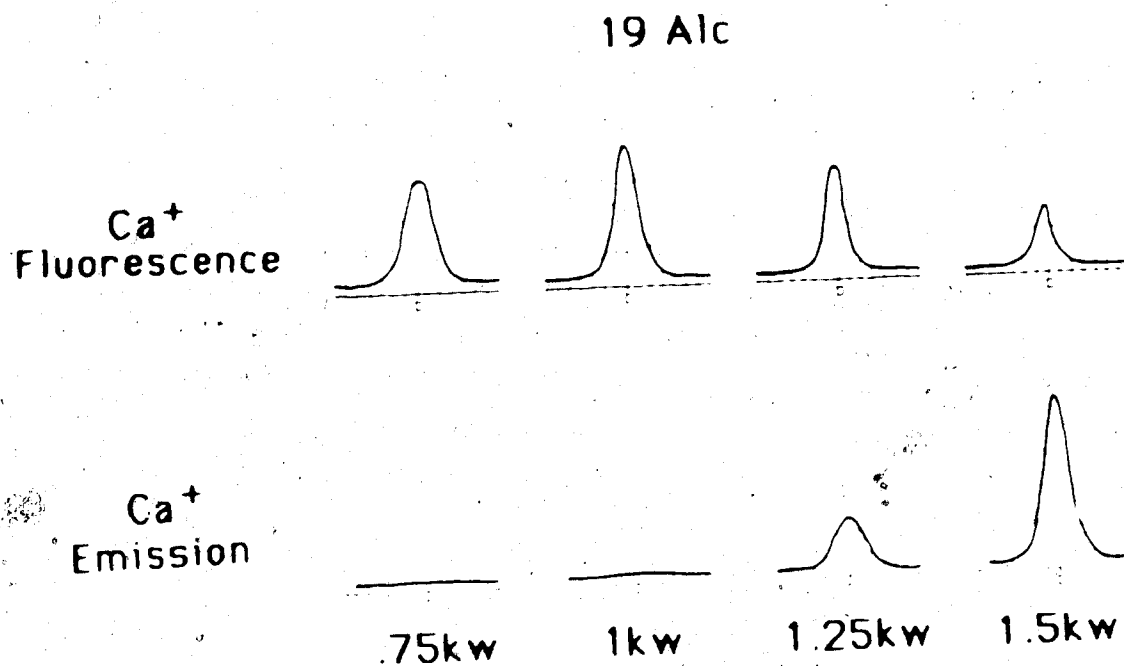
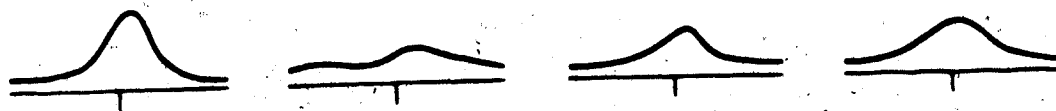
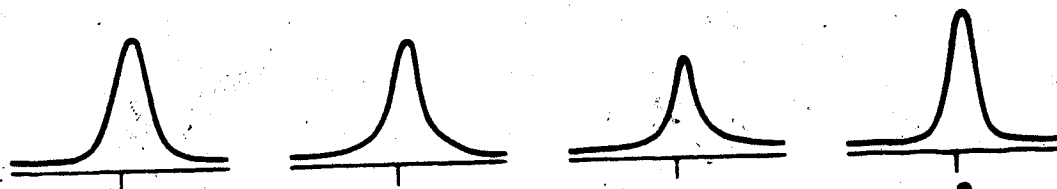


Figure 58. Ca<sup>+</sup> fluorescence and emission profiles at 393.3 nm for 4 powers at an observation height of 19 mm ALC (1 lpm) - MAX torch.

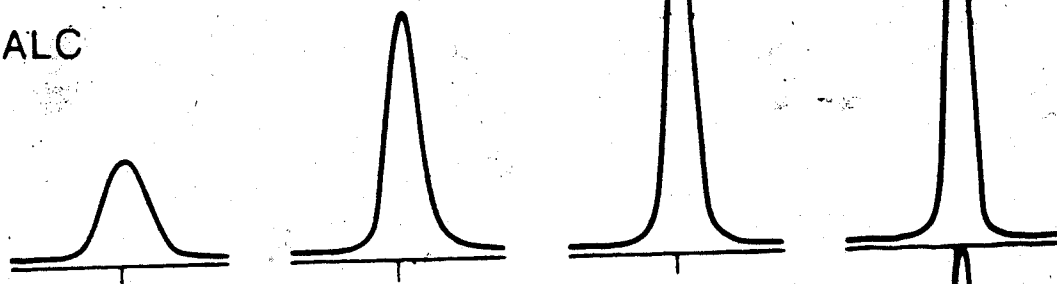
25ALC



19ALC



13ALC



10ALC

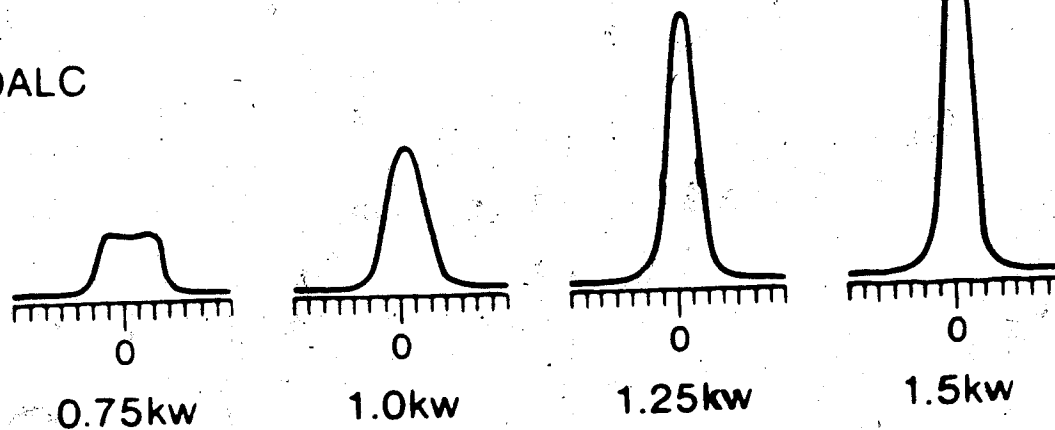


Figure 59. 422.7 nm Ca atom emission power study results, 1 ppm -  
MAK torch.

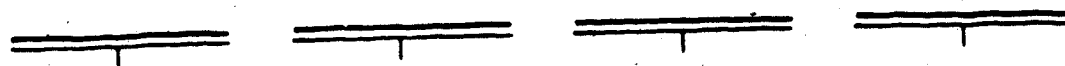


both atom emission and fluorescence are restricted to the central channel low in the plasma. However, Ca atom emission profiles do not seem to "track" ground state Ca atom fluorescence profiles at all in terms of changes in the peak heights as power changes. As will be seen later, the atom emission profiles follow the ground state ion fluorescence profiles more closely.

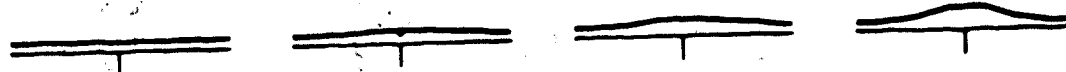
### C.1.3 Ion Emission (.65 lpm)

The flowrate was dropped to .65 lpm and a power study of  $\text{Ca}^+$  emission was done. The results are depicted in Figure 60. Although no emission has appeared for the observation heights represented in the upper part of the figure, for the other conditions (power, observation height) devoid of emission in Figure 56 (1 lpm power study) the emission has shown an increase as the flowrate was decreased (compare the bottom 3 rows of Figures 56 and 60). A puzzling aspect regarding the ion emission is shown in Figure 61. Here the effect of flowrate on  $\text{Ca}^+$  emission and fluorescence at 19 mm ALC is seen (at the 4 powers). Calcium ion fluorescence at all powers is seen to vanish when the flowrate drops to .65 lpm whereas ion emission drops by only a factor of 2. One might expect to see a larger decrease in ion emission if the ion ground state population is dropping drastically.

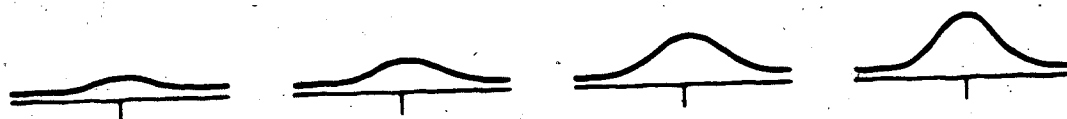
31ALC



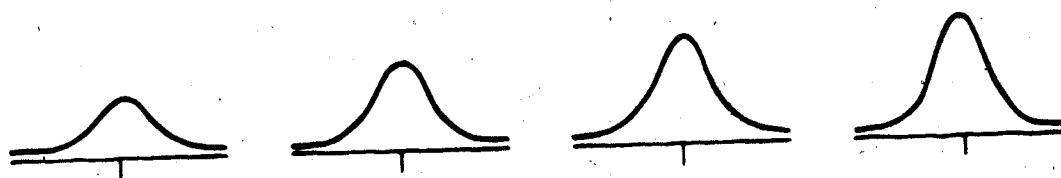
25ALC



19ALC



13ALC



10ALC

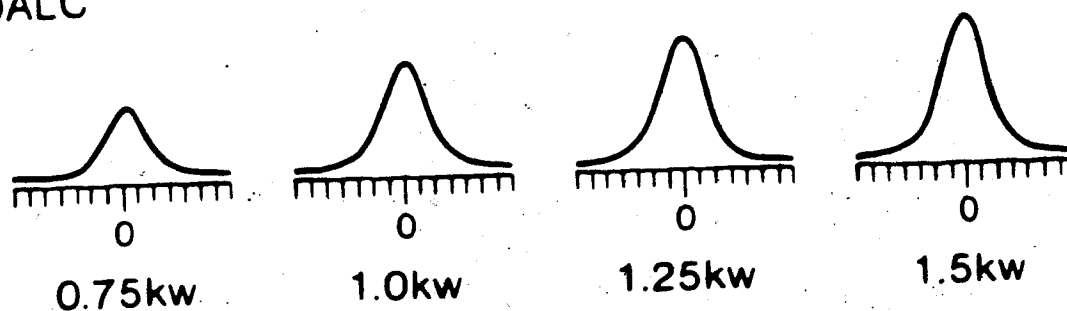


Figure 60. 393.3 nm Ca ion emission power study results, .65 lpm - MAK torch.

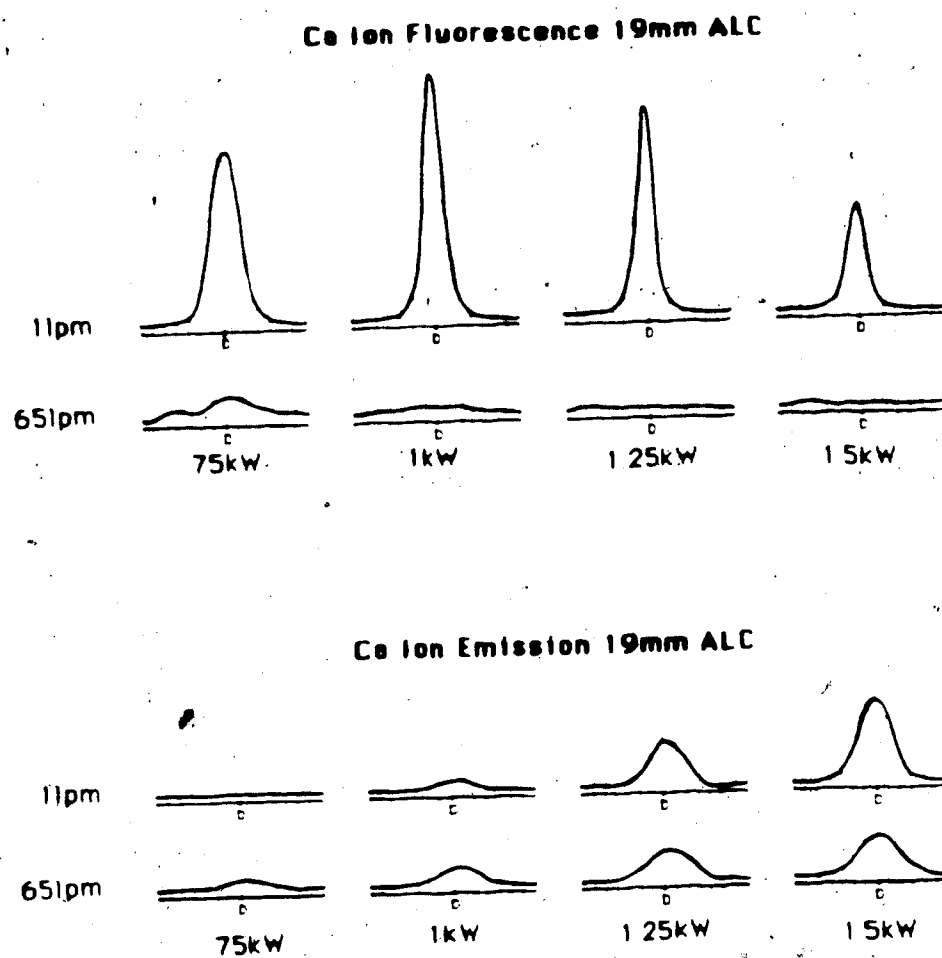


Figure 61. Response of  $\text{Ca}^+$  fluorescence and emission to a decrease in flowrate at 19 mm ALC, 4 powers - MAK torch.

#### C.1.4 Atom Emission (.65) lpm

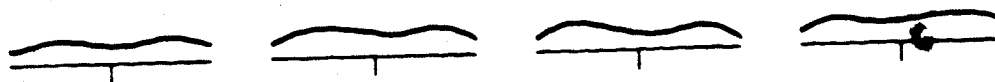
Finally, data from a Ca atom emission power study at .65 lpm is summarized in Figure 62. Here the profiles are somewhat broader with a lower maximum height than the corresponding Ca atom emission profiles at 1 lpm (Figure 59), particularly higher in the plasma. Both these profiles and the set of ion emission profiles in Figure 60 are now much more uniform, i.e. they do not respond as dramatically to changes in power and observation height. For example, as one goes across (a) in either Figure 62 or 60, changes are no greater than a factor of 2 and in many cases no change is observed.

#### C.2 Discussion

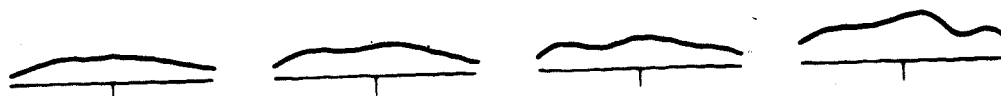
Recall the observation that while  $\text{Ca}^+$  emission at 1 lpm was restricted to a small range of conditions (see Figure 56), large fluorescence signals were observed for most experimental conditions as shown in Figure 43. To give some insight into these observations, it is useful to refer to the energy level diagram in Figure 30 for the following discussion.

With reference to that figure, attention is drawn to the tightly packed energy levels immediately beneath the first ionization limit (i.e. the high lying excited atomic levels). In an environment where energetic electrons exist (for example in the ICP), it is quite likely that a

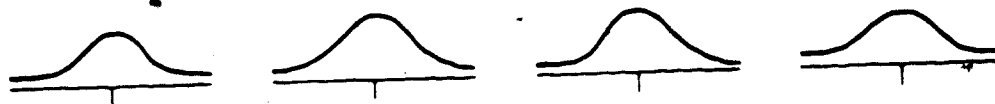
25ALC



19ALC



13ALC



10ALC

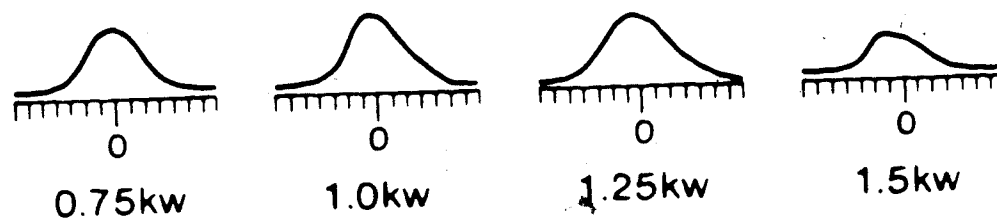
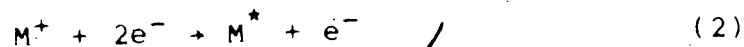
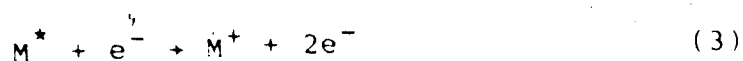


Figure 62. 422.7 Ca atom-emission power study results, .65 lpm - MAX torch

ground state ion will be taken down into the closely spaced levels beneath it by collision with electrons as in Equation (2).



However the chances are also good that some other excited atom will take its place via Equation (3).



This is true even if the average electron energy is low, say on the order of .2 eV. A high population of ground state ions can be maintained under these conditions since a given ion can be thought of as making a series of short "trips" into and out of the excited atom levels, none of which require that much energy be gained or lost.

With this same low electron energy, collisions which successfully excite ground state ions are not frequent due to the large energy gap involved, so excited ion levels will remain sparsely populated. Hence a large ground state ion population can be maintained under conditions where ion emission is very weak.

Even if the average electron energy is higher, the population of a low-lying excited level (ion or atom)

which is strongly coupled to its ground state by a radiative transition can be depleted if the electron density is not high. Normally a species in the plasma is more likely to suffer a collision with an electron before either absorbing or emitting a photon. However as electron density drops, the collision rate and the rates of these radiative processes become more comparable.

Hence radiative effects can then influence the overall steady state population of an excited level. In other words, the steady state population of the excited level is determined by the balance of populating and depopulating collisions and by the balance of emission and absorption of photons when the electron density is low. In the ICP, photons have a good chance of escaping from the plasma (into the jaws of waiting monochromators) since the emitting region is physically small, so the radiative processes do not balance. An underpopulation of the excited level due to this effect can result at lower electron densities.

In light of the foregoing discussion then, by consideration of how the electron density and electron temperature (average electron energy) might vary as power and observation height vary, some understanding of the behavior seen in Figure 56 (ion emission power study, 1 lpm) can be gained. For example, as mentioned in the

introductory chapter, once a volume of plasma flows away from the coil, it starts to decay or lose energy. The electrons lose energy to the heavy particles although the electrons do not recombine very fast. Thus the low intensity of emission high in the plasma might be due to a low electron temperature, although the electron density is still high. It was just discussed that a large ground state ion population could still be maintained under these conditions.

Close to the load coil emission intensity may be linked to a lower degree of dissociation of analyte-containing species at 1 lpm. Also as discussed earlier, the electrons are cooled as they penetrate the central channel so weak emission intensity is again expected on the basis of low electron temperature. At .75 kW, the electron density may be low enough so that radiative depletion of the 3.1 eV excited ion level also becomes significant.

When the flowrate was dropped, there were several interesting observations. One was that ion emission intensity increased markedly for powers and observation heights where it was previously low. Another was that there did not seem to be a correlation between the large drop in fluorescence intensity and the response of the emission profiles (Figure 61).



It is known that as flowrate drops, the electron density in the central channel increases [24]. The central channel is also observed to be hotter, particularly low in the plasma. In this region then, an increase in emission intensity might be understood on the basis of less radiative depletion (due to the increase in electron density) and an increase in electron temperature. The behavior in Figure 61 might be rationalized on the basis of an increase in temperature.

If we assume the total ion population density in the central channel at 19 mm ALC/1.5 kW drops from  $10^{12} \text{ cm}^{-3}$  to  $10^{11} \text{ cm}^{-3}$  as flowrate drops, due to dilution, then the percentage of total ion population in the 3.1 eV level need only change from 0.3% to 1.5% to yield an overall factor of 2 decrease in the density of the 3.1 eV level. (The values .3% and 1.5% were chosen because they are in the range of reasonable close-to-LTE values.)

Overall though, it is fruitless to try to correlate the behavior of the emission and ground state profiles without measurement of actual densities and temperatures. The fraction of ions or atoms excited could change drastically with no apparent change in ground state population. This fraction is very sensitive to temperature whereas the ground state population is less sensitive. One soon gets hopelessly confused looking from

figure to figure, trying to discern trends; inconsistencies abound.

For example, the population of excited levels is closely tied to the ground state ion population by frequent collisions with electrons. One might expect then, that the behavior of the 422.7 nm emission profiles as power and observation height are varied would correlate with the behavior of the ground state ion profiles.

Indeed this is seen at 1 lpm. Compare the bottom 2 rows of Figures 43 and 59, these being power studies of ground state Ca ion fluorescence and Ca atom emission at 1-lpm. The profiles behave quite similarly in terms of response to power. (The atom emission profile at .75 kW/10 mm ALC in Figure 59, would exhibit a central dip if Abel inverted.) This correlation however, breaks down above 13 mm ALC. The correlation also breaks down as flowrate is dropped. In Figure 63 for example, ground state ion fluorescence and excited ion emission are shown as a function of power for an observation height of 10 mm ALC. The atom emission profiles are broad whereas the ion fluorescence profiles are narrow. Also, the emission profiles maintain roughly the same height whereas the ground state ion profiles dwindle dramatically as power increases. This apparently inconsistent behavior does not necessarily indicate that there is anything "wrong" with the fluorescence profiles.

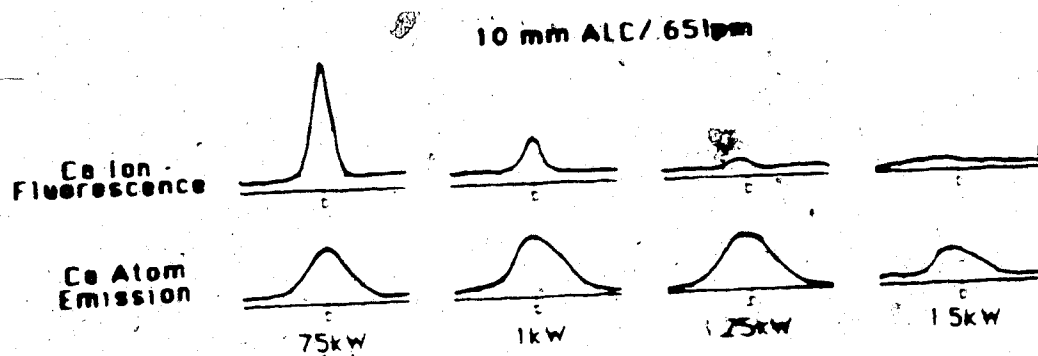


Figure 63. 422.7 nm Ca atom emission profiles and 393.3 nm  $\text{Ca}^+$  fluorescence profiles as a function of power at 10 mm ALC, .65 lpm - MAK torch.

The fact that both ion and atom emission profiles are broad and much more stable in their response to a change in power might be construed as an indication that the plasma moves closer to LTE when flowrate drops. Combined Saha-Boltzmann calculations of level densities of excited Ca ions and atoms indicate that the population of excited levels increases only slowly as electron density increases by an order of magnitude (this simulates the effect of an increase in power).

Finally, a brief comparison to some other radial emission profiles is in order here. At .75 kW, with a 1 lpm flowrate, the profiles at 10 mm ALC (emission and fluorescence) indicate that excited ions, ground state ions and excited atoms all have a toroidal distribution whereas the ground state atom is concentrated in the central channel. This was seen by Rybarczyk [15] in the zone 3 to 6 mm ALC in a 1.25 kW plasma. Furuta [8], however, sees Ca ion and atom radial emission profiles with a central dip at 10 mm ALC in a 1.8 kW plasma. This is surprising since the flowrate is reported to be .9 lpm. No evidence of this was seen above .75 kW at 1 lpm in this work. These examples bespeak the need of a standard ICP system (torch, load coil, nebulizer and spray chamber) for fundamental studies, such as outlined in reference [48].

#### D. Excited State Fluorescence

It was mentioned in Chapter 4 that it is also possible to monitor the population of an excited state species by fluorescence as opposed to emission. The advantage of this technique is that levels that might emit only weakly are more accessible in some cases.

When resonance fluorescence at the 373.7 nm CaII line is attempted, the lower level of the transition is the level from which the 393.3 CaII line originates. In order to get decent signals in this experiment, a concentration of 1600 ppm was used (response was observed to be linear when concentration was varied about this point). The large concentration needed gives another indication of the relative population of the ground and 3.1 eV Ca ion levels since the ground level Ca ion could be probed using a 4 ppm solution.

The results of power studies of  $\text{Ca}^{++}$  resonance fluorescence at 373. nm for flowrates of 1 and .65 lpm are presented in Figures 64 and 65. In Figure 64, some of the same trends seen for the emission profiles shown in Figure 56 (ion emission power study, 1 lpm) are apparent. For example, as one goes up the column at 1.5 kW a peak in fluorescence is seen at 13 mm ALC. The response of these profiles to an increase in power at observation heights of

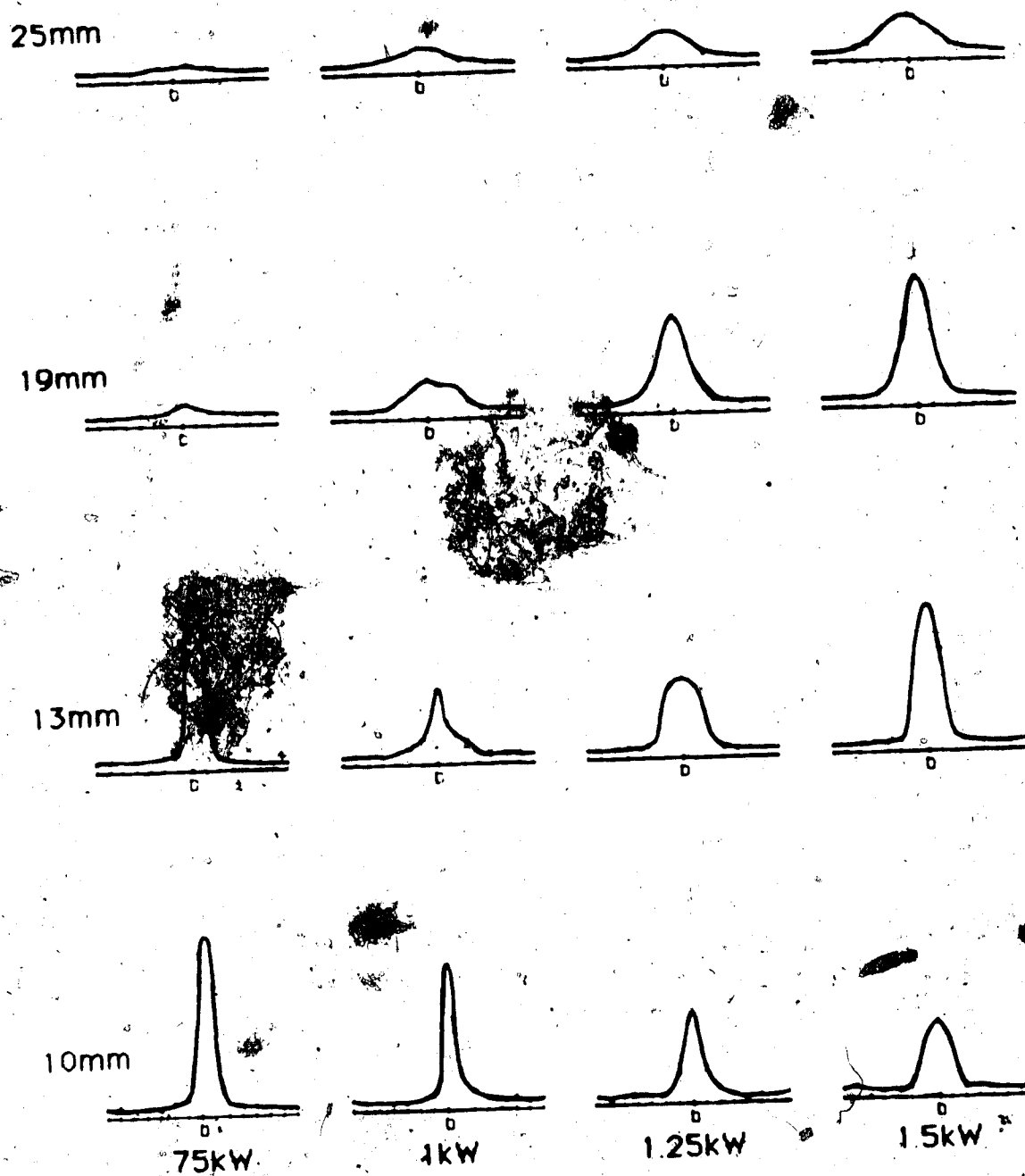
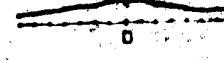
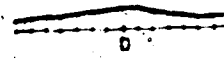
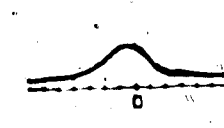
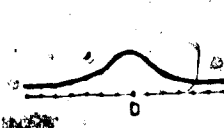
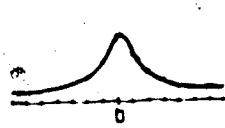
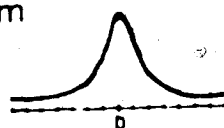


Figure 64. 373.7 nm  $\text{Ca}^+$  fluorescence power study results, 1 lpm - MAK torch.

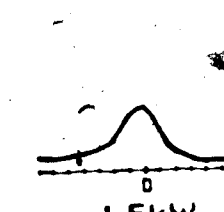
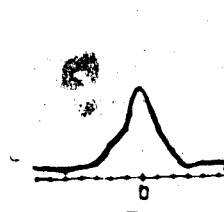
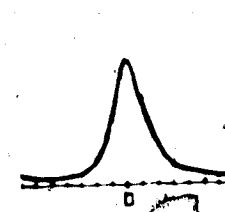
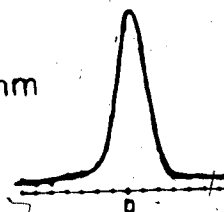
19mm



13mm



10mm



75kW

1kW

1.25kW

1.5kW

Figure 65. 373.7 nm  $\text{Ca}^+$  fluorescence power study results, .65 lpm - MAK torch.

19 and 25 mm ALC is also the same as it was in Figure 56. Lacking from Figure 56, however, are the apparently intense fluorescence profiles seen at 10 mm ALC, .75 and 1 kW and 13 mm ALC, .75 and 1 kW in Figure 64. These signals were seen to vanish when water only is aspirated. The most likely explanation of these profiles is that due to the high concentration of analyte, the plasma is being too heavily loaded at low power so that significant amounts of unvaporized salt particles may persist at 10 and 13 mm ALC.

At .65 lpm, a negative correlation exists between the profiles obtained by 373.7 nm resonance fluorescence (Figure 65) and those obtained by 393.3 nm emission (Figure 60). Fluorescence intensity at all heights decreases as power increases. The figures are rough mirror images.

Although excited state fluorescence appears to work remarkably well at 1 lpm (apart from the scattering effect), evidently it is not accurate at .65 lpm. The hotter environment at .65 lpm increases the likelihood of collisional as opposed to radiative depopulation of the pumped level. It was pointed out in Chapter 4 that resonance fluorescence at 373.7 nm might not work because of the existence of states within .6 eV of the pumped level. Yet if 373.7 nm resonance fluorescence works well



at 1 lpm, it is quite likely that resonance fluorescence at 393.3 nm is not subject to any quenching effects, due to the greater isolation of the upper level.

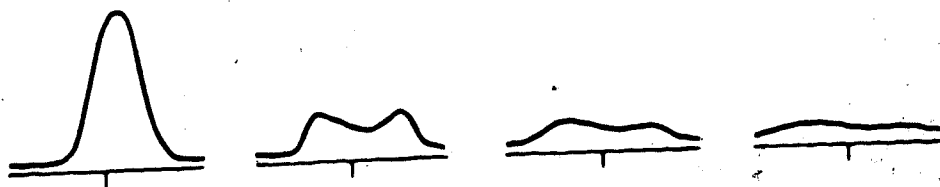
Even though 373.7 nm resonance fluorescence did not work well at .65 lpm, it cannot automatically be concluded that resonance fluorescence at 393.3 nm fails at .65 lpm, again due to the more isolated nature of the upper level.

#### E. Molybdenum Results

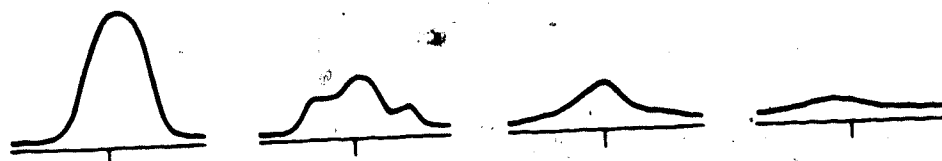
The selection of elements whose ground state ion species can be probed without frequency doubling of our dye laser is fairly limited. A much wider choice exists if ground state atom species are investigated. Molybdenum was selected for study because it had a higher first ionization potential (7.1 eV) than Ca (6.1 eV) and because its ground level can be probed via resonance fluorescence at 390.3 nm. From the information available, this 3.18 eV level appeared to be the lowest lying excited level although there are seven other levels within .8 eV of the 3.18 eV level.

The results of a power study of 1 lpm of Mo atom resonance fluorescence at 390.3 nm are summarized in Figure 66. The concentration used was 1000 ppm. Under the operating conditions for which the largest profiles appeared, concentration was varied by a factor of 10 and

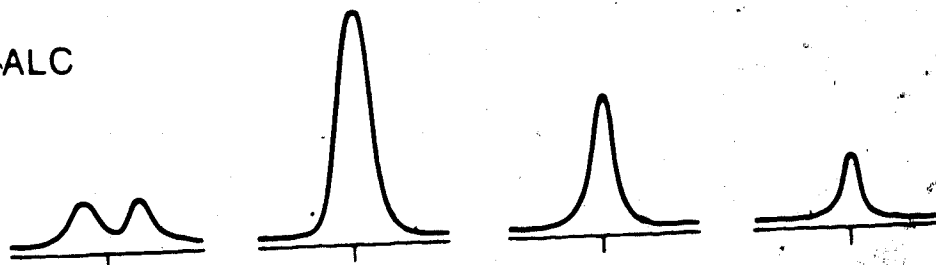
31ALC



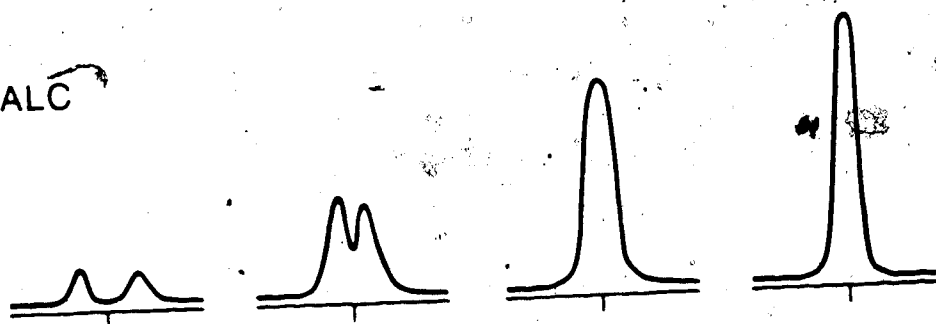
25ALC



19ALC



13ALC



10ALC

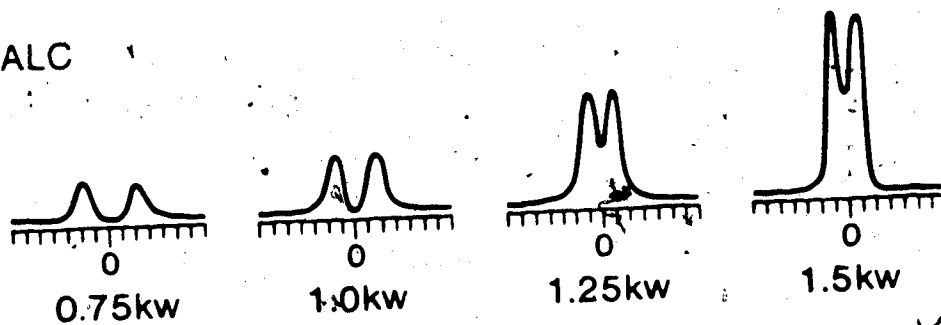


Figure 66. 390.3 nm Mo atom fluorescence power study results, 1 lpm  
- MAK torch.

linear response was seen. Similarly, profiles hollow at 1000 ppm were also hollow at 100 ppm although the symmetry of the hollow profiles speaks against concentration effects.

These profiles (Figure 66) are markedly different from the corresponding Ca atom fluorescence profiles shown in Figure 45. Central minima are prevalent and tend to persist higher in the plasma. A plausible explanation for the observed differences is that Mo forms a more stable oxide than Ca and hence formation of its atomic vapour is delayed (the dissociation energy of MoO is 5 eV and that of CaO  $\approx$  4 eV).

Vertical atom fluorescence profiles for Ca and Mo at various powers are shown in Figure 67. The peak in atom fluorescence likely indicates the point at which ionization begins to compete with excitation. For Mo, this point is not reached until higher in the plasma at low power possibly due to the higher dissociation energy of MoO.

A power study of lateral Mo emission at 390.3 nm for a flowrate of 1 lpm is summarized by the profiles presented in Figure 68. Recall that Ca atom emission at no time was seen to track Ca atom fluorescence profiles, instead following more closely the behavior of the ground state  $\text{Ca}^+$  fluorescence profiles. However, when comparing

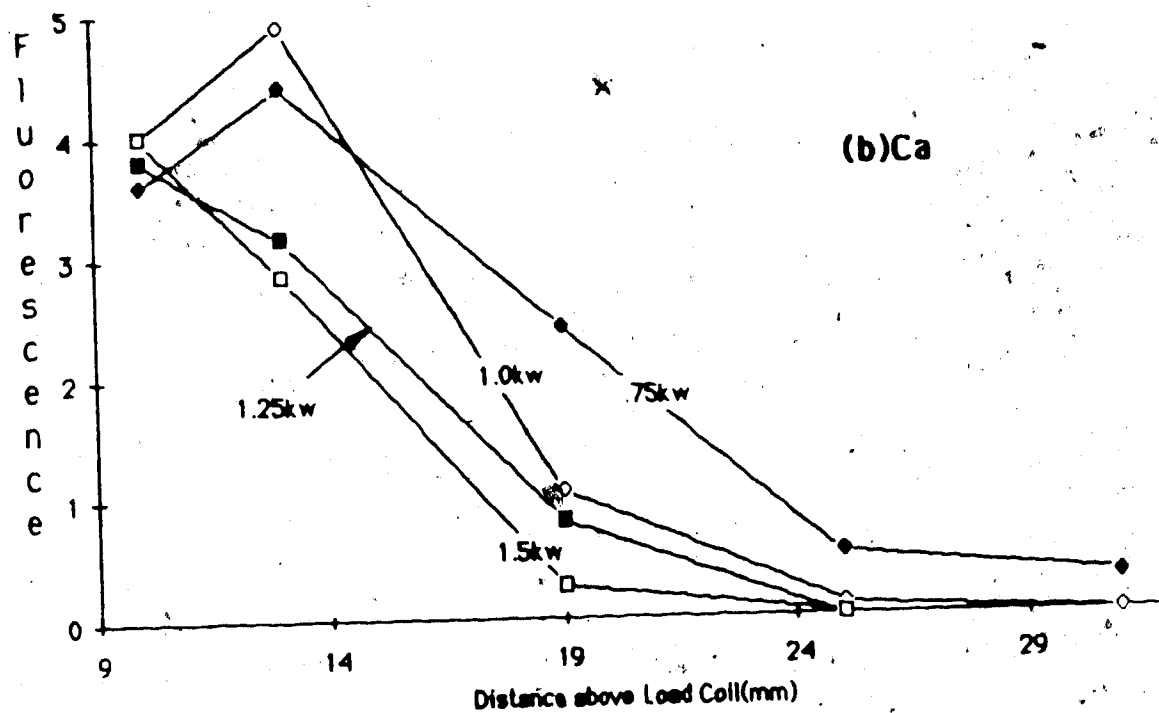
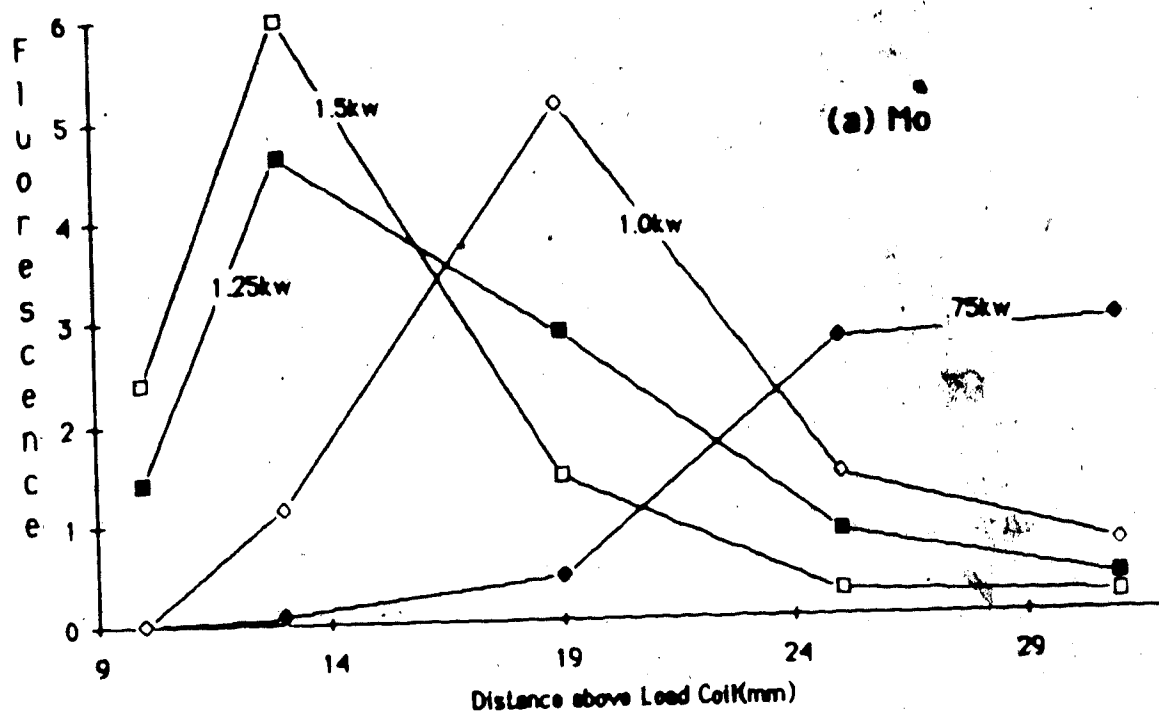
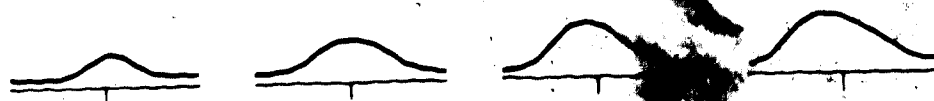
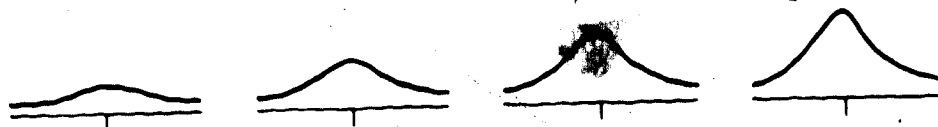


Figure 67. Vertical fluorescence profiles (1 lpm): (a) Mo atom, (b) Ca atom - MAK torch.

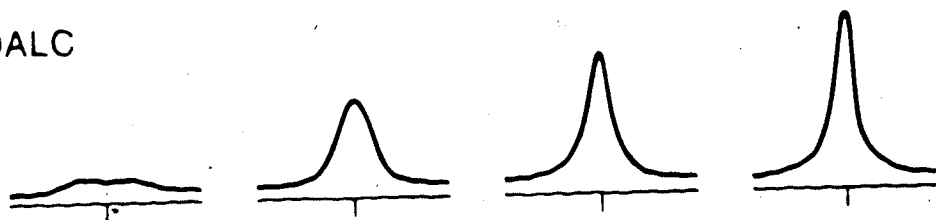
31ALC



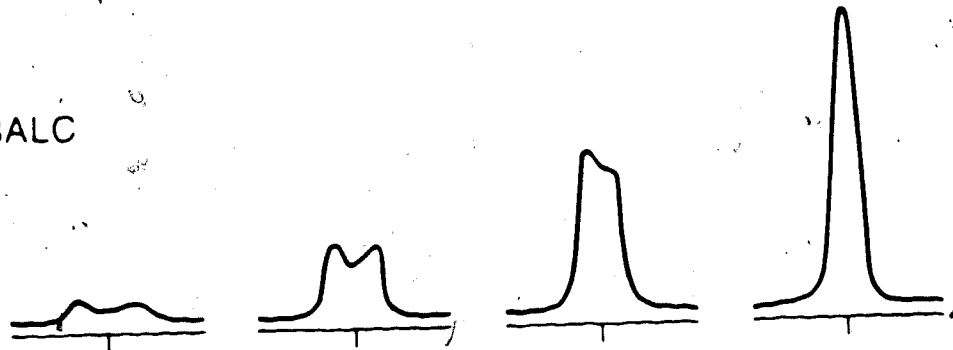
25ALC



19ALC



13ALC



10ALC

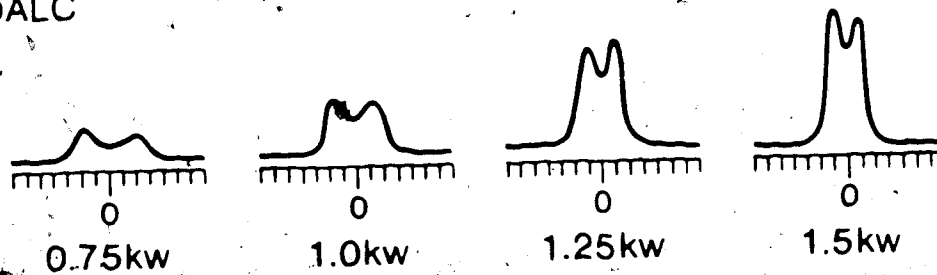


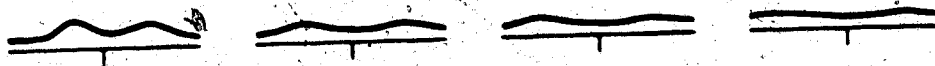
Figure 68. 390.3 nm Mo atom emission power study results, 1 lpm - MAK torch.

the bottom two rows of Figures 66 and 68, it is seen that Mo atom emission, on the other hand, tracks Mo atom fluorescence extremely well, both in terms of profile height and presence or absence of a central minimum in the profile. This correlation breaks down at 19 mm ALC however.

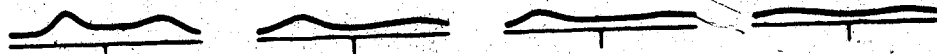
At or below 13 mm ALC, ionization may not be efficient so atom emission and atom fluorescence are closely linked and may depend on the dissociation rate of the oxide [14]. Between 13 and 19 mm ALC, the degree of ionization probably increases so that excited Mo atoms equilibrate with the ground state ion, dissociation being largely complete.

Lastly, 390.3 nm resonance fluorescence and emission power studies at .65 lpm are summarized in Figures 69 and 70. These are shown for comparison to Ca, although nothing startling is revealed by them. Also shown in Figure 69, the Mo atoms visible at .75 kW disappear as power is increased. The now-familiar lobes appear higher in the plasma at powers above .75 kW. The broad Mo atom emission profiles in Figure 70 resemble their Ca counterparts (Figure 62) with the exception that the Mo profiles retain a noticeable central hump at 19 mm ALC whereas the Ca profiles do not.

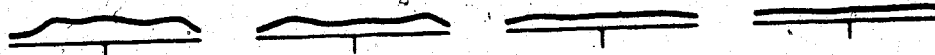
31ALC



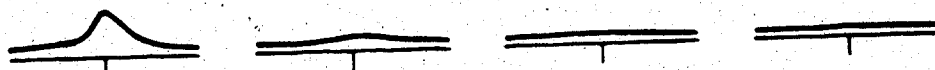
25ALC



19ALC



13ALC



10ALC

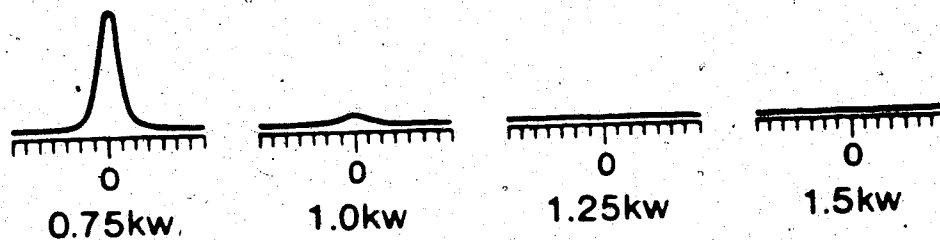
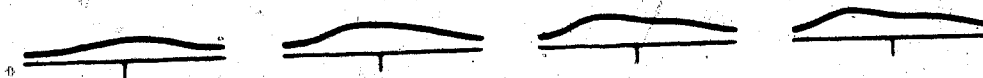
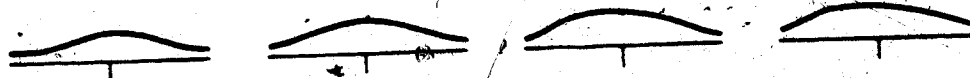


Figure 69. 390.3 nm Mo atom fluorescence power study results, .65 lpm - MAX torch.

31ALC



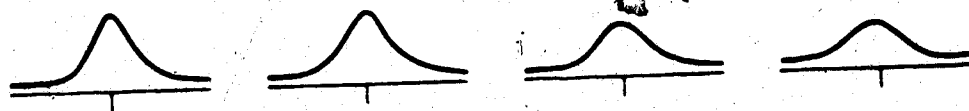
25ALC



19ALC



13ALC



10ALC

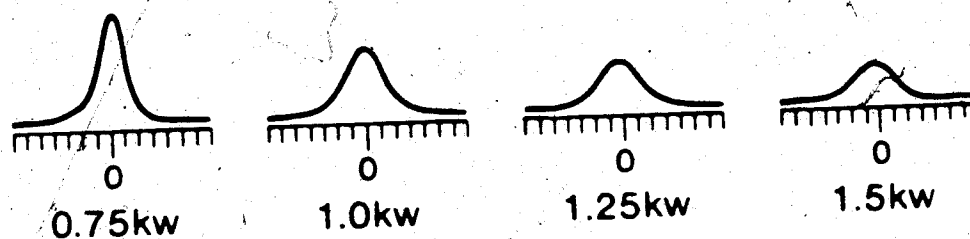


Figure 70. 390.3 nm Mo atom emission power study results, .65 lpm -  
MAX torch.



## F. Summary and Conclusions

Plasmas sustained with the two torches (MAK and Fassel) differed most at a flowrate of 1 lpm. At 1 lpm the MAK torch profiles were narrower, probably indicating greater confinement of analyte within the channel. The lower part of the channel was also cooler in the case of the MAK torch at 1 lpm; ground state atom fluorescence was more evident. These differences most likely arise from the straight-bore injector tube on the MAK torch. The differences however, were ironed out as the flowrate was lowered. At .65 lpm the same loss of analyte due to increased gas expansion occurs in the MAK torch plasma.

Changes in the size and shape of the MAK torch profiles at increasing distances from the load coil (with fixed power) compared quite well with other profiles in the literature.

In one observation zone (17-19 mm ALC) the response of  $\text{Sr}^+$  fluorescence as power and flowrate varied was compared to the response of  $\text{Sr}^+$  count rate by ICP-MS as power and flowrate were varied. Very similar results were obtained, indicating that fluorescence quenching of various types is not important in this zone.

A linear variation of  $\text{Ca}^+$  fluorescence intensity at 393.3 nm seen as laser power was increased indicates, as was surmised in Chapter 4, that fluorescence is not being saturated.

Sets of lateral emission profiles were also acquired for the same range of conditions (power, flowrate and observation height) as the fluorescence profiles. The ground state and excited state species exhibited markedly different patterns in their response to changes in power, observation height and flowrate. Conventional wisdom gathered from ICP-OES does not carry over to ICP-MS. In part, the lack of correlation is due to the great difference in the size of the populations being observed. A systematic analysis of the changes in emission patterns cannot be given without some kind of temperature framework as in references [23] and [24] and knowledge of the actual densities of the levels involved (acquisition of these densities is no simple task).

The spatial distribution of excited analyte species was also probed by resonance fluorescence. At 1 lpm, apart from scattering at low power (due to the high concentration employed) the technique yielded the same information as did direct observation of emission. At a lower flowrate however, the fluorescence was most likely quenched by collisions with electrons, as was expected. If the densities of excited state levels are to be determined by the absolute intensity of saturated fluorescence, strictest attention will have to be paid to quenching effects.

Ground state Mo atom fluorescence exhibited some interesting differences with respect to Ca, including a correlation between the behavior of the ground state atom and the excited atom low in the plasma at 1 lpm. At this flowrate, the attainment of a situation with excited atoms in equilibrium with ground state ions may be delayed by the more refractory nature of MoO relative to CaO.

One basic conclusion regarding ICP-MS can be drawn from comparison of vertical fluorescence and emission profiles. ICP-mass spectrometry should be more "forgiving" than optical emission spectroscopy on the basis of response of signal to changes in power and observation height. For example, in the central channel, a large signal can be obtained at .75 kW or 1.5 kW by varying the observation height. The same is not true for emission. Bear in mind, however, that overall analytical performance depends on the background level and freedom from interelement effects as well as the raw signal strength.

## CHAPTER 6

### EASILY IONIZABLE ELEMENT INTERFERENCE STUDY: MAK TORCH

#### A. Introduction

One area that has received a lot of attention from ICP researchers is the effect of addition of an easily ionizable element (EIE) on the behavior of the analyte. Trace elements are quite often determined by ICP emission spectroscopy in matrices with a high salt content including seawater, biological fluids and/or tissue, and geological samples, i.e. rocks. An understanding of the mechanism of the interference might lead to ways in which it can be reduced or removed.

Of the ways in which the EIE might exert an effect, the five thought to be important include a shift in the analyte ionization equilibrium, enhanced collisional excitation, delayed volatilization, increased ambipolar diffusion and various interferences at the nebulization step. A thorough discussion of these effects appears in reference [18]. No single one of these mechanisms is all-inclusive. For example, it has been shown that in a plasma operated under normal conditions (i.e. 1.5 kW/l, 1pm) increased collisional excitation can explain changes

in emission behavior low in the plasma following addition of an EIE whereas ambipolar diffusion may be important higher in the plasma [18]. This was determined by studying the response of vertical and radial emission profiles to addition of an EIE. By studying ground state species, an assessment can be made of the extent to which analyte ionization equilibrium shifts are important under a variety of operating conditions.

This type of study is of practical interest due to the advent of ICP-MS. Researchers are just beginning to unravel how the major variables, i.e. power, flowrate and observation height, affect ion count rates. It will be advantageous to have an understanding of how EIE's affect the ground state ion population as well, in order to make intelligent decisions on compromise operating conditions. (Compromise operating conditions afford good analytical response, including freedom from interferences, for a wide range of elements.)

A brief summary of ground state studies involving EIE's which have appeared in the literature follows. Kornblum [19] showed radial ground state atom density profiles at various heights in the presence and absence of an excess of cesium, and studied the effect of excess cesium on Mg ion and atom vertical absorbance profiles. As mentioned earlier, this plasma was operated with an

unusually high flowrate. Blades [18] measured Mg atom absorbance as a function of the amount of EIE added; this was done at one spatial location in the plasma with a fixed power and flowrate. Rybarczyk et al. [15] obtained radial profiles of ground state Ca and Mg ions and atoms in the region below 14 mm ALC as discussed earlier. They also studied the effect of an EIE on these profiles. Finally, Nojiri and co-workers [16] studied the effect of addition of an EIE on radial Ca ion and atom absorbance profiles at 3 observation heights for a fixed set of conditions.

It is seen then, that spatial study of the response of ground state species to addition of an EIE has been limited, although there is justification for pursuing such work. Hence ion and atom Ca fluorescence profiles with and without an excess of Na were measured for a variety of operating conditions. Corresponding emission profiles were also acquired. These profiles are presented and discussed in the following sections.

## B. Experimental

Few details need explaining here. The same system and methods discussed in Chapters 4 and 5 were used in this study. The same MAK torch was used. In most cases a 100-fold molar excess of Na was used with a calcium

concentration of 4 ppm.

### C. Discussion

#### C.1 1 lpm

At a flowrate of 1 lpm, power studies of ground state Ca ion fluorescence were done (after the fashion of Chapters 4 and 5) both with and without the EIE. The results are presented in Figure 71. Dotted lines denote the presence of the EIE. It is obvious after a quick glance at the figure, that the general effect of addition of the EIE is to depress ground state Ca ion fluorescence. The effect lessens as power increases and also as one draws away from the load coil (except at .75 kW).

At 1.6 kW, small central depressions in ground state ion absorbance profiles were seen at 7.5 mm and 15 mm ALC by Nojiri as is the case in Figure 71. A large central suppression of ion absorbance in the presence of excess Li was seen by Rybarczyk [15] at 10 mm ALC in a 1.25 kW plasma. This too is seen in Figure 71. Hence these results are in good agreement with existing ground state studies such as they are.

For the combinations of power and observation height for which suppressions are seen, one would like to know the underlying mechanism involved, and whether or not it

# Effect of EIE on $\text{Ca}^{+}$ Fluorescence 393.3 nm 1 lpm

31Alc



25Alc



19 Alc



13Alc



10Alc

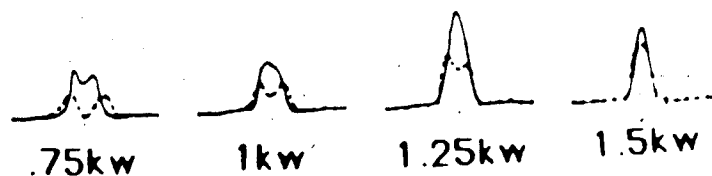


Figure 71. Effect of EIE (100-fold molar excess of Na) on 393.3 nm  $\text{Ca}^{+}$  fluorescence profiles as a function of power and observation height (1 lpm - MAK torch). Profiles obtained in the presence of Na are represented by dashed curves.



varies throughout Figure 71. To get a handle on this, corresponding power/EIE studies were done for other species, including ground state Ca atom, excited Ca ion and excited Ca atom (via 422.7 nm resonance fluorescence, and by emission at 393.3 and 422.7 nm).

In general, the results of these studies indicate that regardless of power, the decrease of ground state ion fluorescence at and below 13 mm ALC coincides with increases in ion and atom emission, but little or no increase in the ground state atom population is seen. Ryharczyk also observed this at 10 mm ALC [15] but only for one power. A typical set of normalized profiles (1.25 kW/10 mm ALC: ion and atom emission, ion and atom fluorescence) is shown in Figure 72 to illustrate the above point. Sets of profiles at other powers, and at 13 mm ALC, are similar. Blades [18] already showed that addition of an EIE caused an increase in the population of the excited Ca ion and atom levels however he did not verify if these enhancements were accompanied by a loss of ground state ions. It is interesting to speculate whether or not the decrease seen in ground state ion populations is due solely to increased collisional excitation of ions. If it is, then addition of Na would likely have to increase the electron temperature by several thousand degrees.

Another point to note is that the broadening of the

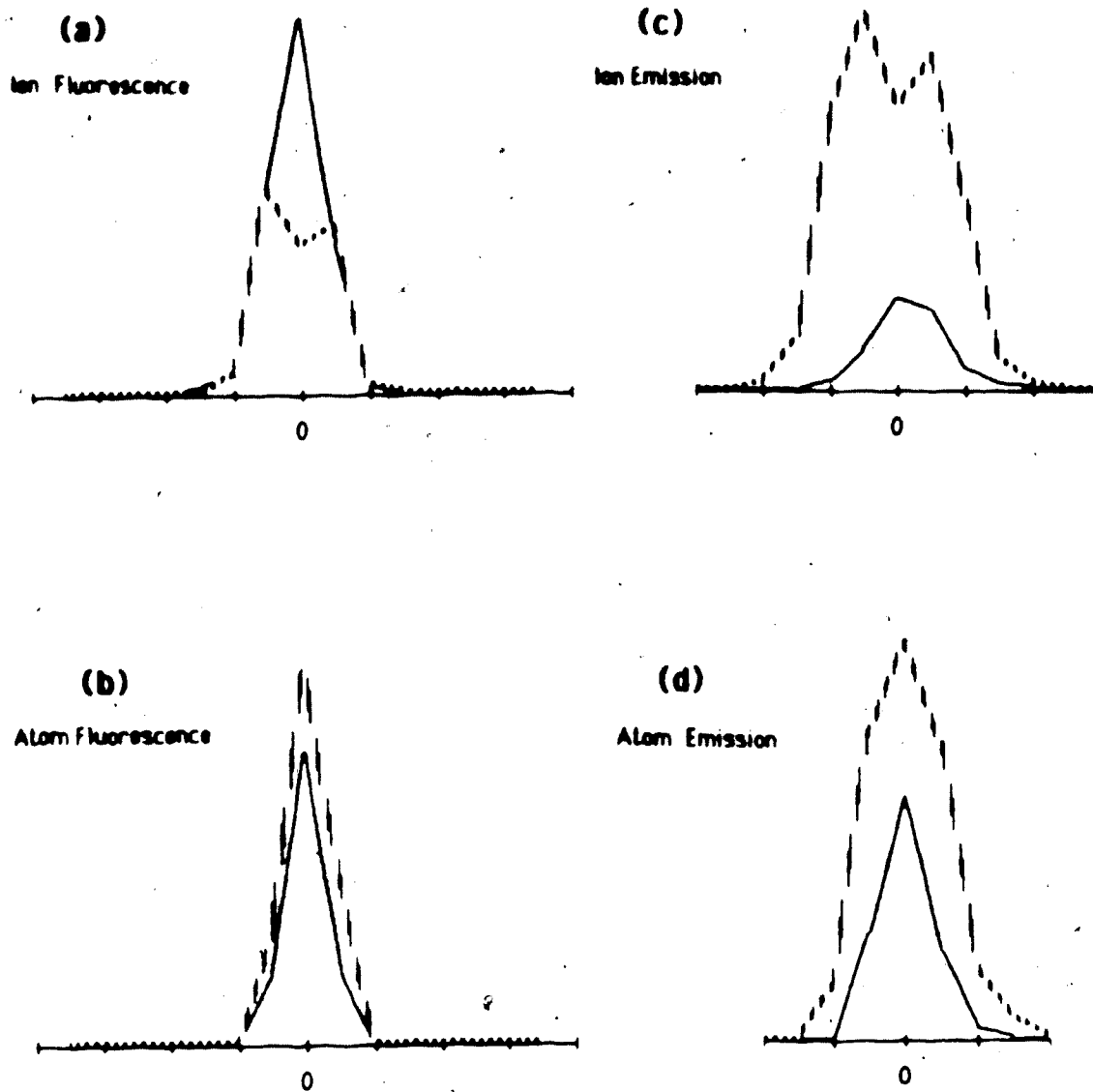


Figure 72. Normalized fluorescence and emission profiles with and without EIE at 10 mm ALC/1.25 kW/1 lpm. Dashed curves denote the presence of the EIE - Mak torch.

profile at .75 kW/10 mm ALC in Figure 71 is probably due to ambipolar diffusion of analyte ion/electron pairs into the surrounding channel.

Looking elsewhere in Figure 71, no evidence of an ionization equilibrium shift appears until 19 mm ALC at 1 kW. As seen in Figure 73 both ion emission (frame (a)) and ground state atom fluorescence (frame (b)) increase when Na is added, indicating that at this power, there may be competition between a buffering effect and increased collisional excitation as one draws away from the load coil. At .75 kW, the Ca atom fluorescence profile at 25 mm ALC can be made to grow dramatically as the concentration of EIE is increased from a 100-fold to a 1000-fold molar excess (Figure 74). No ion emission enhancement however takes place at this height and power. Note that the profile with 2400 ppm Na in Figure 74 now resembles the corresponding ground state ion fluorescence profile in Figure 71.

Higher in the plasma at powers above .75 kW, the atom fluorescence profiles are not visible when put on the same scale as atom fluorescence profiles from lower regions of the plasma. At higher magnification however, the profiles at 31 mm ALC are seen to exhibit lobes and these lobes are enhanced when an EIE is added. This can be seen in Figure 75. This exact behavior was also exhibited by Nojiri's

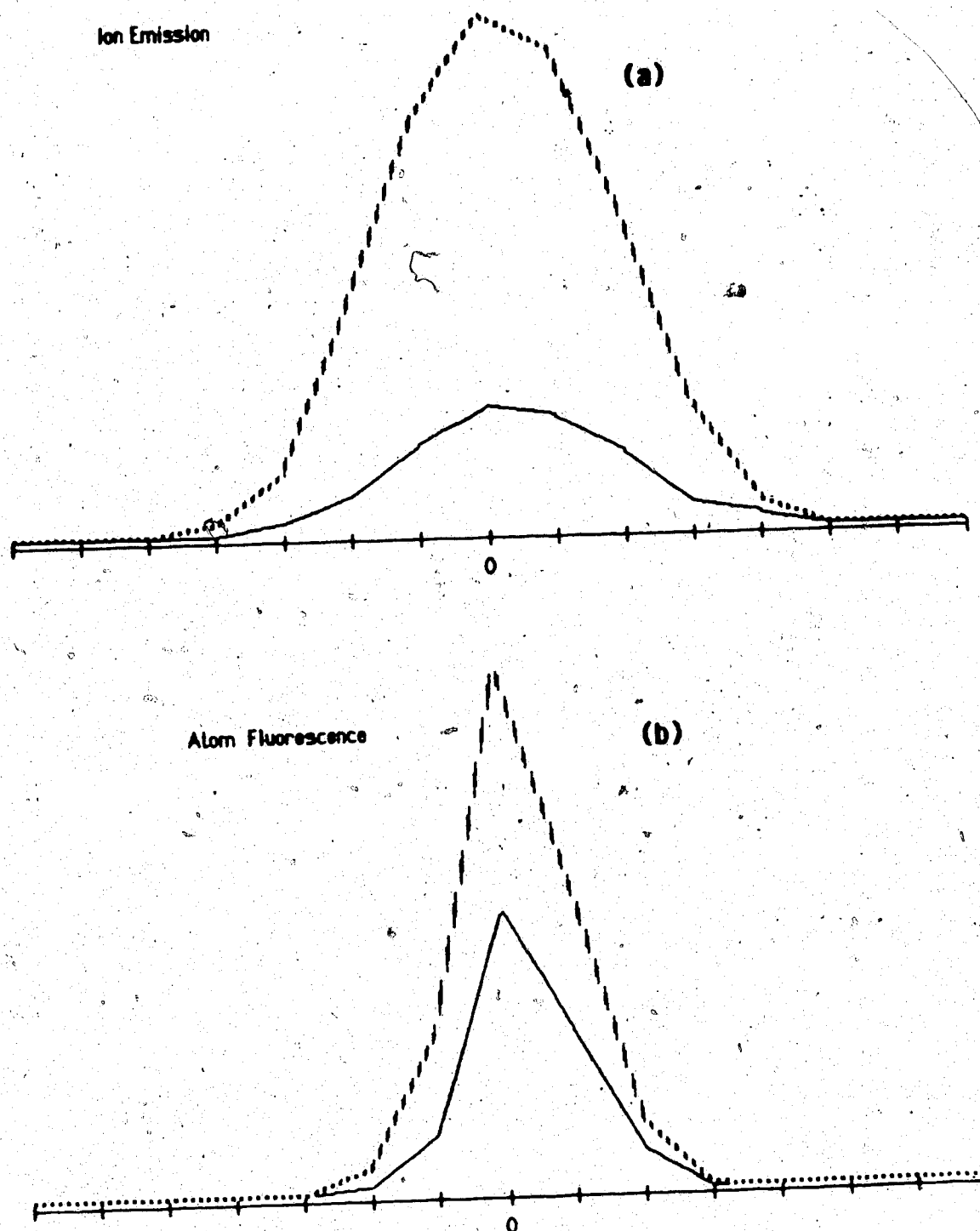


Figure 73. Response of: Ca ion emission (a) and Ca atom fluorescence (b) profiles at 19 mm ALC/1 kW/1 lpm to presence of an EIE.

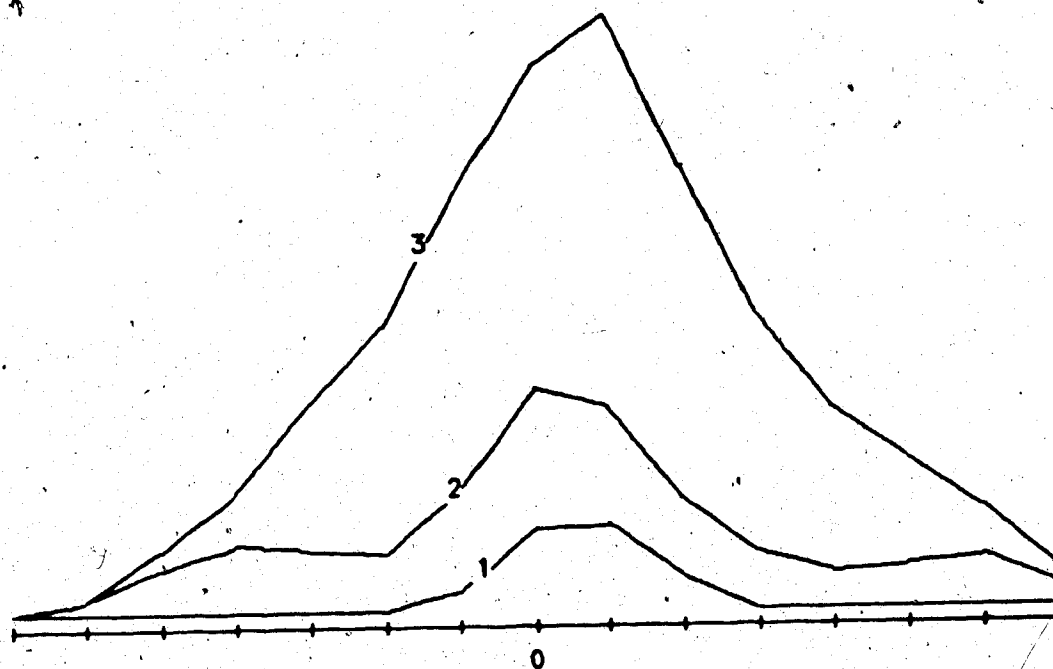


Figure 74. Effect of increased concentration of EIE on  $\text{Ca}^+$  fluorescence at 25 mm ALC/.75 kW/1 lpm - MAK torch. (1) 4 ppm Ca, (2) 4 ppm Ca/240 ppm Na, (3) 4 ppm Ca/2400 ppm Na.

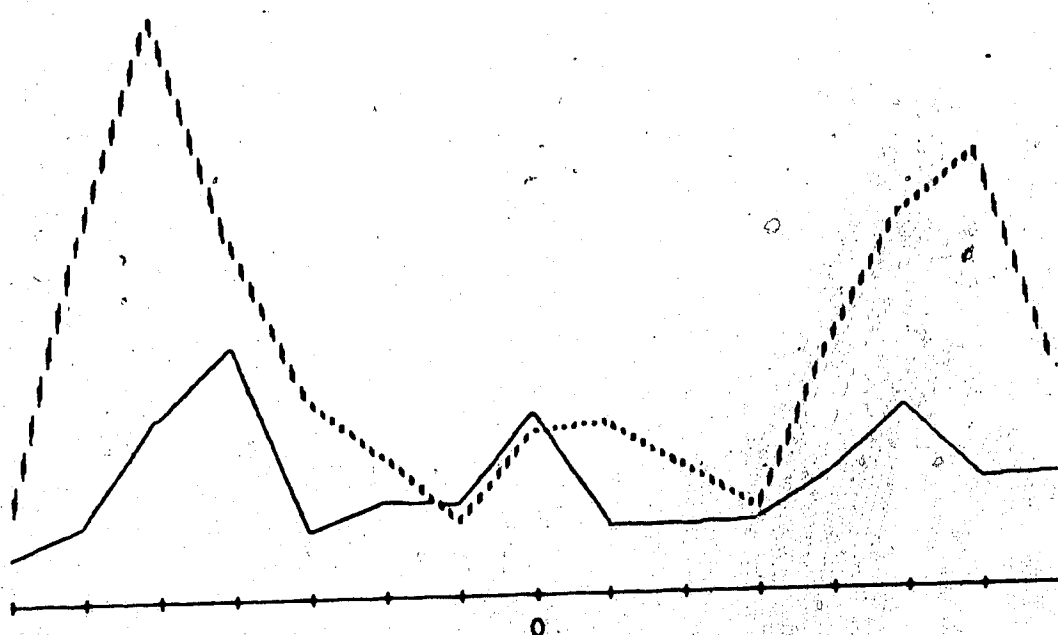


Figure 75. Ca atom fluorescence profiles at 31 mm ALC, 1.25 kW, 1 lpm, MAX torch with (dashed curve) and without (solid curve) excess Na.

[16] atom absorbance profile at 25 mm ALC.

Evidently, as might have been surmised, the analyte ionization equilibrium can be made to shift if one can introduce enough electrons (via an EIE) to significantly alter the "ambient"  $n_e$ . This is most easily achieved at low power but also occurs at the edges of the plasma high above the load coil for higher powers. Why a collisional excitation enhancement mechanism is favored lower in the plasma is not apparent.

#### C.2 .85 and .65 lpm

The effect of flowrate on the response of the ground state ion fluorescence profiles can be seen in Figure 76. Each grid in the figure represents the results of an ion fluorescence power study at the indicated flowrate, done with and without 100-fold molar excess of Na. The presence of a plus, minus or plus/minus in any square within a grid indicates either an enhancement, suppression or mixed effect on the ground state ion fluorescence profile which would be observed (the corresponding set of conditions can be read off the side and bottom of the grid).

As flowrate drops, zeroes denoting no effect gradually invade the grids (this same behavior is also seen for ion emission as well, i.e. an EIE has no effect on ion emission profiles at .65 lpm). Electron density is

# EFFECT OF EIE ON $\text{Ca}^{+}$ FLUORESCENCE

OBSERVATION HEIGHT (mm ALC)	65 lpm					85 lpm					1.0 lpm				
	75	1.0	1.25	1.5	POWER(kw)	75	1.0	1.25	1.5	POWER(kw)	75	1.0	1.25	1.5	POWER(kw)
31	+/-	+/-	0	0		+/-	0	0	0		-	-	0	0	
25	+/-	+/-	0	0		-	0	0	0		-	-	-	0	
19	+/-	0	0	0		-	-	0	0		-	-	-	0	
13	0	0	0	0		-	-	0	0		-	-	-	-	
10	0	0	0	0		-	-	-	0		-	-	-	-	

Figure 76. Schematic representation of effect of excess Na on  $\text{Ca}^{+}$  fluorescence at 3 flowrates. See text for description.



seen to increase sharply in the central channel as the flowrate is dropped from 1.2 lpm to .65 lpm [24] hence one would have to add more EIE to significantly elevate the ambient electron density at .65 lpm. Any collisional enhancement effects are evidently also overridden by the general temperature increase in the central channel as flowrate drops.

The mixed effect denoted by the "+/-" symbol in Figure 76 is illustrated in Figure 77 where the response of the  $\text{Ca}^+$  fluorescence profile at 31 mm ALC/.75 kW to addition of 100- and 1000-fold molar excesses of Na is seen. When increasing amounts of EIE are added, the profile is seen to contract. The decrease at the edges was seen to be accompanied by a large jump in ground state atom fluorescence (not shown) at the edges of the plasma, but the increase in the middle is puzzling. Possibly if the  $\text{Ca}^{2+}$  species is present at that height, an increase in the electron density (due to added EIE) may force it back to the singly charged form much the same as the singly charged ion recombines at the edges of the plasma under the influence of an EIE.

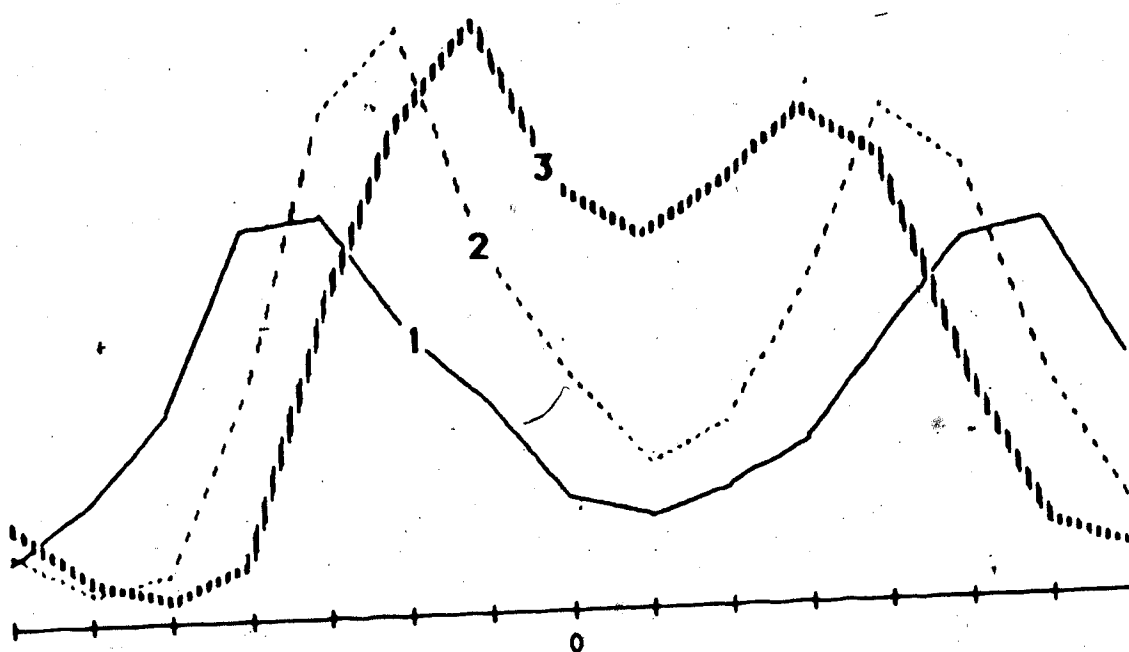


Figure 77. Effect of increasing concentration of EIE on  $\text{Ca}^+$  fluorescence profile at 31 mm ALC, .75 kW, .65 lpm, MAK torch. Numbering of the curves as in Figure 74.

#### D. Conclusion

Low in the plasma the analyte ionization equilibrium does not appear to shift significantly when excess EIE is present. The same is true higher in the plasma at powers above 1 kW. In ICP-MS then, any observation height should be free of EIE interference effects at high power. Freedom from interference effects at lower powers can be achieved by dropping the flowrate but a penalty will be paid in that the analyte is not contained as efficiently within the plasma and overall count rate will drop as a result.

## CHAPTER 7

### CLOSING REMARKS

Recent studies have demonstrated that the partial LTE model is appropriate for explaining many aspects of analyte behavior in the ICP. Admittedly the work in this thesis does not advance the current understanding of the detailed interaction of the analyte and the bulk plasma. This requires spatially resolved measurements of electron density and temperature as well as densities of ground and excited state analyte species.

The picture emerging from this work, however, gives qualitative confirmation of a partial LTE situation. Over a wide range of operating conditions and a range of spatial locations, ground state analyte ions exist in abundance whereas excited ions are virtually nonexistent. This behavior can be understood with reference to the Boltzmann and Saha equations. Emission intensity is seen to be exponentially dependent on electron temperature. The degree of ionization has a more complex dependence on both electron temperature and electron density and can be relatively insensitive to these parameters compared to emission intensity.

The stated goal of acquiring comprehensive spatial

maps of ground state analyte species over a wide range of conditions has been reached. These results offer a clearer superficial understanding of the ICP particularly in its new role as an ion source for mass spectrometry. For example, the ultimately fatal effect that a decrease in flowrate exerts on ion count rates can be understood as a simple dilution effect. (This dilution effect may be compensated for in the case of emission spectroscopy by the increase in temperature accompanying a drop in flowrate.) As another example, it is perfectly clear from this study that 30 mm ALC is an acceptable sampling height for ICP-MS.

There is some cause to question the validity of the results due to the variation of quantum efficiency with operating conditions and spatial location in the plasma, however the general agreement of the results from 3 different techniques (absorbance, fluorescence and mass spectrometry) provides reasonable assurance that the fluorescence results are accurate. As well, the results are in good agreement with published data on Ca ground state species. Certainly the question of quantum efficiency should be carefully explored in further fluorescence work, particularly if elements having many available excited states, e.g. transition metals are studied.

Another point should be made regarding possible ground state studies of elements other than alkaline earths. Although it is true that in the case of the alkaline earths, most of the ions remain in the ground state even at temperatures of 7000 K to 8000 K, the same is not true for other elements. For example, it can be shown that in the case of Fe, roughly only 20% of the total singly charged ion population in a given region will remain in the ground state at 6000 K. Hence in some cases the amount of information to be gained from the study of ground state species may be limited since they will comprise only a small fraction of the total analyte population.

The photodiode array spectrometer and computer controlled torch positioning system developed in the course of this research constitute the nucleus of a powerful system for the automated acquisition of the large bodies of data which will be necessary for further characterization of the ICP at a fundamental level. The work done in this thesis lays the foundation for further studies of ground state analyte species via atomic fluorescence which might be undertaken in this laboratory.

## REFERENCES

1. Y. Shao and G. Horlick, Paper #482, Pittsburgh Conference on Analytical Chemistry, New Orleans, LA, 1985.
2. R. Houk, V. Fassel, G. Flesch and H. Svec, Anal. Chem. 52, 2283 (1980).
3. A. Date and A. Gray, Spectrochim. Acta 38B, 29 (1983).
4. A. Gray and A. Date, The Analyst 108, 1033 (1983).
5. G. Horlick, S. Tan, M.A. Vaughan and C. Rose, Spectrochim. Acta (in press).
6. P. Arrowsmith, A. Boorn and D. Douglas, Paper #335, Pittsburgh Conference on Analytical Chemistry, New Orleans, LA, 1985.
7. J. Fulford, A. Boorn, D. Douglas and E. Quan, Paper #338, Pittsburgh Conference on Analytical Chemistry, New Orleans, LA, 1985.
8. N. Furuta and G. Horlick, Spectrochim. Acta 37B, 987 (1982).
9. G. Larson, V. Fassel, R. Scott and R. Kniseley, Anal. Chem. 47, 238 (1975).
10. T. Edmonds and G. Horlick, Appl. Spec. 31, 536 (1977).

11. D. Kalnicky, V. Fassel and R. Kniseley, Appl. Spec. 31, 137 (1977).
12. H. Kawaguchi, T. Ito, K. Ota and A. Mizuike, Spectrochim. Acta 35B, 199 (1980).
13. M. Blades and G. Horlick, Spectrochim. Acta 36B, 861 (1981).
14. H. Kawaguchi, T. Ito and A. Mizuike, Spectrochim. Acta 36B, 615 (1981).
15. J. Rybarczyk, C. Jester, D. Yates and S. Koirtzmann, Anal. Chem. 54, 2162 (1982).
16. Y. Nojiri, K. Tanabe, H. Uchida, H. Haraguchi, K. Fuwa and J.D. Winefordner, Spectrochim. Acta 38B, 61 (1983).
17. H. Uchida, M. Kosinski and J.D. Winefordner, Spectrochim. Acta 38B, 5 (1983).
18. M. Blades and G. Horlick, Spectrochim. Acta 36B, 881 (1981).
19. G. Kornblum and L. DeGalan, Spectrochim. Acta 32B, 455 (1977).
20. R. Wendt and V. Fassel, Anal. Chem. 37, 920 (1965).
21. P. Ripson and L. DeGalan, Spectrochim. Acta 38B, 707 (1983).
22. E. Choot, Ph.D. Thesis, University of Alberta, Edmonton, Alberta, 1983.



23. B. Caughlin and M. Blades, Spectrochim. Acta 39B, 1583 (1984).
24. B. Caughlin and M. Blades (submitted to Spectrochim. Acta).
25. F. Aeschbach, Spectrochim. Acta 37B, 987 (1982).
26. C. Alkemade, T. Hollander, W. Snelleman and P. Zeegers, "Metal Vapours in Flames", Pergamon Press: Toronto (1982).
27. G. Kornblum and L. DeGalan, Spectrochim. Acta 32B, 71 (1977).
28. P. Boumans and F. DeBoer, Spectrochim. Acta 32B, 365 (1977).
29. J. Alder, R. Bombelka and G. Kirkbright, Spectrochim. Acta 35B, 163 (1980).
30. D. Schram, I. Raaymakers, B. Vander Sijde, H. Schenkelaars and P. Boumans, Spectrochim. Acta 38B, 1545 (1983).
31. I. Raaymakers, P. Boumans, B. Vander Sijde and D. Schram, Spectrochim. Acta 38B, 697 (1983).
32. L. DeGalan, Spectrochim. Acta 39B, 537 (1984).
33. G. Hieftje, J. Mills, J. Carr, G. Rayson, M. Huang and K. Marshall (private communication).
34. R. Lovett, Spectrochim. Acta 37B, 969 (1982).
35. K. Li, Paper #1235, Pittsburgh Conference on Analytical Chemistry, New Orleans, LA, 1985.

36. ~~A.~~ Mitchell and M. Zemansky, "Resonance Radiation and Excited Atoms", Cambridge University Press: London, 1961.
37. N. Omenetto and J.D. Winefordner, Prog. Anal. Atom. Spectrosc. 2, 1 (1978).
38. N. Omenetto and J.D. Winefordner, Appl. Spec. 26, 555 (1972).
39. D. Olivares and G. Hieftje, Spectrochim. Acta 33B, 79 (1978).
40. H. Uchida, M. Kosinski, N. Omenetto and J.D. Winefordner, Spectrochim. Acta 38B, 529 (1983).
41. D. Kalnicky, R. Kniseley and V. Fassel, Spectrochim. Acta 30B, 511 (1975).
42. P. Walters, G. Long and J.D. Winefordner, Spectrochim. Acta 39B, 69 (1984).
43. N. Omenetto, S. Nikdel, R. Reeves, J. Bradshaw, J. Bower and J.D. Winefordner, Spectrochim. Acta 35B, 507 (1980).
44. C. Veillon and M. Margoshes, Spectrochim. Acta 23B, 503 (1968).
45. B. Magyar and F. Aeschbach, Spectrochim. Acta 35B, 839 (1980).
46. H. Human, N. Omenetto, P. Cavalli and G. Rossi, Spectrochim. Acta 39B, 1345 (1984).

47. M. Kosinski, H. Uchida and J.D. Winefordner, Anal. Chem. 55, 688 (1983).
48. G. Rayson, Paper #487, Pittsburgh Conference on Analytical Chemistry, New Orleans, LA, 1985.
49. J. Seto, M.Sc. Thesis, University of Alberta, Edmonton, Alberta, 1983.
50. E. Cordos and H. Malmstadt, Anal. Chem. 44, 2407 (1972).
51. E. Cordos and H. Malmstadt, Anal. Chem. 45, 27 (1973).
52. R. Belchamber and G. Horlick, Spectrochim. Acta 37B, 17 (1982).
53. M. Blades and G. Horlick, Talanta 28, 527 (1981).
54. L. DeGalan, W. McGee and J.D. Winefordner, Anal. Chim. Acta 37, 436 (1967).
55. H. Wagenaar, I. Novotny and L. DeGalan, Spectrochim. Acta 29B, 301 (1974).
56. E. Piepmeier and L. DeGalan, Spectrochim. Acta 30B, 263 (1975).
57. D. Demers, Paper #484, Pittsburgh Conference on Analytical Chemistry, New Orleans, LA, 1985.
58. J.P. Walters, "Contemporary Topics in Analytical and Clinical Chemistry", Plenum Press: New York, 1978.
59. M. Alden, H. Edner, G. Holmstedt, S.S. Vanberg and T. Hogberg, Appl. Optics 21, 1236 (1982).

60. N. Omenetto and H. Human, Spectrochim. Acta 39B, 1333 (1984).
61. J. Carr, M. Blades and G. Hieftje, Appl. Spec. 36, 689 (1982).
62. P. Boumans, Spectrochim. Acta 37B, 75 (1982).
63. R. Houk, H. Svec and V. Fassel, Appl. Spec. 35, 380 (1981).
64. G. Hieftje (private communication).
65. M. Blades and G. Hieftje, Spectrochim. Acta 36B, 881 (1981).
66. J. Mills and G. Hieftje, Spectrochim. Acta 39B, 859 (1984).
67. S. Bashkin and J. Stoner, "Atomic Energy Level and Grotrian Diagrams, Volume 2", North Holland Publishing Company: New York, 1978.
68. L. DeGalan, R. Smith and J.D. Winefordner, Spectrochim. Acta 23B, 521 (1968).



## APPENDIX A



## APPENDIX A

The idea of calculating a temperature based on  $n_e$  and the assumption of LTE in the Saha equation for argon is not new (mention of it was made in 1977 [27]) but it has recently become more popular since it allows a reference LTE framework of e.g. ion/atom emission intensity ratios [23] or degrees of ionization [24] to be constructed from measured electron densities.

Calculation of the  $(n_e, T)$  pairs involves solving a quadratic equation as outlined below. The total argon density is equal to the sum of the density of all argon atom species and the density of all argon ion species:

$$n_T = n_{Ar} + n_{Ar^+} \quad (1)$$

Using the ideal gas law written in terms of density,

$$n_T = \frac{N_A p}{RT} = \frac{7.34 \times 10^{21}}{T} \text{ cm}^{-3} \quad (2)$$

where  $N_A$  is Avogadro's number and  $T$  is the gas temperature (K), and assuming that the electron density is equal to the total argon ion density ( $n_e = n_{Ar^+}$ ) then

$$n_{Ar} = \frac{7.34 \times 10^{21}}{T} - n_e \quad (3)$$

The Saha equation for argon can be written:

$$\frac{n_{Ar} + n_e}{n_{Ar}} = 4.823 \times 10^{15} \frac{Q^+(T)}{Q^0(T)} T^{3/2} 10^{(-5040(E_i)/T)} \quad (4)$$

where  $Q^+(T)$  and  $Q^0(T)$  are partition functions,  $T$  is the ionization temperature (K) and  $E_i$  is the ionization energy in eV. In practice  $Q^0(T) = 1$  and  $Q^+(T)$  can be represented by a polynomial function of  $T$  found in reference [68].

Equation (4) can be written:

$$\frac{n_{Ar} + n_e}{n_{Ar}} = F(T) \quad (5)$$

Letting  $n_e = n_{Ar}^+$  in Equation (5), combining it with Equation (3) and assuming  $T_{gas} = T_{ionization}$  results in:

$$n_e^2 + F(T)n_e - 7.34 \times 10^{21} F(T)/T = 0 \quad (6)$$

which can be solved for  $n_e$  by assuming a value for  $T$  and applying the quadratic formula.

## APPENDIX B



## APPENDIX B

### DETAILS OF CONSTRUCTION AND OPERATION OF THE PHOTODIODE ARRAY SPECTROMETER

#### Mechanical Details

The photodiode array employed was a Reticon model RL-256EC which consists of 256 diodes each  $50\ \mu$  wide. In other words, it was the same length as a standard 512 element array with diodes spaced on  $25\ \mu$  centers. The array (i.e. each element) was  $150\ \mu$  high.

The Minuteman monochromator in which the array was installed is a 1 m Czerny-Turner design, capable of operating as a spectrograph or spectrometer (a folding mirror could be positioned to direct light onto a photomultiplier tube). To facilitate spectrographic operation, the photographic plate holder could be snapped into a moveable carriage and could then be manually racked up and down.

The array came from the manufacturer mounted on a small ( $1\ 1/2'' \times 3''$ ) circuit board together with the circuitry for the first video amplification stage. The array socket was modified so that a copper bar could pass

directly beneath the array. The board was fastened to the copper bar which itself was fastened to two copper arms projecting from the Peltier coolers. Thus the array circuit board and Peltier coolers formed an integral unit. This cooler/holder assembly was mounted within a light aluminum cage which could snap into the movable carriage in exactly the same fashion as the plate holder. The unique feature of the system is that the cooler/holder assembly was affixed within the cage such that it could be rotated  $90^\circ$  with a small crank. The diode array spectrometer could be rapidly converted from a spatial mode to a spectral mode and vice versa.

## Electronics

### Overview

A block diagram of the basic components of the circuitry required to run the array is presented in Figure 78(a). When the integration timer has counted a preset number of pulses from the system clock, an external start pulse is issued. This pulse can be used for example to indicate to a computer that the array is about to read out. The timing circuitry (schematic Figure 78(b)) is responsible for generating a two-phase clock from the system clock and also for outputting an internal start pulse (on the S line) to trigger the self-scanning circuit

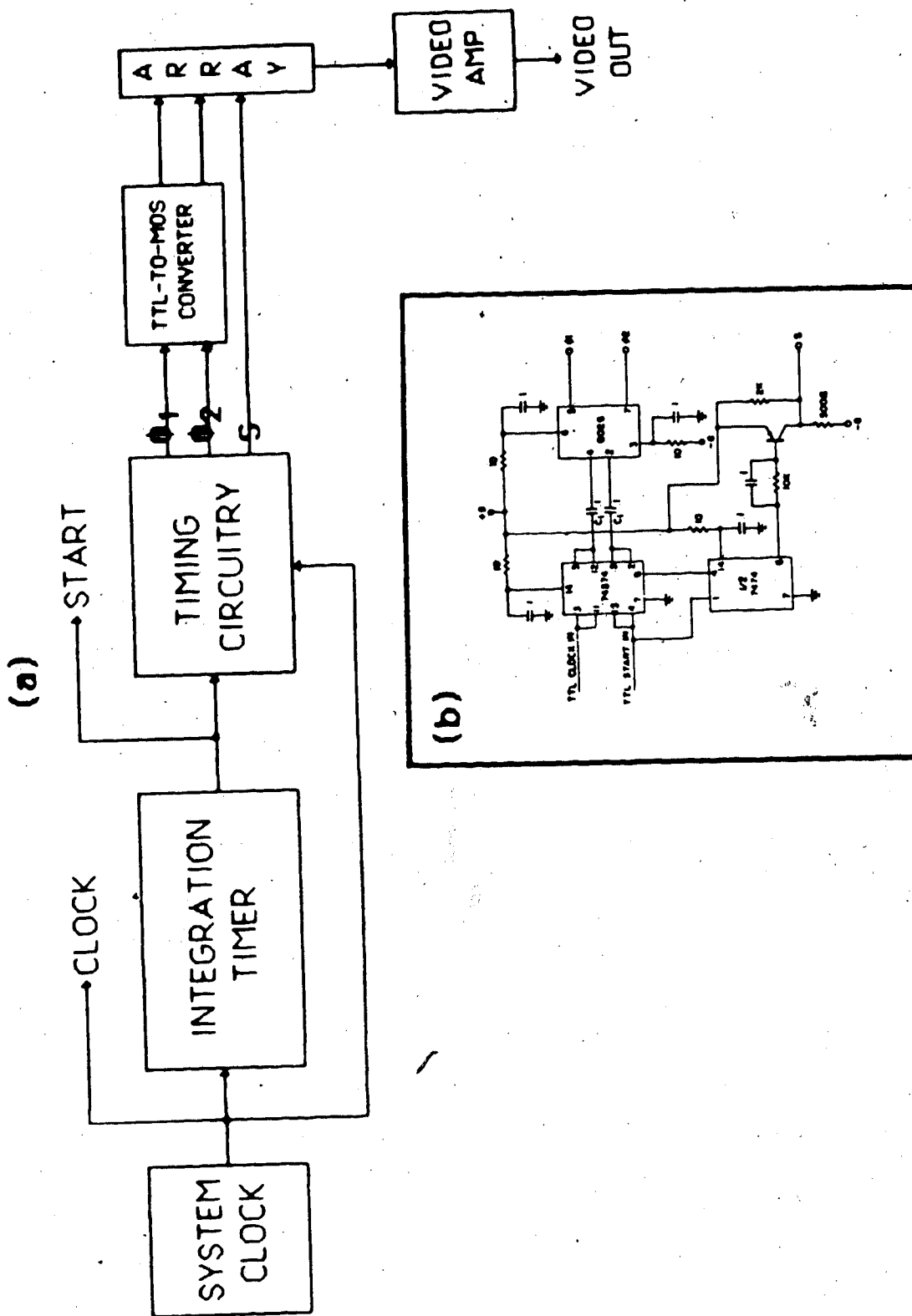


Figure 78. (a) Block diagram of photodiode array driving electronics, (b) schematic diagram of unmodified timing circuitry.

built onto the array chip. Amplification of the resulting chain of video pulses is necessary. Modifications to each of the basic components of the readout electronics are discussed below.

### System Clock

A schematic of the system clock based around a 9602 dual monostable is shown in Figure 79. A separate crystal-controlled oscillator and divider circuit was built to permit the 9602 to lock on to one of 3 preset frequencies. The frequency of the 9602 clock can still be varied continuously if desired, by selecting "VAR" with the CLOCK SELECT switch on the front panel. The output of the 9602 is available externally as a narrow spike for triggering purposes and as a broader negative or positive going pulse of variable width (courtesy of 74121-1) to indicate to a computer that a diode is reading out. These two waveforms are depicted at the top of Figure 80.

### Integration Timer and Timing Circuitry

Refer to Figures 80 and 81 throughout this discussion. The 9602 clock connects directly to the integration timer which consists of a chain of cascaded 74161 counters. The maximum integration time available was extended by inserting 3 more counters into the series. That procedure has been standard practice in our



Figure 79. Clock circuit schematic diagram.



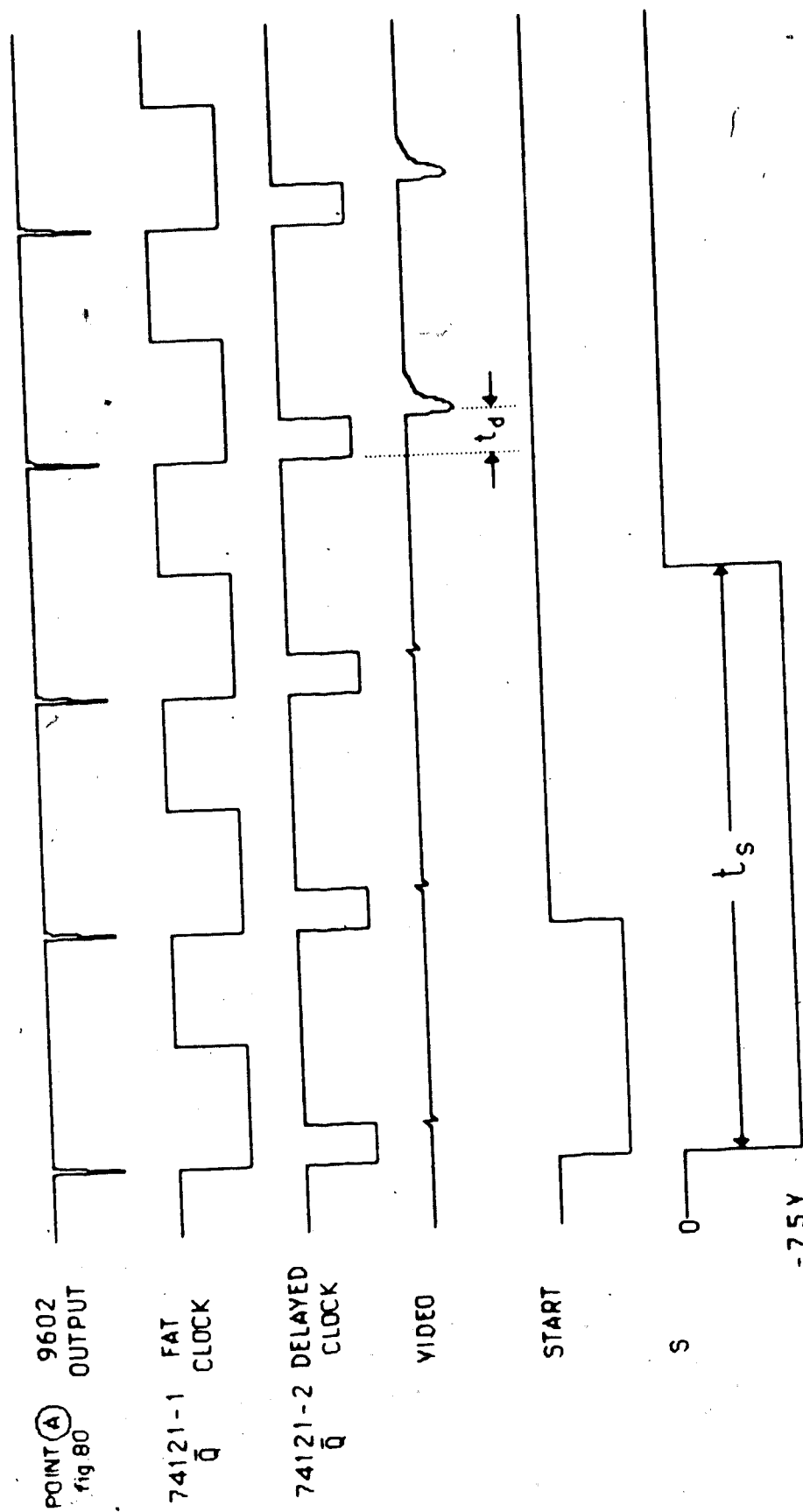


Figure 81. Relevant electronic waveforms for array circuitry.

laboratory and it is not necessary to repeat the details here.

When the timer has reached full count, a negative-going pulse one clock cycle wide is generated. This is brought out to the front panel as the START line and is used to tell a computer that the array is about to read out.

By means of a switch and monostable (74121-2), provision has been made to delay the clock which feeds the timing circuitry. This was done to allow the diode spikes to be sampled by an A-to-D converter. Previously, the timing circuitry was fed directly from the 9602 clock; any given diode would read out concurrently with the rising edge of the spike from the 9602 clock. With the monostable switched in (READOUT DELAY IN/OUT switch) the waveforms appear as in Figure 81. A given diode reads out a time  $t_D$  after the 9602 spike. This time can be set by the 10-turn READOUT DELAY potentiometer on the front panel.

As supplied by the manufacturer, the 9602 clock could not run below 15 kHz since the value of  $C_{VAR}$  in Figure 79 was .001  $\mu$ f. To digitize the array output with the Apple II+ computer however, the clock could not run much above 15 kHz, hence  $C_{VAR}$  was changed to .01  $\mu$ f. This permitted the 9602 to run in the range 5 to 50 kHz. If the clock is



run below 15 kHz, Reticon advises that the two-phase clock be coupled to the level converter via 1  $\mu$ f capacitors instead of .1  $\mu$ f. Hence a switch labelled  $\phi \rightarrow$  PDA was installed to permit the clock to be coupled by either set of capacitors depending on the frequency.

A curious problem manifested itself once all the changes outlined above had been effected. At integration times longer than 400 msec, a false readout pulse would be issued on the S line 400 msec before the end of the nominal integration period. A corresponding pulse did not appear on the START line. The effect was to reduce the maximum integration time available to 375 msec. For example, if the nominal integration time was 10 seconds, the array would integrate merrily for 9.6 seconds, read out due to the action of the false S pulse, then integrate for another 375 msec (readout taking 25 msec with a 10 kHz clock) before reading out again at the prompting of the true S pulse.

Substitution of both 74S74 and 7476 chips which comprised the original timing circuitry (Figure 78(b)) did not remove the problem. Eventually it was solved by replacing the 7476 with a 74121 monostable (74121-3). The monostable was mounted on a small board which piggybacked onto the existing 7476 socket. The trimmer marked  $t_s$  in Figure 80 is also on this board. The width of the S pulse

can be adjusted using this trimmer and is not critical as long as the S line stays low for several clock cycles. The START and S pulses are depicted in Figure 81. If the clock frequency is changed appreciably from 10 kHz, the width  $t_s$  may have to be adjusted.

#### Video Amplifier

A simple amplifier consisting of 4 operational amplifiers (OA's) was built and its schematic appears in Figure 82. Both an inverter and a low pass filter can be switched in or out of the signal path. A gain of 4 is built in at the second OA. Offset can also be added at this point. The gain of the fourth OA can be varied from 1.5 to 15, thus the total gain of the amp is variable from 6 to 60. Provision has been made to switch the entire amp out of the signal path if desired.

#### Interfacing

A schematic of the array and associated electronics interfaced to a computer is found in Figure 83. As mentioned, the electronics were modified to permit the diode spikes to be sampled by an AI13 A-to-D converter. The AI13 can be programmed to open a 125 ns sampling window following the receipt of a trigger pulse. The window does not open until 6  $\mu$ s after the triggering edge. (which can be either positive or negative going).

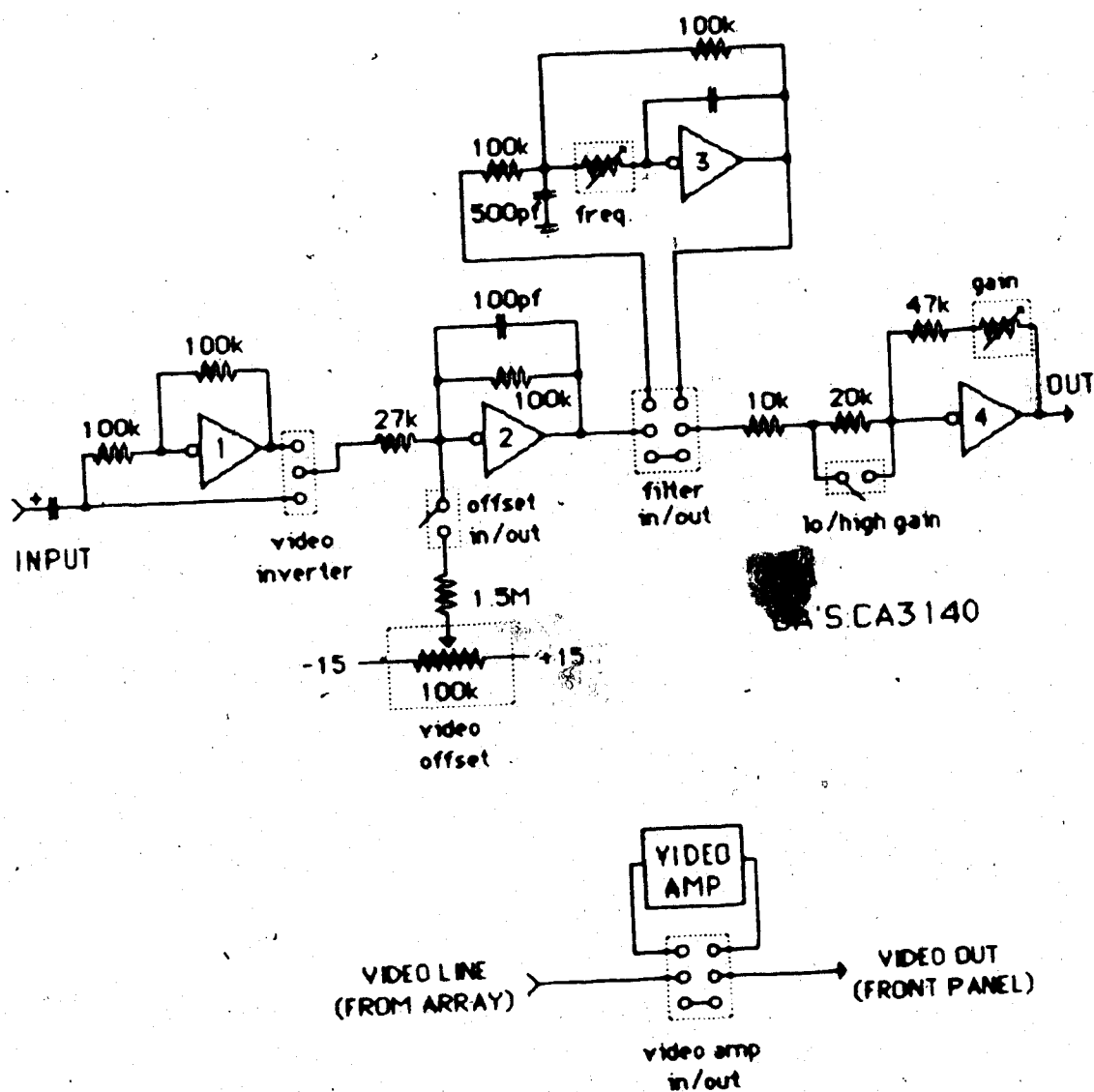


Figure 82. Video amplifier schematic.

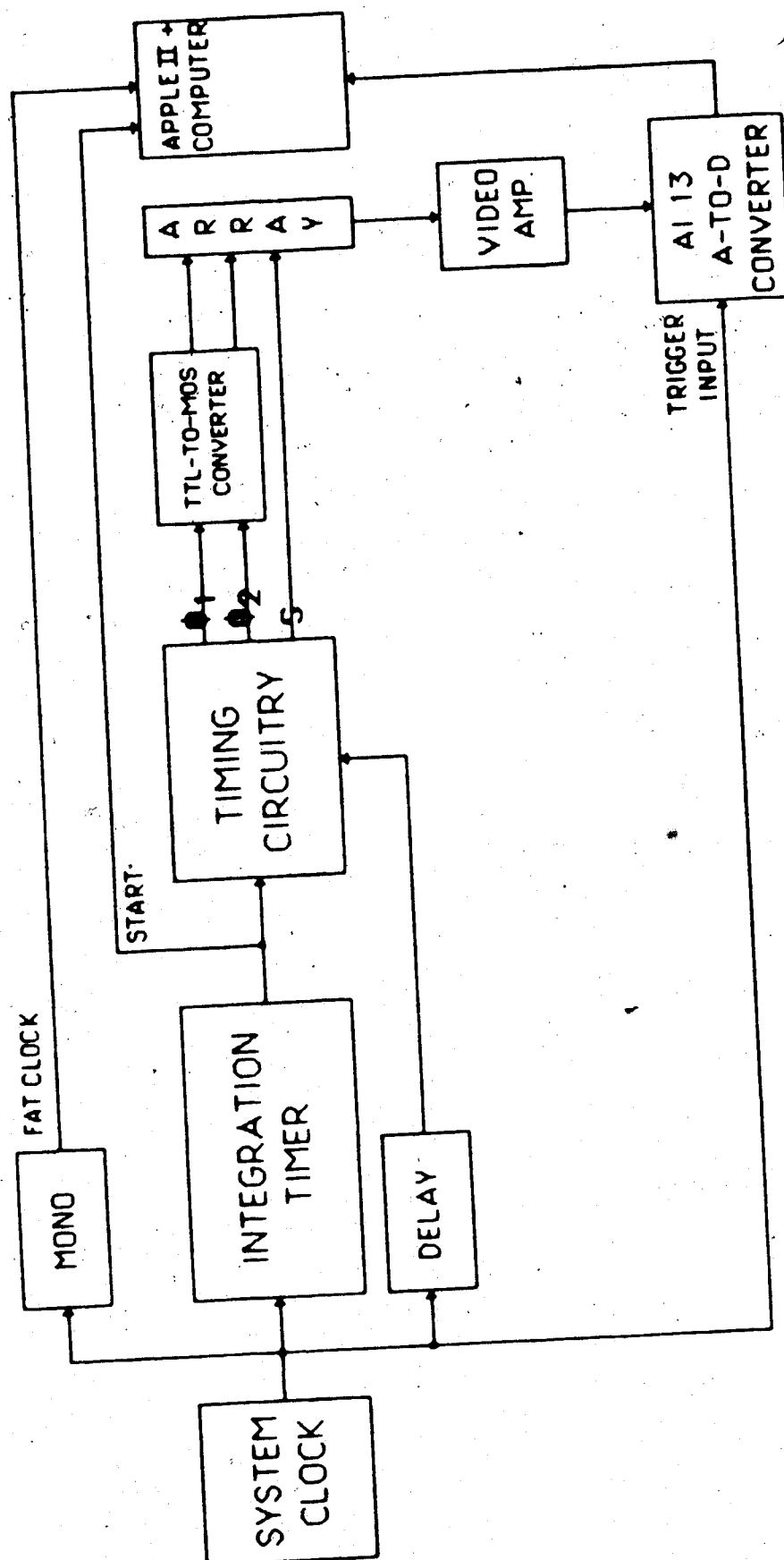


Figure 83. Block diagram of modified array circuitry interfaced to a computer.

No appropriate trigger signal was available from the array electronics in its initial configuration. By permitting the two-phase clock to be delayed relative to the 9602 clock, the 9602 clock can then be used to trigger the AI13. The delay ( $t_d$ ) is then adjusted using the READOUT DELAY potentiometer to ensure that the AI13 samples the signal spikes correctly.

#### Front Panel

A diagram of the front panel is seen in Figure 84. Any components appearing on the front panel have been enclosed by dashed outlines.

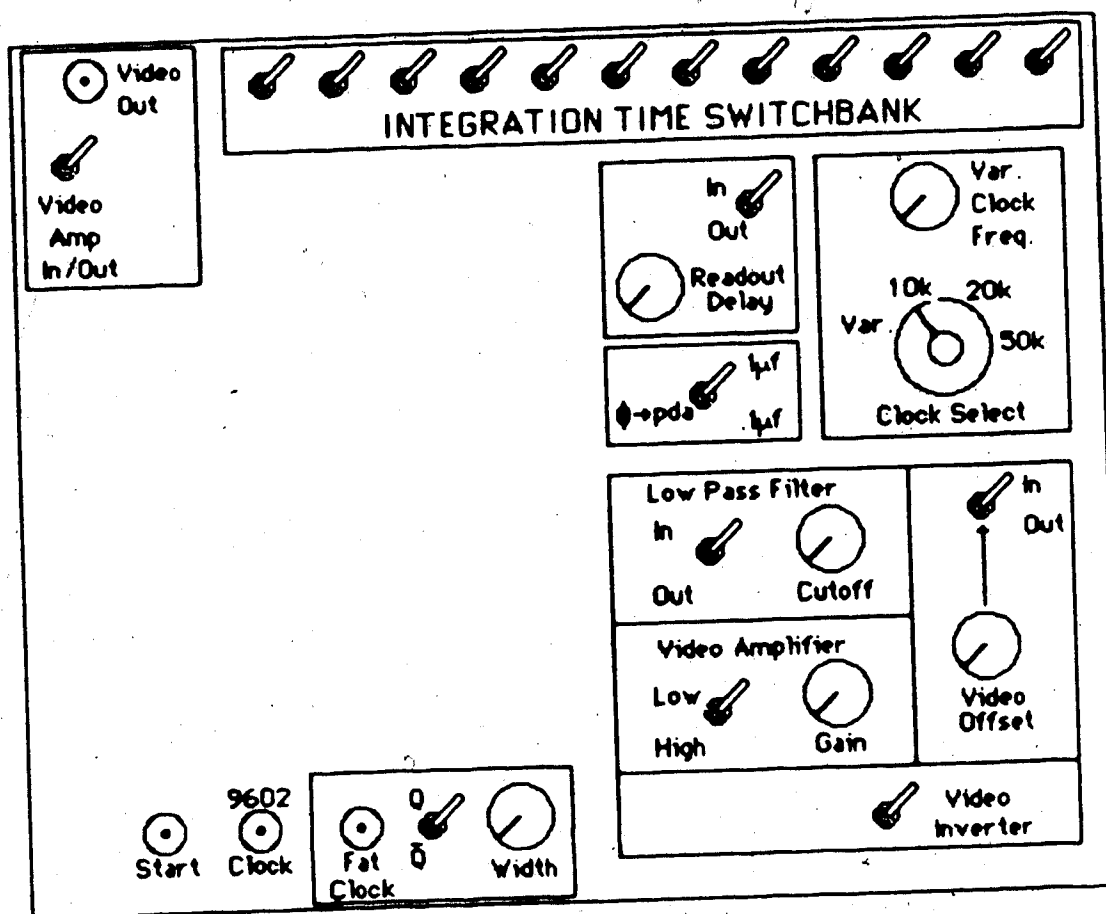


Figure 84. Front panel of unit housing array driving electronics.

## APPENDIX C

## APPENDIX C

### Stepper Motor Interfacing

Very little work was required to fully interface the two stepper motors to the Apple. A timer/driver board plugged into any available expansion slot on the Apple and a ribbon cable ran out to the R2D23 stepper motor driver board.

The R2D23, together with a regulated 5 V logic power supply had to be housed in a small cabinet. A 15 V/6.3 A power supply to run the steppers themselves was housed in another cabinet and its output jumpered into the R2D23.

The 4 phase clock signals plus  $V_M$  lines were taken out to the steppers via 2 octal sockets (see Figure 85). Note that the lines marked ENC, although wired to the sockets, are not connected to the steppers. A wiring diagram for the motors is given in Figure 86. They were operated in the half step mode.

Motor A, which moves the torch box in a horizontal direction, is tuned (as outlined in the Rogers Labs manual) so that it ramps from 8 to 600 Hz in 400 msec, taking 32 ramps steps. Four hundred half steps will move the micrometer 1 mm. If the load is changed appreciably, the tuning will have to be done again.



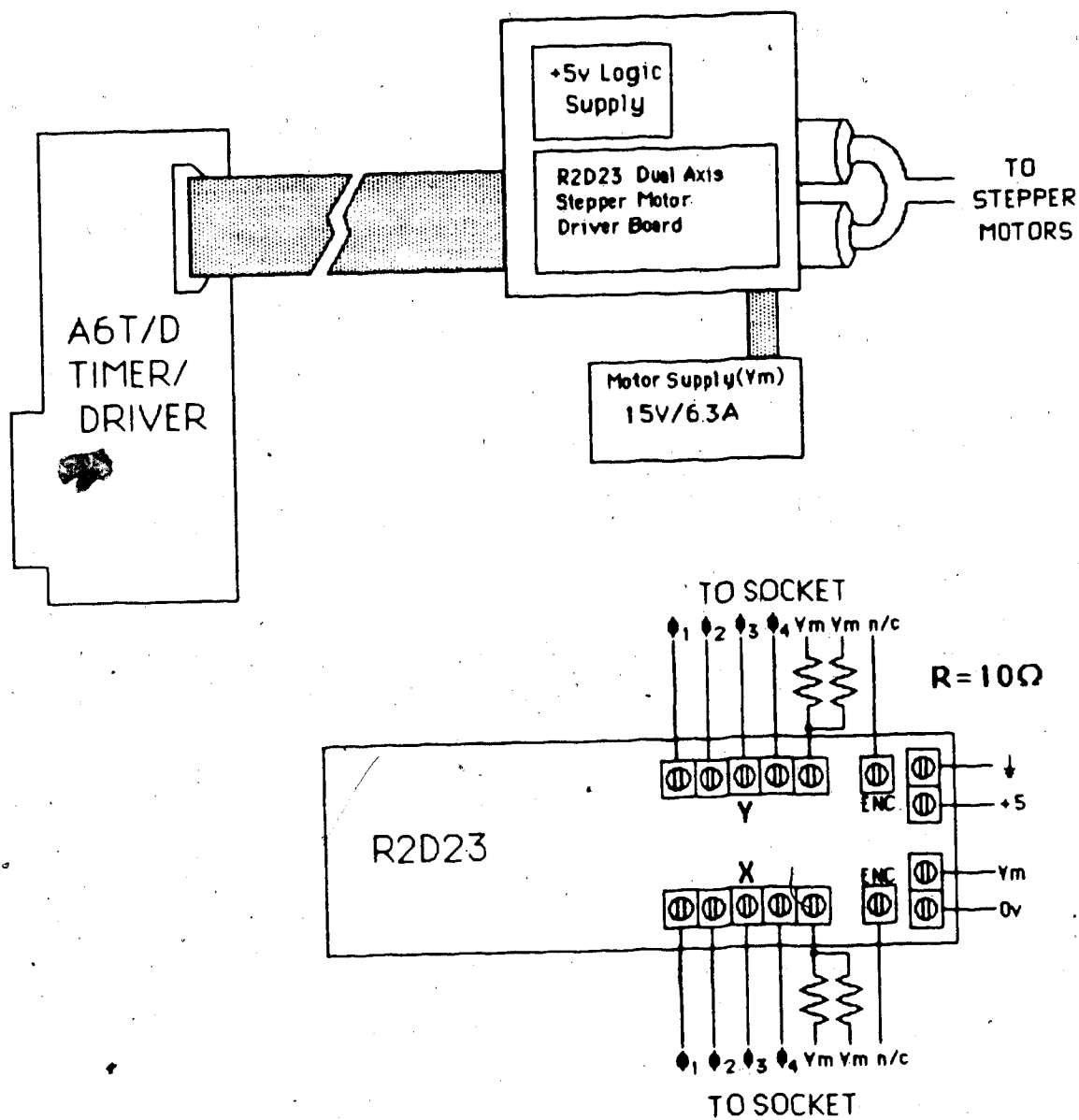


Figure 85. Interfacing of stepper motors.

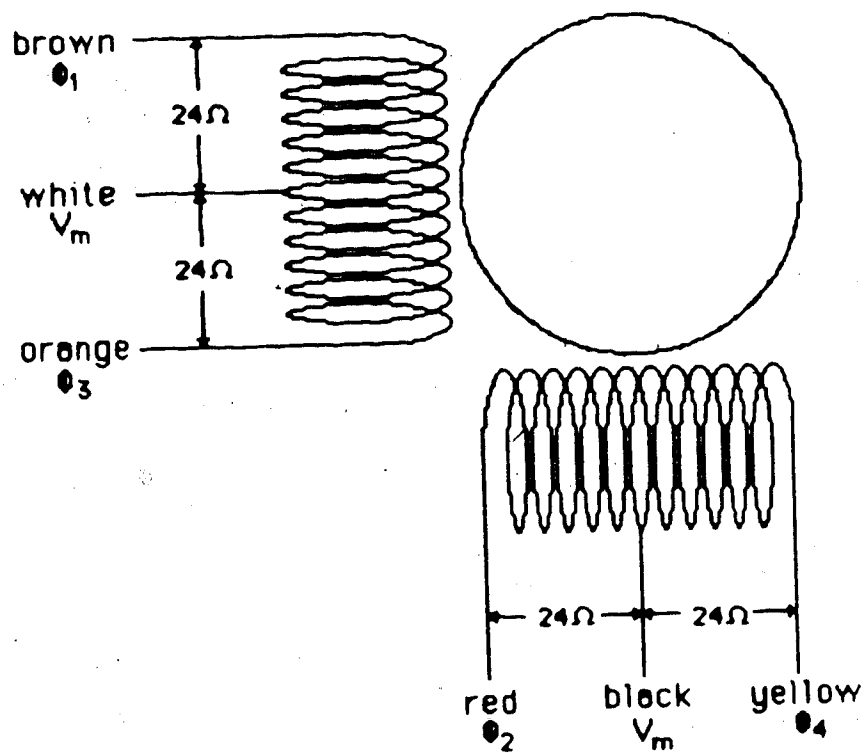


Figure 86. Stepper motor wiring diagram.

Motor B, driving the jack, ramps from 8 to 75 Hz in 1 sec, using 32 ramp steps. It was geared so that 343 half steps equal 1 mm. The same note regarding tuning applies here.

Use of the ampersand (&) calling routines to drive the motors from a BASIC program is clearly explained in the Rogers manual.

The address of the supplier is:

Rogers Labs Inc.  
2710 South Croddy Way  
Santa Ana, CA 92704

APPENDIX D

## APPENDIX D

### Pulse Counting

Each time the gated integrator receives a trigger signal, its BUSY line goes low for 45 microseconds. The BUSY line can then be used to toggle a J-K flip flop as in Figure 87.

A simple algorithm for pulse counting, easily implemented in BASIC, is given below:

1. CLEAR FLIP FLOP (C040 STROBE)
2. SET COUNTER TO DESIRED # OF PULSES
3. ISSUE LASER TRIGGER PULSE (AN0)
4. WAIT A FEW HUNDRED MILLISECONDS
5. IF THE FLIP FLOP ISN'T SET (PB0  $\neq$  1) GO BACK TO 3
6. DECREMENT COUNTER
7. CLEAR FLIP FLOP
8. IF COUNTER  $\neq$  0, GO BACK TO 3
9. DIGITIZE OUTPUT OF INTEGRATOR

Line 4 is the time between laser pulses, set by the user.

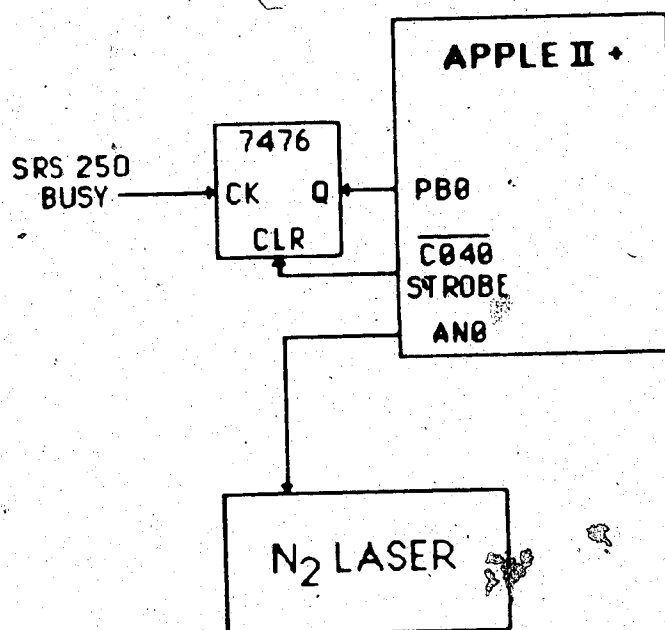
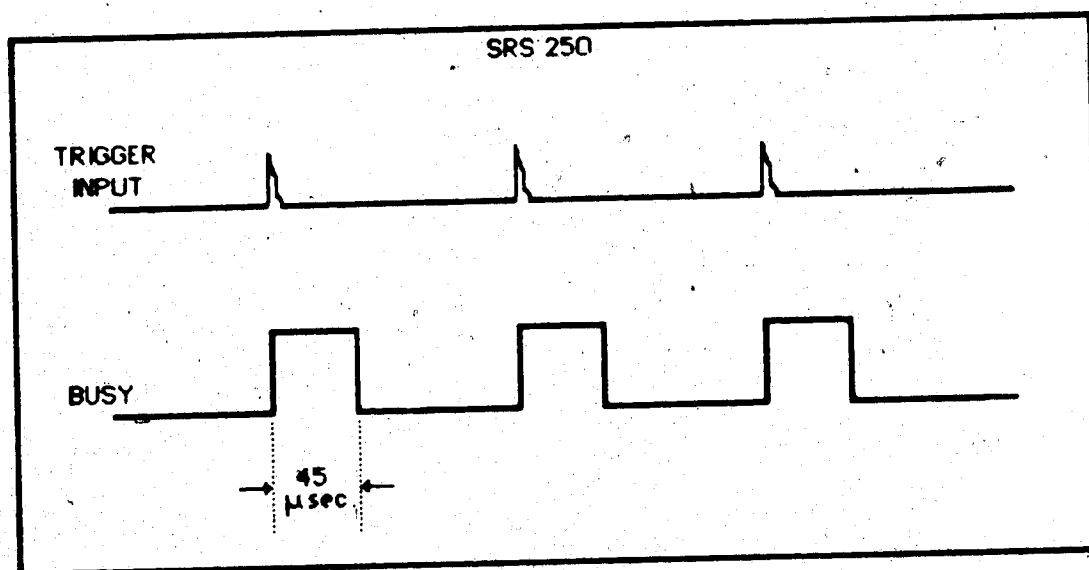


Figure 87. Details of laser pulse counting circuit.